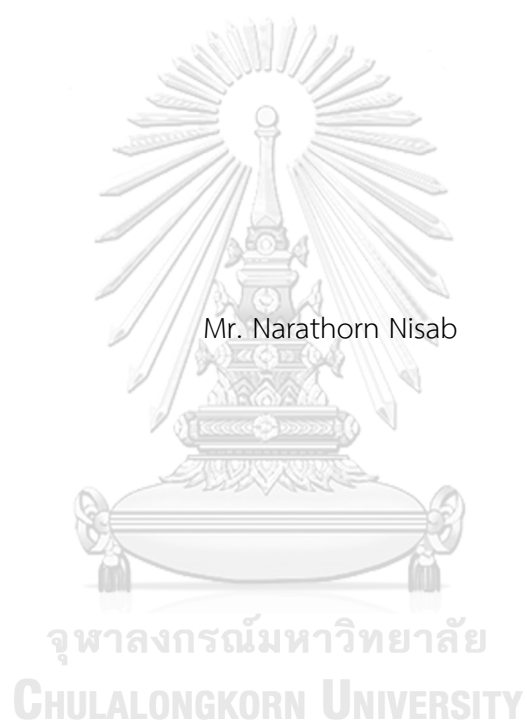


DEVELOPMENT OF BIOSENSOR USING PYRROLIDINYL PNA FOR SCREENING OF
HEPATITIS C VIRUS DNA



A Thesis Submitted in Partial Fulfillment of the Requirements
for the Degree of Master of Science in Chemistry

Department of Chemistry

FACULTY OF SCIENCE

Chulalongkorn University

Academic Year 2019

Copyright of Chulalongkorn University

การพัฒนาตัวรับรู้ชีวภาพโดยใช้พีริโรลิดินิลพีเอ็นเอสำหรับการคัดกรองดีเอ็นเอของไวรัสตับอักเสบบี



วิทยานิพนธ์นี้เป็นส่วนหนึ่งของการศึกษาตามหลักสูตรปริญญาวิทยาศาสตรมหาบัณฑิต
สาขาวิชาเคมี ภาควิชาเคมี
คณะวิทยาศาสตร์ จุฬาลงกรณ์มหาวิทยาลัย
ปีการศึกษา 2562
ลิขสิทธิ์ของจุฬาลงกรณ์มหาวิทยาลัย

Thesis Title	DEVELOPMENT OF BIOSENSOR USING PYRROLIDINYL PNA FOR SCREENING OF HEPATITIS C VIRUS DNA
By	Mr. Narathorn Nisab
Field of Study	Chemistry
Thesis Advisor	Professor Dr. ORAWON CHAILAPAKUL
Thesis Co Advisor	Professor Dr. TIRAYUT VILAIVAN

Accepted by the FACULTY OF SCIENCE, Chulalongkorn University in Partial
Fulfillment of the Requirement for the Master of Science

..... Dean of the FACULTY OF SCIENCE
(Professor Dr. POLKIT SANGVANICH)

THESIS COMMITTEE

..... Chairman
(Associate Professor Dr. VUDHICHAI PARASUK)

..... Thesis Advisor
(Professor Dr. ORAWON CHAILAPAKUL)

..... Thesis Co-Advisor
(Professor Dr. TIRAYUT VILAIVAN)

..... Examiner
(Associate Professor Dr. NATTAYA NGAMROJANAVANICH)

..... Examiner
(Dr. JANJIRA PANCHOMPOO)

..... External Examiner
(Associate Professor Dr. Weena Siangproh)

นราธร นิทรัพย์ : การพัฒนาตัวรับรู้ชีวภาพโดยใช้พีร์โรลิดินิลพีเอ็นเอสำหรับการคัดกรองดีเอ็นเอของไวรัสตับอักเสบบี. (DEVELOPMENT OF BIOSENSOR USING PYRROLIDINYL PNA FOR SCREENING OF HEPATITIS C VIRUS DNA) อ.ที่ปรึกษาหลัก : ศ. ดร.อรรวรรณ ชัยลภากุล, อ.ที่ปรึกษาร่วม : ศ. ดร.ธีรยุทธ วิไลวัลย์

ในงานวิจัยนี้ อุปกรณ์วิเคราะห์ฐานกระดาษชนิดใหม่ซึ่งอาศัยการตรวจวัดฟลูออเรสเซนซ์ได้ถูกพัฒนาขึ้นเพื่อการตรวจวัดดีเอ็นเอของไวรัสตับอักเสบบีโดยปราศจากการติดฉลาก พีร์โรลิดินิลพีเอ็นเอถูกใช้ปรับปรุงพื้นผิวบนกระดาษเซลลูโลสที่มีแบบแผนด้วยพันธะโคเวเลนต์ เพื่อทำหน้าที่เป็นโพรบที่มีความจำเพาะต่อการจับกับดีเอ็นเอเป้าหมายของไวรัสตับอักเสบบีตามหลักการเข้าคู่เบสของวัตสัน – คริก สีย้อมที่จำเพาะต่อดีเอ็นเอสายเดี่ยวซึ่งสามารถเกาะติดด้วยแรงทางไฟฟ้าสถิตกับดีเอ็นเอที่ผูกติดไว้บนพื้นผิวถูกใช้เป็นตัวส่งสัญญาณสำหรับการตรวจวัดฟลูออเรสเซนซ์ ผ่านอุปกรณ์เสริมสำหรับสมาร์ตโฟนและแอปพลิเคชันบนระบบไอโอเอส สำหรับงานวิจัยนี้ได้ตรวจสอบหาสภาวะในการทดลองหลายพารามิเตอร์เพื่อให้ได้ความไวในการตรวจวัดที่ดีที่สุด ได้แก่ ความเข้มข้นของโพรบที่เหมาะสม เวลาที่เหมาะสมในการเข้าคู่กันของโพรบและดีเอ็นเอเป้าหมาย เวลาที่เหมาะสมในการบ่มปฏิกิริยา และปริมาณของสีย้อมฟลูออเรสเซนซ์ที่ใช้ ภายใต้พารามิเตอร์ที่เหมาะสมได้ความสัมพันธ์เชิงเส้นตรง (ค่าสัมประสิทธิ์สหสัมพันธ์ เท่ากับ 0.9956) ระหว่างการเปลี่ยนแปลงของสีเรืองแสงสีเขียวและปริมาณดีเอ็นเอของไวรัสตับอักเสบบีในช่วง 5 ถึง 100 พิโคโมล ชีตจำกัดการตรวจวัดของดีเอ็นเอเป้าหมาย (ความยาว 55 นิวคลีโอไทด์) พบว่ามีค่าเท่ากับ 5 พิโคโมล นอกจากนี้ตัวรับรู้ที่นำเสนอขึ้นยังแสดงการจำแนกที่ละเอียดระหว่างดีเอ็นเอเป้าหมายและโอลิโกนิวคลีโอไทด์ที่มีลำดับเบสไม่ตรงกันกับดีเอ็นเอเป้าหมาย สำหรับการประเมินประสิทธิภาพของตัวรับรู้ที่นำเสนอเพื่อการวิเคราะห์ในตัวอย่างดีเอ็นเอจริง ตัวรับรู้นี้ได้ถูกนำไปใช้ประโยชน์สำหรับการตรวจวัดดีเอ็นเอของไวรัสตับอักเสบบีในตัวอย่างที่มีการขยายจำนวนดีเอ็นเอด้วยเทคนิคพีซีอาร์ พบว่ามีผลลัพธ์เป็นที่น่าพอใจ ดังนั้นอุปกรณ์ที่พัฒนาขึ้นนี้สามารถนำไปปรับใช้เป็นวิธีการเลือกซึ่งบ่งชี้ถึงความเป็นไปได้ในการพัฒนาแพลตฟอร์ม ณ จุดดูแลผู้ป่วย สำหรับการคัดกรองดีเอ็นเอของไวรัสตับอักเสบบีเพื่อวัตถุประสงค์ทางชีวการแพทย์

สาขาวิชา เคมี
ปีการศึกษา 2562

ลายมือชื่อนิสิต
ลายมือชื่อ อ.ที่ปรึกษาหลัก
ลายมือชื่อ อ.ที่ปรึกษาร่วม

6171980423 : MAJOR CHEMISTRY

KEYWORD: biosensor, hepatitis C virus, fluorescence-based detection, pyrrolidinyl peptide nucleic acid

Narathorn Nisab : DEVELOPMENT OF BIOSENSOR USING PYRROLIDINYL PNA FOR SCREENING OF HEPATITIS C VIRUS DNA. Advisor: Prof. Dr. ORAWON CHAILAPAKUL
Co-advisor: Prof. Dr. TIRAYUT VILAIWAN

In this work, a new paper-based analytical device (PAD) that relied on fluorescence measurement was developed for label-free detection of hepatitis C virus (HCV) DNA. Pyrrolidinyl peptide nucleic acid (acpcPNA) was covalently modified onto the patterned cellulose paper to act as a specific probe for capturing the HCV DNA target according to Watson-Crick base-pairing rules. The single-stranded (ssDNA)-specific dye which can be electrostatically attached to the surface-bound DNA was employed as the signaling element for the fluorescence-based detection via a smartphone gadget and an iOS application. To acquire the optimal sensitivity, several experimental parameters, namely acpcPNA probe concentration, hybridization time, incubation time, and the amount of fluorescent dye were examined. Under the optimized conditions, a linear relationship ($R^2 = 0.9956$) between the change of green fluorescent color and the amount of HCV DNA was observed in the range of 5 to 100 pmol. The detection limit of the target sequence (55 nucleotides) was found to be 5 pmol. Moreover, this proposed sensor exhibited excellent discrimination between complementary and mismatch oligonucleotide targets. To assess the efficiency of the proposed sensor for real DNA sample analysis, it was utilized for the detection of HCV DNA in PCR-amplified samples with satisfactory results. Hence, this developed device could be applied as an alternative method which indicates the possibility to develop a point-of-care (POC) platform for screening of HCV DNA for biomedical purposes.

Field of Study: Chemistry

Academic Year: 2019

Student's Signature

Advisor's Signature

Co-advisor's Signature

ACKNOWLEDGEMENTS

First of all, I would like to express a deep sense of gratitude to my principal advisor Prof. Dr. Orawon Chailapakul and co-advisor Prof. Dr. Tirayut Vilaivan for the continuous assistance of my coursework and research with their fortitude, encouragement, inspiration and precious knowledge. Their invaluable supervision supported me in all the time of research and writing of this thesis. I would like to thank my thesis committee, Assoc. Prof. Dr. Vudhichai Parasuk, Assoc. Prof. Dr. Nattaya Ngamrojanavanich, Assoc. Prof. Dr. Weena Siangproh and Dr. Janjira Panchompoo for their direction, devotedness and immense guidance along with this project.

I sincerely appreciate Dr. Prinjaporn Teengam for suggestions in some experiments of this thesis. I really thank her all giving of kindness, support and optimism. Without her helps, it would not be possible to complete this research. I also would like to express my appreciation to Mrs. Chotima Vilaivan for acpcPNA synthesis throughout the experiment. Furthermore, I am grateful to all members of Electrochemistry and Optical Spectroscopy Center of Excellence (EOSCE) for extending their warm friendship towards me and making a delightful environment in the laboratory.

This research was financially supported by the Center of Excellence on Petrochemicals and Materials Technology (PETROMAT) and Electrochemistry and Optical Spectroscopy Center of Excellence, Department of Chemistry, Faculty of Science, Chulalongkorn University. I would like to thank Prof. Pisit Tangkijvanich and Dr. Natthaya Chuaypen for providing real clinical samples used in this research. In addition, I also would like to thank Department of Chemistry, Faculty of Science, Chulalongkorn University for facilities management.

Last but not the least, I must acknowledge with gratitude and love of my family for providing me with inexhaustible support and unceasing consolation throughout my years of master degree's study. This accomplishment would not be possible without them. Thank you.

Narathorn Nisab

TABLE OF CONTENTS

	Page
ABSTRACT (THAI).....	iii
ABSTRACT (ENGLISH).....	iv
ACKNOWLEDGEMENTS.....	v
TABLE OF CONTENTS.....	vi
LIST OF TABLES.....	x
LIST OF FIGURES.....	xi
LIST OF ABBREVIATIONS.....	xv
CHAPTER I INTRODUCTION.....	1
1.1 Introduction.....	1
1.2 Objectives of the research.....	5
1.3 Scope of the research.....	5
CHAPTER II THEORY AND LITERATURE REVIEW.....	7
2.1 Hepatitis C virus and its life cycle.....	7
2.2 Detection methods for HCV diagnosis.....	10
2.2.1 Anti-HCV assay.....	10
2.2.2 HCV Core antigen detection.....	12
2.2.3 Molecular-based HCV assay.....	13
2.3 Paper-based analytical devices.....	15
2.4 Fluorescence-based detection.....	16
2.5 Peptide nucleic acid.....	18
2.6 ssDNA-binding fluorescent dye.....	24

2.7	Fourier transform infrared spectroscopy.....	25
2.8	X-ray photoelectron spectroscopy.....	27
2.9	Literature review.....	28
CHAPTER III EXPERIMENT.....		34
3.1	Instrument and apparatus.....	34
3.2	Chemicals and reagents.....	36
3.3	Chemicals and reagents preparation	38
3.3.1	Synthesis and purification of acpcPNA probe.....	38
3.3.2	Preparation of 0.01 M phosphate buffer saline pH 7.4.....	39
3.3.3	Preparation of stock and working solutions of oligonucleotides.....	39
3.3.4	Preparation of acpcPNA working solution.....	39
3.3.5	Preparation of ssDNA-binding fluorescent dye working solutions	39
3.3.6	Preparation of 2.10 M LiCl in 0.04 M of NaIO ₄	40
3.3.7	Preparation of 0.01 M phosphate buffer saline containing 0.001% v/v Tween-20 (PBST).....	40
3.3.8	Preparation of working solutions for studying behavior of ssDNA- binding fluorescent dye.....	40
3.4	Fabrication of paper-based biosensor	41
3.5	acpcPNA probe Immobilization.....	41
3.6	FT-IR characterization	42
3.7	XPS characterization	43
3.8	Fluorescence-based detection for studying behavior of ssDNA-binding fluorescent dye.....	43
3.9	Hybridization with the target oligonucleotides.....	44

3.10	Fluorescence-based detection on paper-based biosensor.....	44
3.11	Influence of the total length of HCV DNA on the signal response.....	44
3.12	Optimization of the experimental conditions.....	46
3.12.1	Concentration of acpcPNA probe.....	46
3.12.2	Hybridization time.....	46
3.12.3	Incubation time.....	46
3.12.4	Concentration of ssDNA-binding fluorescent dye.....	47
3.12.5	Volume of ssDNA-binding fluorescent dye.....	47
3.13	Analytical performance.....	47
3.14	Specificity study.....	48
3.15	Stability evaluation.....	48
3.16	Sample preparation.....	48
CHAPTER IV	RESULTS AND DISCUSSION.....	49
4.1	Characterization of the acpcPNA-immobilized paper-based sensor.....	49
4.2	Fluorescent behavior of ssDNA-binding fluorescent dye.....	52
4.3	Sensing principle.....	54
4.4	Influence of the total length of HCV DNA.....	55
4.5	Optimization of experimental conditions.....	56
4.5.1	Effect of acpcPNA concentration.....	56
4.5.2	Effect of hybridization time.....	57
4.5.3	Effect of incubation time.....	59
4.5.4	Effect of fluorescent dye concentration.....	60
4.5.5	Effect of fluorescent dye volume.....	62
4.6	Analytical performance.....	63

4.7 Specificity study.....	66
4.8 Stability evaluation	67
4.9 Real sample analysis	68
CHAPTER V CONCLUSIONS AND FUTURE PERSPECTIVE.....	71
5.1 Conclusion.....	71
5.2 Future perspective.....	72
REFERENCES	72
APPENDIX.....	87
VITA.....	94



LIST OF TABLES

	Page
Table 3.1	List of instruments and apparatus.....34
Table 3.2	List of chemicals and reagents.....36
Table 3.3	List of synthetic oligonucleotides.....37
Table 4.1	F-test for the determination of detection limit..... 65
Table 4.2	t-test for the determination of detection limit.....65
Table 4.3	The concentration of HCV-RNA and viral load in test samples.....69
Table A1	Chemical compounds that interfere with the ssDNA-binding fluorescent dye (QuantiFluor [®] ssDNA System) [93].....90
Table A2	The regression analysis of the calibration plots in Figure A3.....91
Table A3	T-distribution table (one tail).....92
Table A4	F distribution table (one tail) at significant level of 0.05.....93

LIST OF FIGURES

	Page
Figure 2.1	HCV genome and information in relation to viral polyproteins.....8
Figure 2.2	Schematic illustration of the intracellular life cycle of HCV [3].....10
Figure 2.3	Chemiluminescence ELISA of the detection of HCV-specific antibody [42].....12
Figure 2.4	Perrin–Jablonski diagram illustrating electronic states and transition related to the generation of fluorescence [67].....17
Figure 2.5	Overview of the point-of-care detection of ZIKV NS1 using the novel smartphone-based fluorescent LFIA platform [73].....18
Figure 2.6	Examples of preorganized constrained aegPNA systems [29].....19
Figure 2.7	General structure of DNA and selected PNA molecules.....20
Figure 2.8	The fabrication of the paper-based sensor by immobilizing acpcPNA onto filter paper and the detection of target DNA by cationic dye staining [30].....22
Figure 2.9	Detectable ranges of commercial ssDNA-binding fluorescent dyes [93].....25
Figure 2.10	Simplified chart of IR stretching frequencies regarding functional groups.....26
Figure 2.11	Evanescent wave as a result of attenuated total reflection [97].....26
Figure 2.12	The photoemission process of K (1s) photoelectron related to XPS analysis. The circles represent electrons and the bars stand for energy level within the material being measured.....28
Figure 2.13	The basis of detection procedures in the developed electrochemical assay for the selective determination of HCV DNA [13].....29

Figure 2.14	Schematic illustration of HCV DNA detection by naFRET probe [19].	32
Figure 2.15	Overview of the solid-phase assay for DNA detection using immobilized quantum dots as donors in FRET (left). Pseudocolor epifluorescence images generated using the multiple imaging channel (right) [70].	33
Figure 3.1	The design of paper-based sensor in top view (left) and side view (right) that composed of hydrophilic region (1), hydrophobic region (2) and transparent tape (3).	41
Figure 3.2	The procedure to produce acpcPNA-immobilized paper-based sensor.	42
Figure 3.3	Schematic of fluorescent camera for smartphone consisting of (1) 4 pieces of 340 nm light source, (2) 500 nm long-pass filter with anti-reflection filter, (3) body part for covering the paper-based sensor and preventing the interference of external light, (4) USB-C charging port, (5) switch and (6) smartphone case attachment.	45
Figure 3.4	The mean color intensity obtained from ColorMeter RGB Colorimeter application (version 1.95, developed by White Marten).	45
Figure 4.1	ATR-FT-IR spectra of (A) Whatman cellulose sheet, (B) aldehyde-modified paper and (C) acpcPNA-immobilized sensor.	50
Figure 4.2	High resolution XPS spectra of (A) C 1s, (B) O 1s and (C) N 1s on the surface of acpcPNA-immobilized paper-based device.	51
Figure 4.3	Fluorescence spectra of ssDNA-binding dye solution (0.5% v/v) with the addition of acpcPNA probe and target ssDNA (55 oligomers). All concentration of acpcPNA and ssDNA are 0.3	

	μM . The inset is the photographs of the assay solutions under UV light (365 nm).....	53
Figure 4.4	The proposed schematic representation of ssDNA-binding dye behavior.....	53
Figure 4.5	The detection concept of acpcPNA-immobilized PAD in the absence (A) and presence (B) of target sequence.....	54
Figure 4.6	Influence of the total length of HCV DNA on the signal intensity.....	55
Figure 4.7	Fluorescent images of 50 μM of HCV DNA at different total lengths (25–55 nucleotides).....	56
Figure 4.8	Effect of acpcPNA concentration on the fluorescence response of 50 μM of HCV DNA.....	57
Figure 4.9	Fluorescent images of target HCV DNA (50 μM) at different probe concentrations (25–75 μM).....	57
Figure 4.10	Effect of hybridization time on the fluorescence response of 50 μM of HCV DNA.....	58
Figure 4.11	Fluorescent images of target HCV DNA (50 μM) at different hybridization times (5–30 minutes).....	58
Figure 4.12	Effect of hybridization time on the fluorescence response of 50 μM of HCV DNA.....	59
Figure 4.13	Fluorescent images of target HCV DNA (50 μM) at different incubation times (0–30 minutes).....	60
Figure 4.14	Effect of fluorescent dye concentration on the fluorescence response of 50 μM of HCV DNA.....	61
Figure 4.15	Fluorescent images of blank and target HCV DNA (50 μM) at different fluorescent dye concentration (0.5–5% v/v).....	61

Figure 4.16	Effect of fluorescent dye volume on the fluorescence response of 50 μM of HCV DNA.....	62
Figure 4.17	Fluorescent images of target HCV DNA (50 μM) at different fluorescent dye volume (5–30 μL).....	62
Figure 4.18	The enhancement of green colors onto the proposed DNA sensor for various amounts of incubated HCV DNA (pmol).....	63
Figure 4.19	The calibration plot of ΔI_G value against the amount of incubated HCV DNA.....	63
Figure 4.20	ΔI_G values obtained from the paper-based sensor after hybridization of target, mis-1, mis-2 and ncDNA, respectively. All concentration of test DNA are 50 μM	67
Figure 4.21	The digital images of paper-based sensor in specificity test.....	67
Figure 4.22	Long-term stability of the proposed sensor for detecting 50 μM of HCV DNA (45 nucleotides) in room temperature (red line) and 4°C (blue line).....	68
Figure 4.23	The ΔI_G values for the detection of real HCV DNA in PCR-amplified samples (n=3).....	69
Figure 4.24	The schematic illustration for real sample analysis (upper) and ΔI_G response of the proposed DNA sensing-device in the occurrence of negative control and C132 samples (1x, 2x) (lower).....	70
Figure A1	Nucleotide sequences report from NCBI BLAST database.....	88
Figure A2	MALDI-TOF mass spectrum and the specific information of HCV acpcPNA probe.....	89
Figure A3	The calibration plots of the proposed DNA sensor in multiple color channels.....	91

LIST OF ABBREVIATIONS

acpcPNA	pyrrolidinyl peptide nucleic acid
DNA	deoxyribonucleic acid
FT-IR	Fourier transform infrared spectroscopy
HCV	hepatitis C virus
IU	international unit
L	liter
LOD	limit of detection
M	Molar
mg	milligram
mL	milliliter
nm	nanometer
PCR	polymerase chain reaction
pg	picogram
pmol	picomole
RNA	ribonucleic acid
SD	standard deviation
ssDNA	single-stranded deoxyribonucleic acid
UV	ultraviolet
XPS	X-ray photoelectron spectroscopy
μ L	microliter
μ M	micromolar
$^{\circ}$ C	degree Celsius

CHAPTER I

INTRODUCTION

1.1 Introduction

Hepatitis C virus (HCV) is a kind of blood-borne virus that its infections can induce various liver diseases such as cirrhosis, hepatic fibrosis, liver failure and hepatocellular carcinoma [1]. According to World Health Organization (WHO) report, it is shown that at least 185 million people all over the world succumbed from hepatitis C viral infection, and approximately 350,000 patients died each year from chronic HCV-related illnesses [2]. HCV infection can be treated; however, infected individuals do not become aware of the noticeable symptoms until their hepatic cells have been severely destroyed. Although it is a serious global public health issue, no effective vaccination and therapy against HCV are recently available [3]. The HCV monitoring in clinical samples, blood and its product, is operated to identify active infections; moreover, it can be utilized for determining treatment duration and response of the patient's body to antiviral drugs [4]. Consequently, it is urgent to develop reliable, rapid and simple screening assays for the determination of HCV.

Enzyme-linked immunosorbent assays (ELISA) are employed as standard screening techniques for HCV identification by detecting HCV-specific total antibodies (Anti-HCV). Nevertheless, these indirect serological methods are incapable of discrimination between active and resolved infections [5]. Furthermore, HCV antibodies can only be observed in the serum samples after the infection for a while (approximately 45–68 days) [6]. Thereby, these methods could not be used for early stage detection. Through the years, many direct assays have been developed for HCV diagnosis. These methods rely on the quantification of hepatitis C viral components, namely HCV Core antigen and HCV RNA. HCV Core antigen can be detected in the antibody window period and its levels are used to categorize active from resolved HCV infection [7]. Although HCV Core antigen detection could be a promising screening test, its

sensitivity is not high enough to overcome molecular HCV assays [8]. In terms of molecular-based methods, HCV RNA serves as a significant marker in early HCV infection within 1–3 weeks after exposure. Also, these assays provide a considerable sensitivity with a lower limit of detection <50 IU/mL [9]. Real-time reverse transcription-polymerase chain reaction (known as real-time RT-PCR) is the well-known molecular assay of reference for the determination of HCV RNA levels according to European and American guidelines [10]. The assay generates double-stranded DNA that complementary to HCV RNA in reverse-transcription (RT) processes. After that, millions of HCV DNA copies were created via PCR operation. The amount of HCV DNA can be quantified in real-time by fluorescence chemistry for each of the DNA amplification cycles. Even though these quantitative PCR exhibit acceptable results in comparison with other nucleic acid amplification technologies, there are some drawbacks since they rely on sophisticated instruments, expensive reagents, large sample volumes as well as the requirement of trained operators. Moreover, reading and interpretation procedures are complicated and therefore time-consuming [11]. These limitations make previous HCV diagnosis unattainable for point-of-need purposes, especially in developing areas. Thus, the establishment of a rapid, easily manipulated and cost-effective strategy for the early-stage detection of HCV is in high demand.

Over the past decades, several analytical methods have been reported for the detection of HCV DNA, for example, electrochemical detection [12-15], optical enzyme-linked oligosorbent assay (ELOSA) [16] and electrochemiluminescence [17]. However, most of these methods have their own disadvantages, for instance, cumbersome apparatus, complicated procedure, portable incapability, long time interval analysis and large sample amounts requirement. To solve these problems, the detection assay should be able to provide simple, portable, time-saving and miniature sensing platforms which is still challenging. Fluorescence detection has been accepted as an impressive analytical technique by reason of its high sensitivity and selectivity,

simple operation, fast-response and can be directly recognized by naked-eyes under the UV control system [18]. To the best of our knowledge, there is only one piece of scientific publication that presented the HCV DNA quantitation using fluorescence-based detection [19]. This system based on fluorescence resonance energy transfer (FRET) system of labeled DNA probes and exhibited a very low background signal as well as high sensitivity with the detection limit in the range of nanomolar. However, it requires a large amount of sample and chemical reagent. Hence, the development of fluorescence-based detection to overcome the abovementioned drawbacks is crucial and attractive to obtain a new sensor that acts as an alternative approach for screening of HCV DNA in clinical settings.

Nowadays, paper-based analytical devices (PADs) have obtained considerable interest to serve as an efficient sensing platform to use in low and middle-income countries. PADs exhibit a multitude of advantages, such as being biocompatible, disposable, portable, low-priced, small-sized, lightweight and easy-to-handle. Additionally, fluorescence detection can be manipulated as the detection method that can be employed with PADs to improve the sensitivity and selectivity in such devices [20-24]. Accordingly, the coalescence of PADs and fluorescence-based detection is a well-suited sensor for the practical determination of numerous biomarkers regarding a clinical diagnosis for point-of-care (POC) applications in developing regions.

In terms of specific DNA detection, a selective recognizing receptor is an essential factor that influences the validation of the detection method. Peptide nucleic acids (PNA) recently received significant attention to utilizing as a probe for DNA sequence analysis. This noticeable molecule is an uncharged DNA-analog model comprised of a synthetic peptide-mimic backbone. The hybridization between PNA probe and target oligonucleotide presented an extremely strong affinity and distinguished selectivity compared to original DNA probes [25]. The DNA-binding process exclusively follows the expected Watson–Crick rule [26]. Moreover, the neutral backbone exhibited excellent

durability of DNA–PNA hybrids over a broad range of ionic strengths [27]. The synthetic structure of PNA also provides outstanding stability against protease and nuclease in biological specimens [28]. Lately, Vilaivan group [29] has demonstrated a unique design of a rigid PNA molecule. The pyrrolidinyI PNA class consists of a D-prolyl-2-aminocyclopentanecarboxylic acid backbone (known as acpcPNA). This acpcPNA system shows superior probe/target recognition in terms of desirable binding affinity and sequence specificity over the conventional PNA. Besides, the acpcPNA probe can be covalently tethered onto a modified cellulose-filter paper and operated as an effective device for in vitro detection of the target DNA of interest [30-32]. Given the aforementioned benefits, PADs that merged with the acpcPNA-based sensor provide the prospects of POC DNA diagnosis.

In order to develop the new approach for screening HCV DNA in biological media, the novel POC platform is created by using acpcPNA chemically immobilized on PADs combined with fluorescent and visual detection. This research could serve as an alternative and simple-to-fabricate tool for the rapid screening of HCV DNA in clinical diagnosis. The improvement of this work over the previous publications is a new sensing strategy composed of portable size, rapid detection, small sample volume requirement, long-term storage, uncomplicated fabrication and straightforward operation. In addition, the proposed platform can achieve the objective of real sample measurement effectively.

1.2 Objectives of the research

The objectives of this research are separated into two parts as follows:

- 1) To develop a novel paper-based biosensor using a specific acpcPNA probe for screening of hepatitis C virus DNA.
- 2) To apply the proposed sensor for clinical sample analysis.

1.3 Scope of the research

The novel sensing platform for screening of hepatitis C virus DNA using selective acpcPNA probe covalently immobilized on cellulose substrate coupled with fluorescent and visual detection was first established. In the interest of developing a strategy for the detection of HCV DNA, the various procedures were performed. Firstly, the behavior of ssDNA-binding fluorescent dye related to the hybridization between acpcPNA and target oligonucleotide was examined using fluorescence spectroscopy. For verification of the probe existence on cellulose devices after immobilization steps, the Fourier transform infrared spectroscopy (FT-IR) and X-ray photoelectron spectroscopy (XPS) were operated to investigate the characteristic functional groups of the paper-based biosensor. The effect of the total length of incubated DNA on the signal intensity was also evaluated by fluorescence-based detection on the paper-based biosensor. To obtain the high sensitivity of HCV DNA measurement, all experimental conditions on paper-based devices consisted of the amount of acpcPNA, concentration and volume of fluorescent dye were optimized. In addition, the assay time such as hybridization time and incubation time were also considered to reach optimal conditions. For analytical performance, the different amounts of HCV DNA were analyzed to identify the linear dynamic range versus the green fluorescent signal. Moreover, the detection limit was also calculated. To evaluate the sequence specificity of acpcPNA probe, the green signal response of single-base-mismatch, two-base-mismatch and non-complementary oligonucleotides were examined and compared to complementary HCV DNA. Furthermore, the shelf-life time of acpcPNA-

immobilized paper-based sensor was also studied to assess the long-term stability. Finally, the proposed sensor was utilized to detect target DNA in PCR products for confirmation of applicability for screening of HCV DNA in real samples.



CHAPTER II

THEORY AND LITERATURE REVIEW

2.1 Hepatitis C virus and its life cycle

Hepatitis C is a severe liver disease resulting from infection with the hepatitis C virus (HCV), which is a small, enveloped, single-stranded and hepatotropic RNA virus belonging to the genus Hepacivirus, a member of the family Flaviviridae. This spherical viral particle, of which dimensions range around 30–60 nm, is composed of an RNA genome with approximately 9,500 nucleotides in length. The positive-sense HCV RNA can be translated into a great number of viral polyproteins comprising about 3,000 amino acids in the host cell. [33, 34]. The viral genome is constituted by a translational open reading frame (ORF) that responsible for encoding four-type structural (Core, p7, glycoproteins E1 and E2) and six non-structural (NS2, NS3, NS4a, NS4b, NS5a, NS5b-RNA polymerase) viral proteins. The region of ORF and information regarding HCV proteins is shown in Figure 2.1. The genomic feature of HCV displays significant variability by a reason of imperfect proofreading activity in viral RNA polymerase. This genetic variability allows classification into seven main HCV genotypes, identified by 1–7. Each of HCV genotype contains multiple subtypes, designated by small letters of English alphabets (1a, 1b, and so on) [35]. Among various HCV genotypes, subtypes 1a and 1b become more prevalent worldwide and represent 60% of all cases. Due to a highly genotypic distribution, there is no curative vaccination accessible for against HCV presently [36]. Common groups at risk of infection include people who make contact with infected blood and its product, injection procedures without adequate sterilization, haemodialysis, sexual relationship with HCV-infected person and mother-to-child transmission. HCV infection can generate acute hepatitis C within six months of acquiring infection. Subsequently, 50–80% of acute HCV patients progress to chronic liver disease. Infected patients have a high possibility of chronic inflammatory disease, which might proceed to liver

fibrosis, cirrhosis, hepatocellular carcinoma (HCC) and even death [2]. Therefore, effective diagnosis and rapid screening of HCV infection are deeply critical processes to prevent the propagation of HCV-associated liver disease and also decrease the rate of viral transmission.

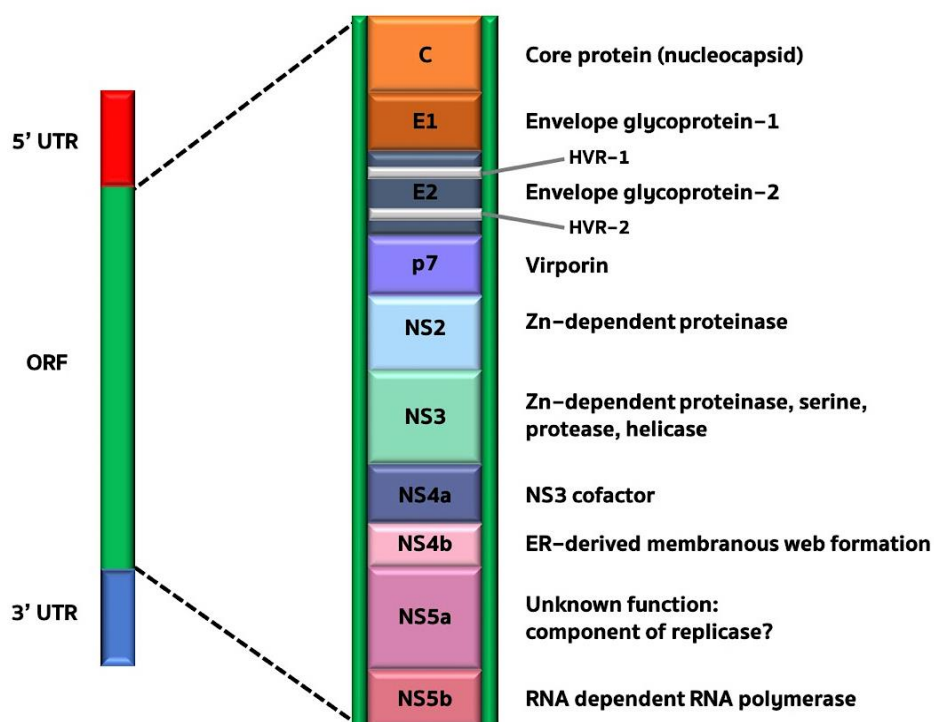


Figure 2.1 HCV genome and information in relation to viral polyproteins.

For the life cycle of HCV in liver cell, as illustrated in Figure 2.2 [3], beginning at viral attachment process that associates with apolipoproteins on the hepatitis C viral surface and the two types of structural protein (glycoproteins E1 and E2). Glycosaminoglycans and the low-density lipoprotein receptor (LDLR) appear to be related to the low-affinity of host cell binding initially. After that, HCV glycoproteins communicate with CD81 protein and scavenger receptor class B member 1 (SRB1), while claudin 1 and occludin are needed for cell entrance [37]. This HCV-receptor complex serves as an intermediate in uptake and determines species specificity. Subsequent to attachment, the HCV molecule accesses into the host cell via clathrin-mediated endocytosis, accompanied by merging between the viral vesicle and host

cytoplasmic membrane, which results in the penetration of the viral nucleocapsid into the cytoplasm. Uncoating of the HCV nucleocapsid can release the positive-sense of viral genome into the cytoplasmic matrix. This genomic RNA acts as messenger RNA (mRNA) to synthesize the various types of HCV polyprotein. The translational ORF region is encoded at the membrane of endoplasmic reticulum (ER), followed by the production of the four structural and the six non-structural viral proteins. Two common cellular peptidases of the host, such as signalase and signal peptide peptidase are essential with a role in the protein processing of HCV structural elements. In case of non-structural protein, peptidolysis during protein maturation is required at least a couple of viral enzymes (NS2 and NS3/4a). Then, the replication process is induced by the catalytic ability of NS5b protein and NS3 helicase, whereas NS4b is utilized as an integral membrane protein that plays an important factor in the formation of replication complex (also known as membranous web) that facilitates and insulates HCV replication. The positive-sense RNA employs as a template stand to generate an intermediate of negative polarity. Hereafter, negative-sense genomes become templates for the establishment of abundant positive-stranded genomes. These numerous positive-strands are subsequently exploited for the polyprotein synthesis, the reproduction of intermediates of replication and packaging into new virus particles [38]. MicroRNA-122 (miR-122) is a liver-specific microRNA for effective HCV replication and RNA stabilization. Finally, the viral assembly step is triggered by the cooperation of the genomic RNA, core and NS5a proteins in cytoplasmic membrane-enclosed vesicles. At the end-stage of viral particle formation, HCV lipoviroparticles are completely formed and released to the outside via a very-low-density lipoproteins (VLDL) production pathway [39].

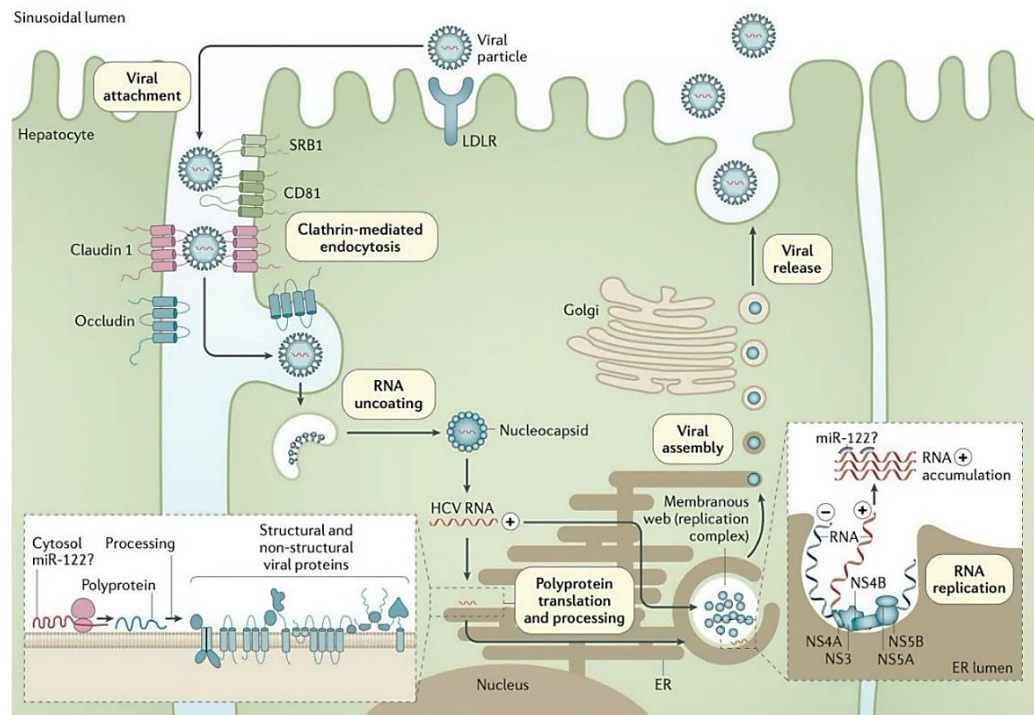


Figure 2.2 Schematic illustration of the intracellular life cycle of HCV [3].

2.2 Detection methods for HCV diagnosis

The traditional method for HCV identification for clinical purposes is demonstrated through the detection of three major types of analytes, namely HCV-specific antibodies (Anti-HCV), HCV Core antigen and RNA viral component. Throughout the last decade, both direct and indirect techniques have been developed to improve the sensitivity and specificity of these critical biomarker assays.

2.2.1 Anti-HCV assay

Since 1989, when the cloning of HCV genome was successfully generated by Choo *et al.* [40]. HCV infection has been primarily diagnosed using Enzyme-linked immunosorbent assays (ELISA). These immunologic methods relied on the observation of HCV-specific total antibodies (IgM and IgG) against multiple HCV antigens (Core, NS3, NS4 and NS5 viral proteins) in plasma or serum specimens. Currently, Anti-HCV assays can be fully automated and extensively applied in accredited laboratories [41]. Briefly, recombinant HCV

antigens are coated on microwells or other solid supports, for example, magnetic and paramagnetic particles. Then, controls and samples are incubated into the antigen-immobilized solid phases, followed by a washing step. The conjugate antibody, also known as mouse anti-human IgG labeled with horseradish peroxidase (HRP), is added to the microwells. After removing the unbound materials, a reagent solution containing a luminogenic substrate and electron transfer agent are dropped into the assay solution. The HRP in the bound conjugates will induce the oxidation of the substrate leading to the generating light from the chemiluminescent phenomenon as shown in Figure 2.3 [42]. Finally, the light signals are recorded by an automated optical system and normalized as relative light units (signal/cut-off ratio). For interpretation, patient's samples with a relative light unit of ≥ 1.00 are considered positive results. In addition, diverse POC technologies have been evolved to test for HCV antibodies outside of clinic settings [43]. Although these assays are simple, rapid, cost-effective and non-instrumented approaches for Anti-HCV detection, results from such methods should be interpreted carefully by trained personnel. The only commercial platform presently approved by the U.S. Food and Drug Administration (FDA) is the OraQuick HCV Rapid Antibody Test (OraSure technologies) [44]. This test is based on an indirect lateral flow immunoassay using three-types of HCV synthetic peptides, such as NS3, NS4 and Core proteins are tethered on the surface of nitrocellulose substrate. The reddish-purple line is directly visualized by protein-labeled gold nanoparticles in the existence of HCV antibodies.

Anti-HCV immunoassays are employed as indirect serological methods for effective screening of HCV exposure. However, Anti-HCV assays have several drawbacks [45], including: (1) the inability to distinguish active from resolved HCV infections; (2) the prolonged duration of the window period, approximately 45-68 days after acquiring infection [6]; (3) the occurrence of false-positive results from the non-specific adsorption of multiple circulating immunoglobulins that require additional confirmatory tests; and (4) the high

likelihood of false-negative results in immuno-suppressed patients after implantation with the human immunodeficiency virus (HIV) or those who are undergoing haemodialysis owing to detectable antibodies inadequacy.

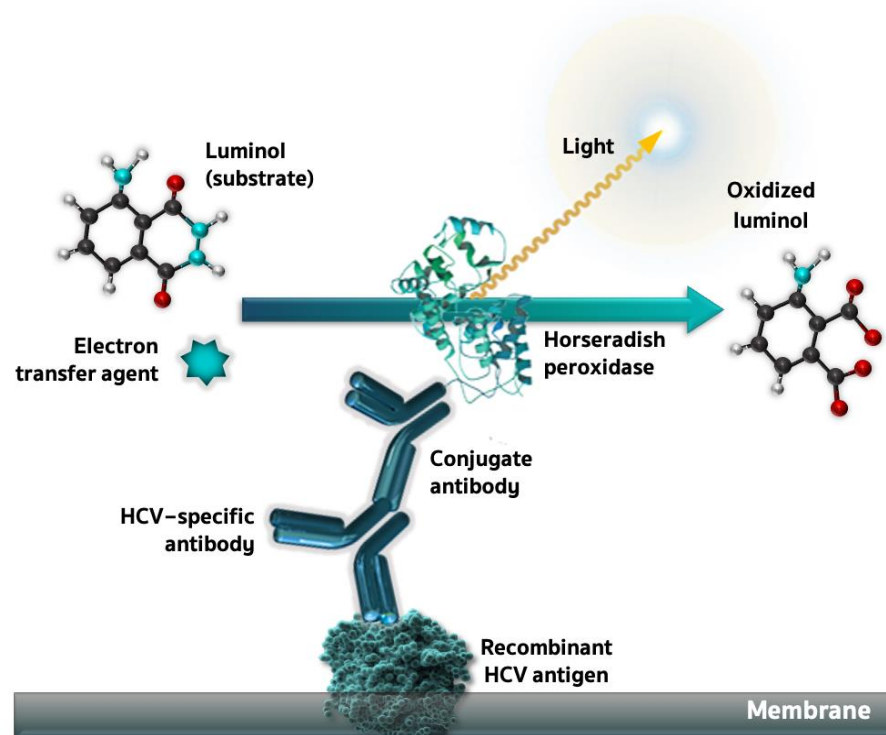


Figure 2.3 Chemiluminescence ELISA of the detection of HCV-specific antibody [42].

2.2.2 HCV Core antigen detection

The HCV Core antigen is a kind of HCV structural component that expressed on the nucleocapsid protein. This epitope also serves as a viral delegate of HCV replication. The HCV Core antigen levels can be observed and quantified in the blood of HCV-infected people, and its amounts are closely correlated with those of HCV RNA [46, 47]. One picogram of this antigenic determinant is equivalent to approximately 8,000 IU of HCV RNA [48]. The direct HCV diagnosis for detecting the Core antigen exhibits reasonable cost over HCV RNA assays and can be efficiently applied in resource-constrained settings. Consequently, they could be employed as an alternative way in the prognosis of HCV infection and treatment monitoring for five significant reasons: (1) the

ability to discriminate between active and resolved infections; (2) the HCV identification in the antibody window period [7, 49]; (3) the practical performance for the diagnosis in hemodialysis patients at great risk for HCV infection [50]; (4) the determination of the Core antigen could be utilized to control the antiviral response in chronically HCV-infected individuals [51]; and (5) The complicated and multiple of detection steps can be fully automated in the form of commercial assay (Abbott Architect HCV Ag testing). This sensitive technology for the quantitation of HCV Core antigen based on chemiluminescent microparticle immunoassay rely on specific interaction between the Core antigens and murine anti-HCV Core monoclonal antibodies that are coated onto paramagnetic particles. The acridinium-labeled anti-HCV conjugates act as secondary antibodies and light-generating sources in the assay solution. The chemiluminescent response is triggered by alkaline hydrogen peroxide and measured as relative light units (RTUs). This approach provides the detection limit of 0.06 pg/mL for the recombinant Core antigen of the HCV genotype 2a [7]. However, this analytical method is not sensitive enough to replace the RNA viral load assay according to the current clinical practice guidelines [8].

2.2.3 Molecular-based HCV assay

The molecular virological techniques for the HCV RNA identification make a significant contribution to several clinical needs. The highly sensitive molecular-based methods with a limit of detection < 50 IU/mL are exploited in both acute and chronic HCV diagnosis because HCV RNA can be observed in the serum before the appearance of HCV specific antibodies (within 1–3 weeks after infection) [9]. In addition, molecular assays are required to confirm the HCV infection in seronegative patients who are non-reactive with Anti-HCV [52]. Furthermore, HCV RNA testing is useful to guide and monitor the antiviral capability of medical treatment.

The standard molecular-based system for the quantification of HCV RNA is a real-time reverse transcription-polymerase chain reaction

(abbreviated to real-time RT-PCR) as reported by European and American guidelines [10]. This viral RNA test incorporates with viral genome extraction, complementary DNA (cDNA) production, PCR amplification and real-time detection of target DNA sequences, respectively. As mentioned earlier, the HCV genome is a single-stranded RNA. For that reason, reverse transcription is always a prerequisite for the quantitative PCR technology, which demands a DNA template. The highly conserved primer of 5' untranslated region (UTR) acts as the HCV RNA template for the production of a single-stranded cDNA by reverse transcriptase [53]. After that, multiples of double-stranded DNA copies are synthesized by DNA polymerase in PCR amplification. Due to detection and amplification of PCR amplicons have to be done simultaneously, a fluorescent probe (oligonucleotide labeled with a quencher and reporter molecule) attaches to target cDNA between the two PCR primers and is released by DNA polymerase during the production of cDNA. When the probe is degraded, it induces the discrimination of fluorescent reporter and quenching molecules, which results in the fluorescence emission from the reporter. The amount of PCR product is proportional to the amplification plot between the relative fluorescence unit (y-axis) and cycle number (x-axis). Quantification in absolute values is achieved by the correlation of amplification kinetics between target and internal control [54]. Although real-time RT-PCR presents a desirable sensitivity with broad dynamic range for the determination of HCV RNA in clinical samples, it has some limitations, for instance, long-time analysis, sophisticated technical equipment, high-cost reagents, dedicated laboratory areas, large sample volumes and requirement of skilled personnel for operation and result interpretation [11].

2.3 Paper-based analytical devices

To date, paper-based analytical devices (PADs) have received significant attention since their initial development by the Whiteside's group in 2007 [55]. PADs generally contain the defined pattern of the hydrophilic and hydrophobic regions on the paper substrate using various fabrication techniques, including wax printing, inkjet printing, flexographic printing, plasma etching, laser treatment, photolithography and chemical vapor-phase deposition [56]. Compared to conventional platforms using glass and polydimethylsiloxane (PDMS) materials, PADs have a multitude of benefits, such as lower cost, strong capillary force, excellent biological compatibility, portable, easy-to-manipulate, straight-forward fabrication process, and can be miniaturized. Various types of paper-based materials can be used as a PADs substrate, e.g., cellulose chromatographic paper, graphite paper, and glass fiber paper [57-59]. Among these materials, the cellulose-based paper has gained considerable interest because of its cost-effectiveness. Additionally, it can be functionalized for applying in the immobilization of various probes [60]. There are seven common analytical methods that can be utilized in combination with PADs for sensitivity enhancement [61], namely colorimetry, fluorescence, chemiluminescence, electrochemiluminescence, electrochemistry, photoelectrochemistry, nanoparticle detection and surface-enhanced Raman spectroscopy. As a result, PADs have been widely used for applications in the pharmaceutical analysis, environmental monitoring, clinical diagnosis, food manufacture and chemical industry fields [62-66]. Given the advantages mentioned above, this sensing platform provides high-performance in term of diagnostic tool for point-of-care purposes in the low and middle-income regions where they face the challenges of constrained resources and the rising number of patient visits.

2.4 Fluorescence-based detection

Fluorescence is another kind of luminescence phenomenon in which the molecular absorption of electromagnetic energy induces the rapid emission in the form of photons with a longer wavelength. The production of fluorescence in a generic molecule can be illustrated in the Perrin–Jablonski diagram as presented in Figure 2.4 [67]. The unique molecules (fluorochrome) is originally stable at the lowest (ground) electronic state (S_0). After absorbing a photon with a certain energy, the fluorochrome is excited to the given vibrational level of the first (S_1) or second excited state (S_2). The excited molecule has a short lifetime (typically 1–10 nanoseconds) and will easily come back to the ground state by releasing the surplus energy along the way as fluorescent radiation and non-radiative relaxation. Due to the energy lost through various processes, such as collisional quenching, internal conversion and intersystem crossing, the energy of an emitted photon is decreased which results in a longer wavelength than the excitation photon. The inequality of wavelength between fluorescence emission and excitation source is called Stokes' shift. This characteristic shift manages to isolate fluorescence from excitation photons which leads to a low background signal in fluorescence-based detection.

Presently, many sensing platforms of fluorescent detection coupled with PADs have been exploited to detect abundant pathogenic bacteria and disease biomarkers [20-24]. Emitting fluorescence is an important aspect to the development of PADs, whether detecting the mere presence/absence of target species or quantifying the amounts of analytes. The fluorescent biosensor exhibits a high sensitivity and selectivity resulting from characteristic Stokes' shift and spectral bandwidth. Moreover, the paper-based fluorogenic devices require a simple operation process and little amount of sample and reagent [68]. Additionally, the smartphone camera can be employed as a detector to take the digital image of fluorescent platform under illumination of UV light. The pixels of a spectral image are subsequently converted into their RGB value

or the other mode of color intensity for determining fluorescence intensity. Accordingly, the smartphone-based detection integrated with fluorogenic PADs leads to the evolution of promising strategies for point-of-care applications offering the benefits of portability, simplicity, user-friendly design and rapid data transmission [69-73]. For example, Rong *et al.* [73] presented the combination of fluorescent lateral flow immunoassay (LFIA) and smartphone-based platform for the highly sensitive determination of Zika virus nonstructural protein 1 (ZIKV NS1) as depicted in Figure 2.5. This assay utilized quantum dot microspheres as fluorescent probes to obtain bright red color under UV radiation. The proposed fluorescent LFIA provided the rapid and inexpensive determination of ZIKV NS1 with a detection limit of 0.15 ng/mL in human serum samples.

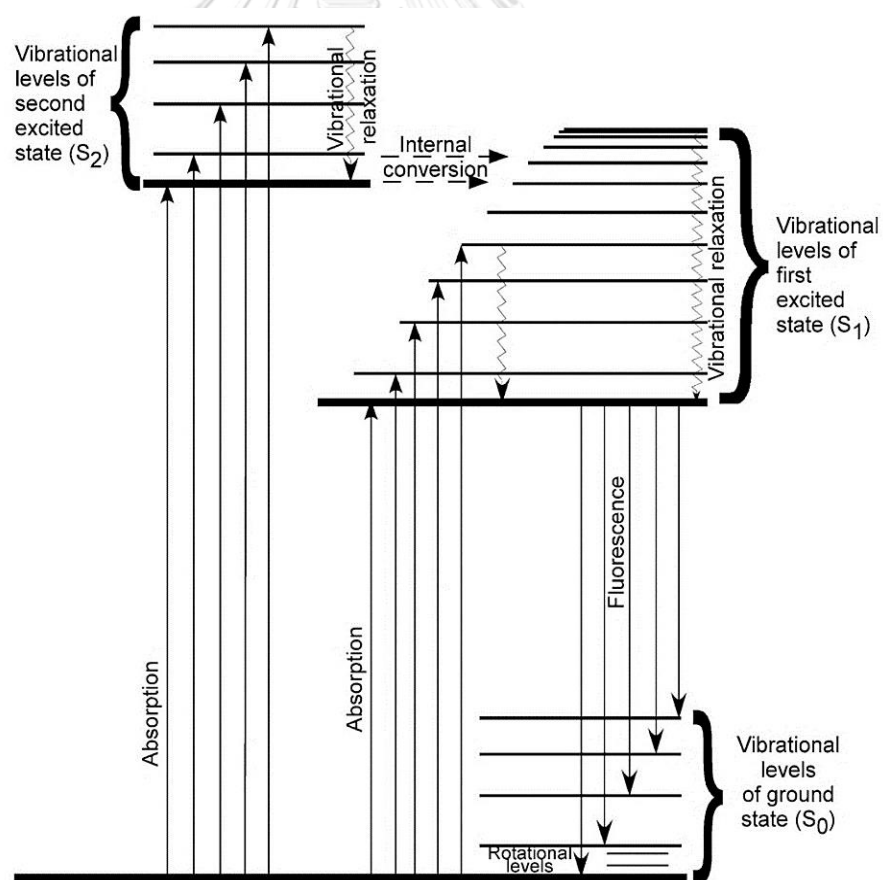


Figure 2.4 Perrin-Jablonski diagram illustrating electronic states and transition related to the generation of fluorescence [67].

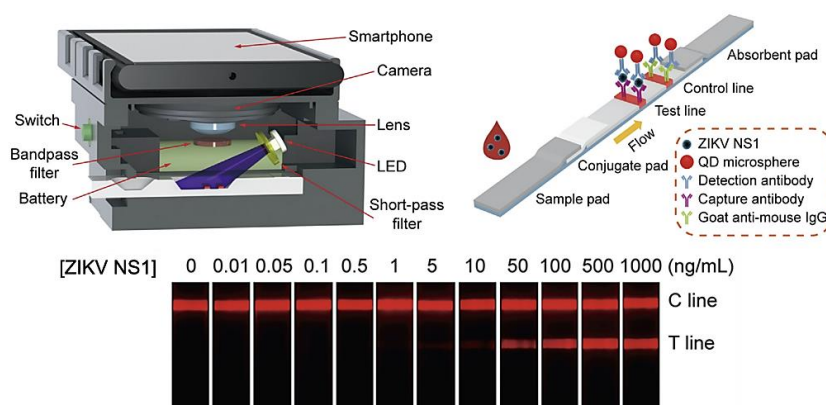


Figure 2.5 Overview of the point-of-care detection of ZIKV NS1 using the novel smartphone-based fluorescent LFIA platform [73].

2.5 Peptide nucleic acid

Peptide nucleic acids (PNA) are the most intriguing class of synthetic oligonucleotide-analog models which are constructed from entirely replacing the sugar-phosphate structure in natural nucleic acids with an uncharged pseudopeptide backbone. In 1991, Nielsen *et al.* [74] initiated the primitive PNA molecule which possessed an *N*-2-aminoethylglycine scaffold (designated as aegPNA). This distinct DNA-mimics exhibit the highly specific affinity between two complementary nucleobases (A-T, C-G) via the predictable Watson-Crick base-pairing. In particular, aegPNA presents an even stronger affinity and better identification between complementary and mismatched sequence targets than natural DNA probes [25, 26]. The electrostatically neutral peptide-mimic structure of PNA is responsible for desirable advantages not recognized in other systems of nucleic acid mimics with negatively charged phosphate backbones. These include the unusually outstanding stability over ionic strength variations of the solvents [27] as well as the relative insensitivity of DNA-PNA or RNA-PNA hybrids toward enzymatic degradation in biological environment [28]. However, the uncharged nature of aegPNA causes some inherent weaknesses, including a relatively low solubility in aqueous media, the non-specific binding on hydrophobic surfaces and the tendency to form self-aggregation [75, 76].

The backbone modification of original PNA leads to the establishment of new PNAs having improved various properties and functionalities (Figure 2.6) [29]. In 2004, Pokorski *et al.* [77] incorporated the (*S,S*)-*trans*-cyclopentane diamine units into the *N*-2-aminoethylglycine backbone as a result of the improvement of thermal stability and sequence specificity to complementary DNA. On the contrary, Govindaraju *et al.* [78] designed *cis*-aminocyclohexylglycyl PNA by the stereospecific imposition of aegPNA with the 1,2-*cis*-cyclohexyl moieties. This preorganized PNA showed selective binding with RNA over DNA targets. Moreover, structural preorganization arising from a substitution of L-serine at γ -position (C^γ) in Nielsen's PNA considerably increases its binding affinity [79]. Additionally, the water solubility of PNA can be enhanced by attachment C^γ with a hydrophilic (*R*)-diethylene glycol unit [80]. Several functional moieties can also be placed at γ side chain to facilitate cell permeability, such as a guanidinium group, ethyleneamine, ethyleneguanidine, azidomethylene and azidobutylene [81-83].

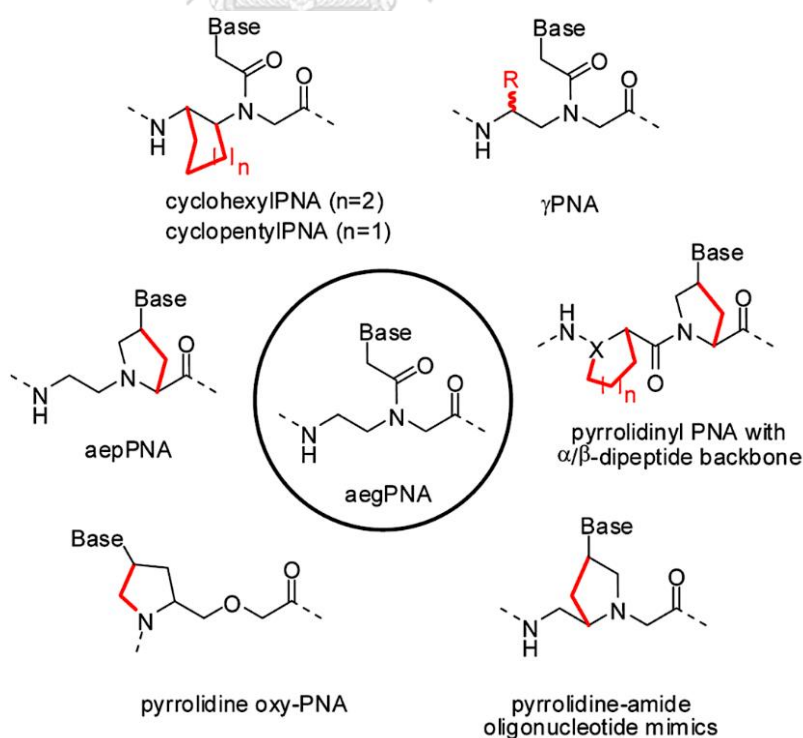


Figure 2.6 Examples of preorganized constrained aegPNA systems [29].

On account of well-defined stereochemistries of proline derivative, the modern design of PNAs have extensively utilized the pyrrolidine ring as a constraint backbone. In 1996, Lowe *et al.* [84] firstly proposed a solid phase method for pyrrolidine-containing PNA synthesis. This configurationally constrained PNA composes of nucleobase-modified prolines in a dipeptide backbone. After that, Vilaivan group [29] introduced a new family of conformationally pyrrolidinyl PNA having a D-prolyl-2-aminocyclopentanecarboxylic acid (acpc) backbone (Figure 2.7). The duplex formation between acpcPNA and complementary DNA dictated favorable affinity and remarkable mismatch discrimination over the well-established PNA. It also hybridizes to RNA with a high specific sequence in spite of lower affinity than target DNA. Additional characteristics include the preference for forming only antiparallel hybrids with DNA and a low propensity for self-pairing. Furthermore, acpcPNA can directly bind to double stranded DNA via a double duplex invasion or triplex formation without sequence-related limitations. These properties of acpcPNA make its potential as a promising probe for targeting structured nucleic acid targets.

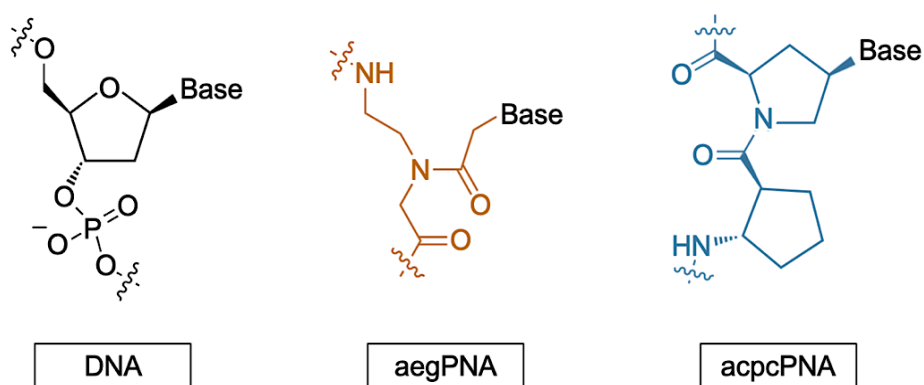


Figure 2.7 General structure of DNA and selected PNA molecules.

Throughout the last two decades, abundant acpc-based detection platforms have been developed for specific DNA sequencing. For instance, Ananthanawat *et al.* [85] synthesized the thiolated-modified acpcPNA that was used as a DNA probe on gold-coated piezoelectric quartz crystal. DNA hybridization on the probe-immobilized platform was determined by quartz crystal microbalance (QCM) with a detection limit of 5 μM . Then, the same group suggested the label-free method to improve the detection efficiency of their previous research. This method provided the lowest concentration of target DNA at 0.2 μM using surface plasmon resonance (SPR) technique [86].

In 2012, Thipmanee *et al.* [87] reported the non-labeling approach for DNA sequencing using capacitance detection of acpcPNA-immobilized gold electrode. The immobilization process of C-terminal lysine-modified acpcPNA relied on alkanethiol self-assembled monolayers (SAMs). The modified acpcPNA electrode gave a relatively low detection limit in the range of picomolar.

Afterward, Jampasa *et al.* [88] proposed a selective biosensor for the quantification of human papillomavirus (HPV) DNA type 16. This sensor utilized the voltammetric response of anthraquinone-labeled acpcPNA probe that immobilized on a screen-printed carbon electrode. The electrochemical DNA sensor exhibited a desirable sensitivity with LOD as low as 4×10^{-9} M.

In 2015, Jirakittiwut *et al.* [30] demonstrated a cellulose-based model (Figure 2.8) for the investigation of target oligonucleotides by using specific properties of acpcPNA that was covalently immobilized onto partially oxidized cellulose paper combined with the visual detection of cationic dye (Azure A) staining via photography. This useful model offers numerous advantages, including straightforward signal-reading, ease-of-use, portable, sample-saving and low-cost. At the optimal condition, the lowest concentration of complementary DNA that produced distinguishable color intensity from the background was found to be 200×10^{-9} M.

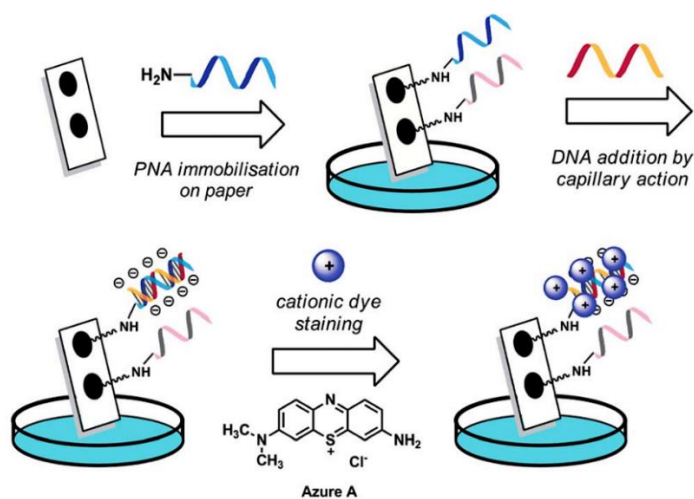


Figure 2.8 The fabrication of the paper-based sensor by immobilizing acpcPNA onto filter paper and the detection of target DNA by cationic dye staining [30].

In 2017, Teengam *et al.* [89] introduced a multiplex paper-based sensor for colorimetric detection of three different kind of oligonucleotides, including HPV type 16, *Mycobacterium tuberculosis* (MTB) and Middle East respiratory syndrome coronavirus (MERS-CoV). The proposed assay depended on the aggregation and deaggregation of citrate anion-stabilized silver nanoparticle (AgNPs) induced by acpcPNA probes on a cellulose-based substrate. In this sensing platform, a single positively-charged moiety was incorporated at C-terminus of acpcPNA and caused aggregation of AgNPs in the absence of DNA targets. In the occurrence of complementary DNA, the hybridization between acpcPNA probes and anionic DNA strands generated deaggregation of AgNPs resulting in the detectable color change. The colorimetric PAD enabled a detection limit of 1.03, 1.27 and 1.53×10^{-9} M for DNA detection of HPV type 16, MTB and MER-CoV, respectively.

Thereafter, Jampasa *et al.* [90] developed a signal-on electrochemical platform for the simultaneous determination of HPV DNA type 16 (SiHa) and 18 (HeLa). A new DNA sensor design based on a sandwich-hybridization among two types of acpcPNA probes and target sequence. The unlabeled-acpcPNA that bounded on a screen-printed carbon electrode employed as a capture probe,

whereas an acpcPNA probe labeled with an anthraquinone moiety used as a signaling element for electrochemical measurement. The detection limits were found to be 150 (HPV type 16) and 153×10^{-9} M (HPV type 18). Moreover, this proposed sensor was successfully applied to identify the two high-risk HPV DNA sequences in a PCR product from positive human cancer lines.

Next, Teengam's group [31] illustrated a novel paper-based electrochemical sensor for label-free detection of MTB. The unlabeled-acpcPNA probes were directly tethered onto the aldehyde-modified cellulose paper providing the regeneration by PAD replacement. The synthetic oligonucleotides of MTB can be quantified by measuring charge transfer resistance of ferri/ferrocyanide redox couple using electrochemical impedance spectroscopy (EIS), and limit of detection was found to be 1.24×10^{-9} M.

Lately, Srisomwat *et al.* [32] designed a pop-up origami-based electrochemical sensor for label-free hepatitis B virus (HBV) DNA detection. The modified acpcPNA with a lysine moiety at the C-terminus was chemically immobilized onto the cellulose substrate and used as a probe to hybridize with target HBV DNA. In the presence of HBV DNA, the decrease of the electrochemical response of $[\text{Fe}(\text{CN})_6]^{3-/2-}$ was observed by differential pulse voltammetry. The novel pop-up DNA device demonstrated noticeable performance for sensitive HBV DNA detection with the detection limit at a low picomolar level. Besides, the proposed 3D sensor can be identified HBV DNA level in the range of 10^2 – 10^4 copies/ μL in DNA extracted from plasmid constructs.

According to these applications, specific acpcPNA probes serve as the key aspect to improve the performance of plentiful DNA detection methods. Various analytical approaches can be combined with acpcPNA to obtain acceptable sensitivity. Additionally, acpcPNA-based biosensor integrated with PADs has the potential to be a preferred platform for detecting and screening in infectious diagnostics.

2.6 ssDNA-binding fluorescent dye

As the majority of natural biomolecules cannot provide the fluorescence response, the observation of non-fluorescent substances using a fluorescence-based assay can be achieved with the aid of fluorescence probes, such as fluorescent dyes, quantum dots, carbon dots, upconversion nanoparticles and metal nanoclusters [69]. In these classes of fluorescent materials, fluorescent dyes have been frequently utilized as signaling agents in the paper-based sensor because of its small size, easy surface modifications, good biocompatibility and high fluorescence intensity [91, 92].

Numerous commercial fluorescent dyes have been developed for various biochemical assays especially the quantification of single-stranded DNA (ssDNA) [93], for example, Quant-iT™ Oligreen, QuantiFluor® ssDNA and Qubit® ssDNA dyes. These ssDNA-binding fluorescent dyes can be used with a common spectrofluorometer or may be scaled up for measurement in a microplate reader at the suitable excitation and emission wavelengths. The typical binding of fluorescent dye with ssDNA is invoked by electrostatic interaction between the cationic moiety of dye and negatively-charged of phosphate backbone. Also, the dye stacking between two adjacent bases on the oligonucleotide strand could be another factor associated with the binding interaction [94]. The fluorescent-based detection using commercial ssDNA-binding dye exhibits rapid detection at the low amount of ssDNA in purified samples with a widely detectable range as shown in Figure 2.9 [93]. Moreover, the common contaminants that are found in nucleic acid preparation, including salts, ethanol, chloroform, urea, detergents, protein and agarose are well tolerated in the assay solution [95].

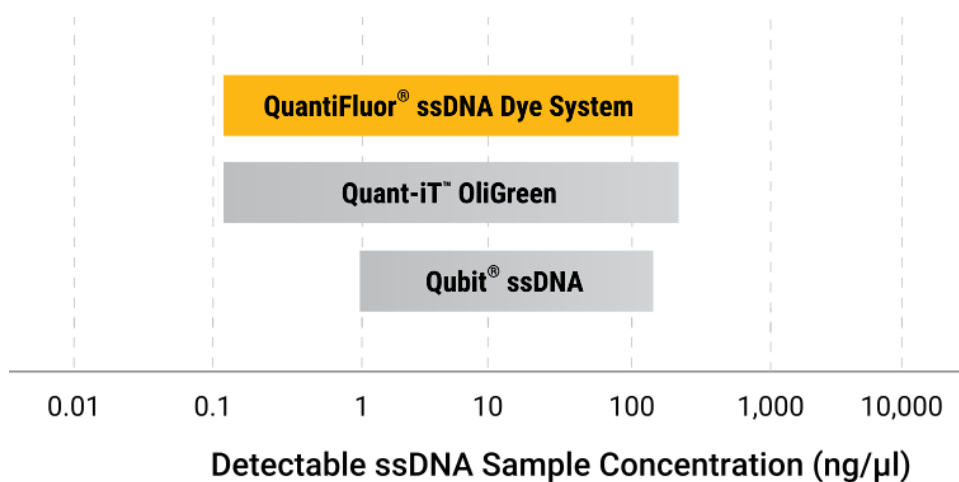


Figure 2.9 Detectable ranges of commercial ssDNA-binding fluorescent dyes [93].

2.7 Fourier transform infrared spectroscopy

Fourier transform infrared spectroscopy (FT-IR) is a powerful method for chemical characterization and structure elucidation in many kinds of samples, including organic powders, polymers, biological materials, free-flowing aqueous solutions, viscous liquids and gases [96]. In FT-IR analysis, Infrared radiation travels through a sample and can be partially absorbed at specific frequencies by molecular vibration of the sample's constituents. The FT-IR interferometer with a moving mirror obtains the IR spectrum by Fourier transformation of the infrared interferogram. The resulting spectrum commonly presents in a plot of IR transmittance (or absorbance) on the vertical axis versus frequency in a unit of cm^{-1} (known as wavenumber) on the horizontal axis. In the IR region with higher wavenumber than 1500 cm^{-1} , various characteristic bands can be observed to identify chemical composition and bonding arrangement as shown in Figure 2.10.

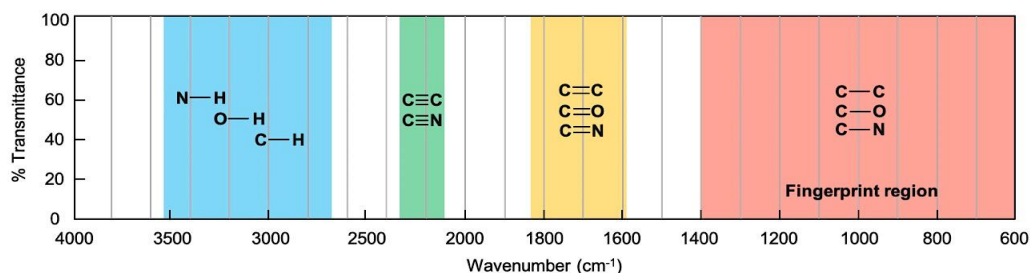


Figure 2.10 Simplified chart of IR stretching frequencies regarding functional groups.

Recently, the novel spectrometer with attenuated total reflection (ATR) mode is constructed for revolutionized FT-IR measurement. For this approach, a single crystal with a high refractive index, e.g., diamond, zinc selenide or germanium is used as a special probe to contact the sample. A beam of IR radiation penetrates the ATR crystal and totally reflects within the inner surface of the ATR probe, resulting in an evanescent wave that passes through the sample surface with a few micrometers penetration depth (d_p) as depicted in Figure 2.11 [97]. Then, the transmitted beam is recorded when it exits the crystal probe for FT-IR analysis. The increased signal-to-noise ratio of ATR-FT-IR offers better sensitivity than the conventional FT-IR method. Thus, FT-IR analysis with ATR accessory has significantly recognized as a practical tool for the characterization of paper-based substrates and other solid platforms [98, 99] with the simplicity of sample preparation.

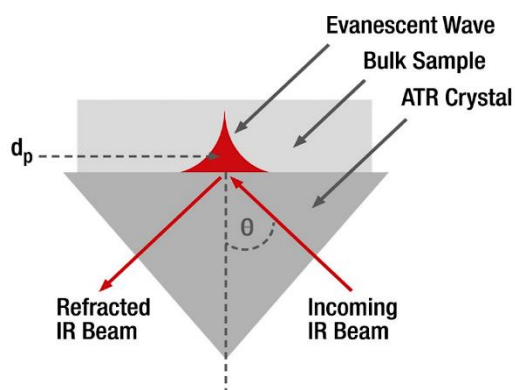


Figure 2.11 Evanescent wave as a result of attenuated total reflection [97].

2.8 X-ray photoelectron spectroscopy

X-ray photoelectron spectroscopy (XPS), also used as an alternate word for electron spectroscopy for chemical analysis (ESCA), is another type of the non-destructive methods for surface characterization of solid material. XPS obtain much useful information associated with surface chemistry, including the chemical constitution, empirical formula, chemical state and electronic state of the elements within the surface of defined material. For XPS measurement, X-ray radiation with a constant energy ($h\nu$) in an ultrahigh vacuum system (generally better than 10^{-7} pascal) is irradiated to the sample for producing photoelectrons as displayed in Figure 2.12. The photoelectrons are ejected from the top layer approximately 1–10 nm of the material surface with characteristic kinetic energy (KE) depending upon the incident energy of X-ray photon and the binding energy (BE) of the inner electron to the atom's nucleus. The BE values can be calculated from the XPS instrument by the simple equation; $BE = h\nu - KE$. By capturing and analyzing the KE of the emitted electrons, it can demonstrate XPS spectrum that exhibits the relationship between the signal intensity (y-axis) connected to the amount of measured photoelectron and the BE in a unit of electron volt (x-axis). The peaks or bands which appear at different positions in XPS spectrum involve the kinds of element and orbital from which the photoelectron is generated, and they also connect to the chemical environment of the atom from which the electron is ejected. Apart from qualitative identification of elements, XPS can achieve semi-quantitative analysis in the form of the relative amount of the constituents in the surface region. Additionally, XPS analysis shows the high performance to detect light elements, such as carbon, nitrogen and oxygen which cannot be observed in the spectrum of X-ray fluorescence spectroscopy (XRF) that has been regularly used for elemental identification in scanning electron microscopy (SEM) [100]. Consequently, XPS could be employed as the adventurous tool for surface-sensitive detection which allows probing the

element composition and chemical state of paper-based biosensor and other biomolecule-modified substrates.

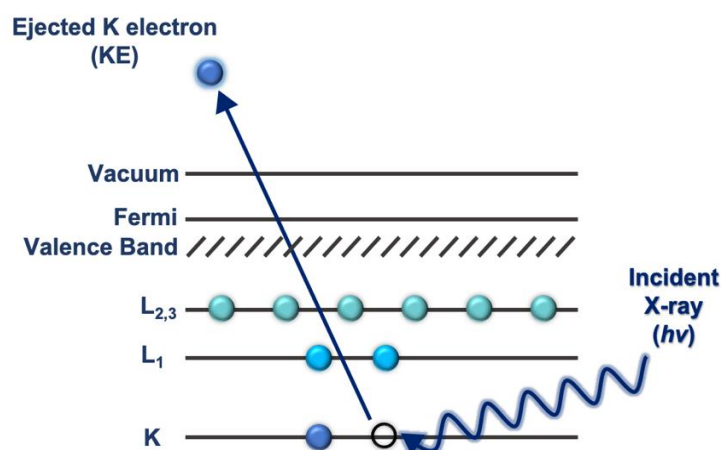


Figure 2.12 The photoemission process of K (1s) photoelectron related to XPS analysis. The circles represent electrons and the bars stand for energy level within the material being measured.

2.9 Literature review

The diagnostic strategy for HCV DNA identification has been extensively established and applied to the clinical setting. By focusing on the strategy for point-of-need applications, various research groups have proposed a number of alternative approaches to investigate HCV DNA particularly electrochemical detection. The details of each work are explained below.

Liu *et al.* [12] presented an electrochemical molecular assay for both qualitative and quantitative measurements of HCV DNA. They utilized the thiolated-modified oligonucleotides labeled with thionine as DNA probes which were immobilized on the surface of a gold electrode via Au-S bonding. After hybridization with complementary DNA, BamHI endonuclease was added into the assay solution for inducing the site-specific cleavage of DNA hybrid. The voltammetric signal of thionine decreased with the increasing concentration of HCV DNA after enzymatic digestion. The obtained results indicated that the

proposed method can be applied to quantify HCV DNA (21-base sequences were produced by RT-PCR) in serum samples and the limit of detection was found to be 0.02 μM .

In 2011, the previous model of DNA-BamHI endonuclease was developed to improve the detection limit for the determination of HCV DNA. The synthetic thiol-capped DNA probe assembled on the *p*-aminobenzoic acid (ABA)-modified glassy carbon (GC) electrode through forming a carbon-nitrogen linkage between the carboxylic group of ABA and the amine moiety at the 3'-terminus of DNA probe. This assay reported the use of specific cleavage by BamHI nuclease incorporated with gold enhancement to improve the sensitivity of HCV DNA quantification. On the basis of detection (Figure 2.13) [13], the variation of electrochemical response of thionine that attached to the 5'-terminus of the specific probe was measured by differential pulse voltammetry for both before and after the enzymatic digestion of duplex target. The developed system showed the outstanding sensitivity for selective identification of HCV DNA genotype 1b (244 mer) with a detection limit as low as 3.1×10^{-22} M in the clinical environment.

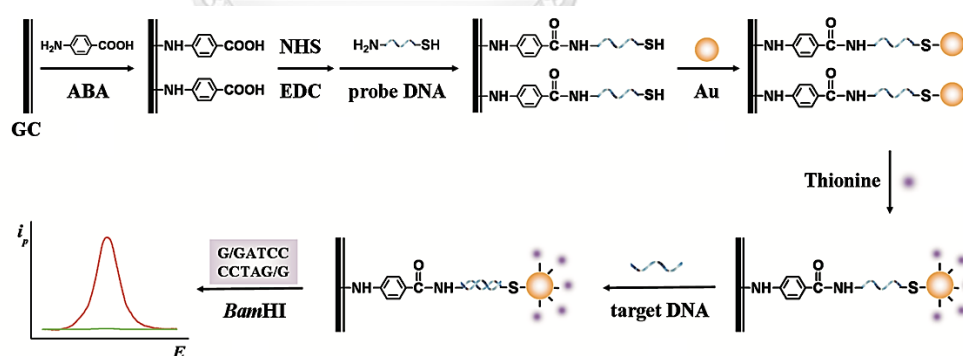


Figure 2.13 The basis of detection procedures in the developed electrochemical assay for the selective determination of HCV DNA [13].

Donmez *et al.* [14] established a cost-effective and disposable biosensor for the label-free detection of HCV DNA genotype 1a for the first time. The nucleic acid biosensor was prepared by utilizing the electropolymerization of poly(L-glutamic acid) on pencil graphite electrode (PGE), followed by covalent immobilization with inosine-substituted 20-mer probes. In their approach, the peak current from the oxidation of guanine was measured by square wave voltammetry to examine the hybridization event of the probe with the complementary target DNA onto the PGE-modified biosensor. Under the optimal condition, a detectable range from 50×10^{-9} M to 1.0×10^{-6} M with a desirable detection limit of 40.6×10^{-9} M was achieved.

Singhal *et al.* [15] fabricated a novel impedimetric DNA-based platform for the non-labeling quantitation of HCV genotype 1 in human serum. Unlabeled-ssDNA probes were physically anchored on a fluorine-doped tin oxide (SnO_2/F) electrode which was earlier incubated with methylene blue (MB) doped silica nanoparticles (SiNPs). The MB in the immunosensor served as an electrochemical indicator while SiNPs were used to facilitate signal amplification. Upon incubation with target DNA, the change in charge transfer resistance (ΔR_{ct}) of modified electrode related to the logarithmic concentration of target HCV DNA was obtained by electrochemical impedance spectroscopy. The renewable impedimetric biosensor enabled an excellent linear relationship in the range of 10^2 – 10^6 copies/mL, and the limit of detection was 90 copies/mL in patient serum samples.

Lereau *et al.* [16] prepared the state-of-the-art polythiolated oligonucleotides for application in rapid HCV genotyping. The polythiolated probes were employed as recognition elements that were compatible with the electrochemical biosensor and optical enzyme-linked oligosorbent assay (ELOSA). Innovative polythiolated probes were tethered with good strength to use as specific DNA probes on both gold electrodes and on maleimide-activated microplates (MAM). In the electrochemical assay, multiple electroactive ferrocene moieties were capped at the 3'-terminus of

polythiolated probes. Differential pulse voltammetry was operated for real-time electrochemical detection of HCV amplicons with a detection limit as low as 10×10^{-15} M. In addition, the high throughput assay by ELOSA test enabled a detection limit of 10×10^{-9} M to be reached with remarkable sensitivity and selectivity for HCV diagnosis in human plasma.

As reported by these literature surveys, while electrochemical detection merged with various biosensor obtain extremely high sensitivity with a noticeable detection limit for specific HCV DNA monitoring, this approach still has obvious limitations, including the complicated-steps of electrode preparation and requirement of the elaborate instrument and infrastructure. Hence it is not convenient to utilize as POCT system for clinical HCV diagnosis.

To overcome the drawbacks of the aforementioned techniques, fluorescence-based detection is a promising way to develop the easy-to-handle and sensitive DNA sensor for selective determination of HCV DNA. From the literature survey, there is only one publication reported by Zeng *et al.* [19] that suggests the utilize of the fluorescent sensor for HCV quantification. In their work, a triple-helix DNA structure of a nucleic acid fluorescence resonance energy transfer (naFRET) system which composed of one-donor (FAM-labelled hairpin structure) and multiple-acceptors (BHQ-1-labelled ssDNA strands) assembly was designed (Figure 2.14). The demonstrated fluorescent probe exhibits the high fluorescent intensity with low background signal for the investigation of HCV DNA in real serum samples. At optimized condition, the limit of detection was determined to be 24.6×10^{-9} M. However, this naFRET system still require a large volume of sample and high-cost reagent to obtain the sufficient fluorescent signal from spectrofluorometer.

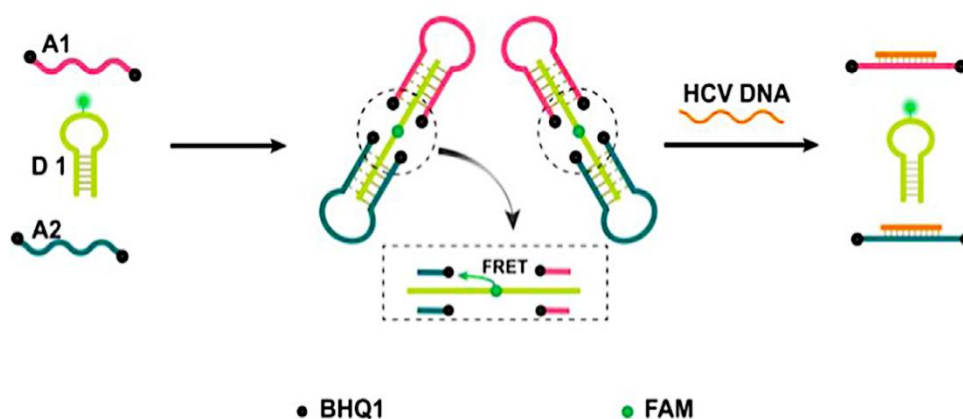


Figure 2.14 Schematic illustration of HCV DNA detection by naFRET probe [19].

To solve the mentioned problem of conventional fluorescence technique, the miniaturization of fluorescent detection in the form of fluorogenic PADs is an interesting strategy for the observation of HCV DNA in the constrained resources. Additionally, this small system can be combined with smartphone-based detection to serve as an economical, portable and rapid diagnostic tool in developing countries. From the literature review, there are some research groups which suggested the fluorogenic PADs for the evaluation of target DNA as shown below

Noor *et al.* [70] exhibited solid-phase assay of DNA hybridization on paper-based substrate using a FRET mechanism combined with camera-based ratiometric transduction. The conjugates of quantum dots and specific oligonucleotide probes were chemically tethered on the surface of imidazole-modified paper. Hybridization between the immobilized probe and the Cy3-labeled oligonucleotide target provided the significant change of fluorescent signal in digital images as shown in Figure 2.15. This assay afforded a detection limit of 300×10^{-15} mole without any amplification steps.

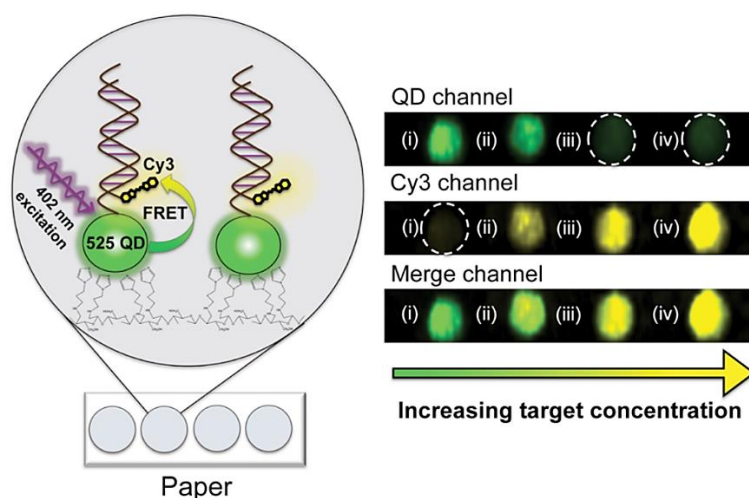


Figure 2.15 Overview of the solid-phase assay for DNA detection using immobilized quantum dots as donors in FRET (left). Pseudocolor epifluorescence images generated using the multiple imaging channel (right) [70].

Yang et al. [71] designed paper-origami DNA microfluidics integrated with Loop mediated isothermal amplification (LAMP) for the multiplex diagnosis of three pathogens (*Leptospira*, *Brucella* and BoHV-1) that cause bovine reproductive diseases. In the presence of the target genomic DNA, the positive result was detected as a green fluorescent response using either naked-eyes detection or smartphone-based detection combined with hand-held UV flashlight (365 nm). The LOD for *Leptospira*, *Brucella* and BoHV-1 in semen samples were evaluated to be 50 organisms, 50 colony forming units (CFU) and 1 TCID₅₀, respectively.

Based on the above literature reviews, there is no report for the utilization of fluorogenic PADs as the detection method to observe HCV DNA in clinical sample. To address the challenge, the ease-of-use, rapid-response and cost-effective DNA sensor using acpcPNA as a recognition probe onto functionalized-cellulose material combined with fluorescence-based detection was developed. Moreover, this recent work also concentrates on the use of a smartphone camera to develop the point-of-care system for screening of HCV DNA.

CHAPTER III

EXPERIMENT

This chapter provides the detail of chemicals and reagents used in this work as well as the preparation of all working solutions. The sensor fabrication, detection methodology, instrument operation and sample preparation for real sample analysis are also described.

3.1 Instrument and apparatus

The instrument including detection device which used in all experiments are listed in Table 3.1.

Table 3.1 List of instruments and apparatus.

Instruments and apparatus	Suppliers
Analytical balance, ME204	Mettler Toledo, Switzerland
Autopipette	Eppendorf, Germany
Centrifuge tubes	Plusmed, Thailand
Fluorescence spectrophotometer, Cary Eclipse	Agilent, United states
Fluorescent camera for smartphone	EOSCE, Thailand
FT-IR spectrophotometer, Nicolet iS50	Thermo Fisher Scientific, USA
Hot air oven	Memmert, USA
Hotplate stirrer, C MAG HS 7	IKA, Germany

Instruments and apparatus	Suppliers
iPhone SE, 32 GB	Apple, USA
Matrix-assisted laser desorption ionization time-of-flight (MALDI-TOF) mass spectrometer, Microflex series	Bruker Daltonik GmbH, Germany
Microcentrifuge tubes	Axygen scientific, USA
Micro fluorescence cuvette (700 μ L), CV10Q700FS	Thorlabs, United states
Millipore Milli-Q water system	Merck Millipore, USA
Reverse-phase (C-18) high performance liquid chromatography (HPLC), Water Delta 600 pump system equipped with Water 996 photodiode array detector	GenTech Scientific, USA
Ultrasonic sonicator, IL 60061	Elma, German
Universal pipette tips	Plusmed, Thailand
Volumetric flask and other glassware	SCHOTT, Germany
Vortex mixer	Scientific industries, United states
Wax printer, ColorQube 8570	Fuji Xerox, Japan
X-ray photoelectron spectrometer, Axis ultra DLD	Kratos, Unites states

3.2 Chemicals and reagents

All analytical grade chemicals and reagents utilized in this research were handled without further purification. The list of chemicals and reagents are shown in Table 3.2. The sequences of synthetic oligonucleotides used throughout the experiment are listed in Table 3.3. The HCV DNA sequences were designed according to the previous report [16].

Table 3.2 List of chemicals and reagents.

Chemicals and reagents	Suppliers
Acetonitrile (ACN)	Merck, Germany
acpcPNA probe	Vilaivan's group, Thailand
Ethanol (Absolute for analysis)	Merck, Germany
Lithium chloride (LiCl)	Wako Pure Chemicals, Japan
<i>N,N</i> -dimethylformamide (DMF)	Merck, Germany
Phosphate buffered saline (PBS) tablet pH 7.4	Sigma–Aldrich, USA
Sodium cyanoborohydride (NaBH ₃ CN)	Acros Organics, USA
Sodium periodate (NaIO ₄)	CARLO ERBA Reagents, Italy
ssDNA-binding fluorescent dye, QuantiFluor [®] ssDNA System	Promega Corporation, USA
Synthetic oligonucleotides	Pacific Science, Thailand
Tween-20, Polysorbate 20	Glentham Life Sciences, USA
Whatman chromatography paper No. 1	Sigma–Aldrich, USA

Table 3.3 List of synthetic oligonucleotides.

Synthetic oligonucleotide	Sequences (5'→3')
Complementary HCV DNA (25 nucleotides)	<u>GCTCCGGGACTGCACCATGCTCGTG</u>
Complementary HCV DNA (35 nucleotides)	<u>GCTCCGGGACTGCACCATGCTCGTGTGTGG</u> CGACG
Complementary HCV DNA (45 nucleotides)	<u>GCTCCGGGACTGCACCATGCTCGTGTGTGG</u> CGACGACTTAGTCGT
Complementary HCV DNA (55 nucleotides)	<u>GCTCCGGGACTGCACCATGCTCGTGTGTGG</u> CGACGACTTAGTCGTTATCTGTGAA
Non-complementary DNA (45 nucleotides)	<u>ATGTTAAACTGATCT</u> CATGCTCGTGTGTGGC GACGACTTAGTCGT
Single-base-mismatch (45 nucleotides)	<u>GCTCCGGC</u> ACTGCACCATGCTCGTGTGTGG CGACGACTTAGTCGT
Two-base-mismatch (45 nucleotides)	<u>GCTCTGGGACTCC</u> ACCATGCTCGTGTGTGGC GACGACTTAGTCGT

- Underline letters represent the expected binding region of synthetic nucleotides with acpcPNA probe.

- Red letters represent base mismatch in complementary HCV DNA (45 nucleotides).

3.3 Chemicals and reagents preparation

3.3.1 Synthesis and purification of acpcPNA probe

The conformationally constrained acpcPNA used in this research was designed for specific binding with HCV DNA [16]. The acpcPNA probe with a sequence of GTGCAGTCCCGGAGC (written in the N → C direction) was obtained from Ms. Chotima Vilaivan, Organic Synthesis Research Unit. Briefly, the PNA was synthesized on a Tentagel S RAM resin by standard Fmoc solid-phase peptide synthesis according to the previous work [101]. At the N-terminus of acpcPNA, the amino group was end-capped by acetylation. Whereas, L-lysine residue was also incorporated at the C-terminus to serve as a solubility enhancer and a handle for subsequent immobilization onto the aldehyde-modified cellulose paper via the amino group on the lysine side chain. MALDI-TOF Mass analysis using a Microflex MALDI-TOF mass spectrometer was performed to monitor the progress of the reaction. After completion of the reaction, the nucleobase protecting groups were removed from the acpcPNA molecules via the treatment with 1:1 (v/v) aqueous ammonia: dioxane in a sealed tube at 60°C overnight. The acpcPNA was obtained after cleavage from the resin by treatment with trifluoroacetic acid (TFA), followed by purification using reverse-phase HPLC (C18-AR column, 0.1% (v/v) TFA in water-methanol gradient). The purity of the synthesized acpcPNA was evaluated to be >90% by reverse-phase HPLC analysis. The identity of acpcPNA was verified by MALDI-TOF MS, which showed a characteristic peak at m/z 5268.4 corresponding to the quasi-molecular ion as expected.

3.3.2 Preparation of 0.01 M phosphate buffer saline pH 7.4

The 400 mL of 0.01 M phosphate buffer saline (PBS) pH 7.4 was prepared in ultra-purified water ($18.2 \text{ M}\Omega\cdot\text{cm}^{-1}$ at 25°C) obtained from a Millipore Milli-Q water system. Two commercial PBS tablets were added into 400 mL Milli-Q water and the mixture was sonicated at room temperature until the PBS tablets dissolved completely. The volume was adjusted so that the final solution composed of 0.01 M PBS (pH 7.4 at 25°C), 0.137 M NaCl and 0.0027 M KCl.

3.3.3 Preparation of stock and working solutions of oligonucleotides

All stock and working solutions of synthetic oligonucleotides were prepared in 0.01 M PBS pH 7.4 and kept at 4°C prior to use. The concentration of each stock solution should be measured by UV-visible spectroscopy at 260 nm. The working solutions were prepared by diluting the stock solution with 0.01 M PBS solution to various concentrations at 50, 35, 20, 10, 5 and $2.5 \mu\text{M}$ in $200 \mu\text{L}$ centrifuge tubes.

3.3.4 Preparation of acpcPNA working solution

The concentration of acpcPNA stock solutions in the level of μM was determined spectrophotometrically from the calculated molar extinction coefficients ($145,200 \text{ L/mol}\cdot\text{cm}$) at 260 nm. The acpcPNA working solutions were prepared by diluting stock solution to 75, 62.5, 50, 37.5 and $25 \mu\text{M}$ with DMF containing NaBH_3CN (1 mg/mL) for using as a solvent in $200 \mu\text{L}$ centrifuge tubes. Both stock and working solution were kept frozen (-20°C) for long-term storage until use.

3.3.5 Preparation of ssDNA-binding fluorescent dye working solutions

The QuantiFluor[®] dye was stored in the dark at -30°C to -10°C to maintain the fluorescent properties. Since the manufacturer did not provide

the exact concentration, the stock fluorescent dye is defined as 100% v/v. Before dilution, the frozen QuantiFluor[®] dye was thawed at room temperature and protected from light. The working solution of the ssDNA-binding dye was prepared by diluting the stock solution to 5, 2.5, 1 and 0.5% v/v in 1 mL centrifuge tube with 0.01 M PBS (pH 7.4). These working solutions were protected from light by covering with foil or placing in the dark and were stable for 2–3 hours at 25°C.

3.3.6 Preparation of 2.10 M LiCl in 0.04 M of NaIO₄

The mixture solution of 2.10 M LiCl and 0.04 M NaIO₄ was prepared by weighing 0.0856 g of NaIO₄ (Mw = 213.89 g/mol) and 0.8902 g of LiCl (Mw = 42.39 g/mol) into a 10 mL of centrifuge tube, then dissolving in Milli-Q water and adjusting the volume to 10 mL. This prepared solution was utilized for surface modification of cellulose-based filter paper.

3.3.7 Preparation of 0.01 M phosphate buffer saline containing 0.001% v/v Tween-20 (PBST)

The 100 mL of PBST solution was prepared to use as a washing solution for removing non-hybridized oligonucleotides from the proposed paper-based biosensor. A PBST solution was prepared by pipetting 0.1 mL of Tween-20 and diluting with 0.01 M PBS solution to final volume of 100 mL.

3.3.8 Preparation of working solutions for studying behavior of ssDNA-binding fluorescent dye

To study the behavior of ssDNA-binding fluorescent dye in the assay solution, 0.3 μM of acpcPNA, 0.3 μM of complementary HCV DNA (55 bases) and the mixture of equal concentration of acpcPNA and target oligonucleotide (55 bases) mixture were separately prepared in 1 mL centrifuge tube using 0.5% v/v QuantiFluor[®] dye as a solvent. All prepared solutions were stored in the dark at 4°C prior to fluorescence measurement.

3.4 Fabrication of paper-based biosensor

A wax-printing method was employed for the fabrication of the paper-based biosensor in this work. First, the designed pattern of the proposed sensor was created through a graphic program (Adobe Illustrator) and subsequently printed onto the Whatman grade 1 chromatographic paper (A4 sheet) using a commercial wax printer. The patterned paper was then melted on a hotplate at 175°C for 50 seconds allowing the wax colors penetrated the paper. The area covered with the blue wax is a hydrophobic region that prevented the liquid leaking from the side of the paper. Whereas, the area without wax is hydrophilic which was utilized as a detection region as shown in Figure 3.1. Finally, the obtained paper-based device was attached below with transparent tape.

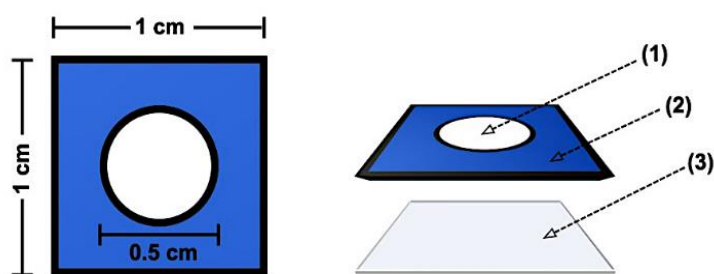


Figure 3.1 The design of paper-based sensor in top view (left) and side view (right) that composed of hydrophilic region (1), hydrophobic region (2) and transparent tape (3).

3.5 acpcPNA probe Immobilization

The overall immobilization procedures of the acpcPNA probe onto the cellulose-based platform with uncomplicated modification steps [31] are summarized in Figure 3.2. First, 2 μL of a LiCl (2.10 M) in 0.04 M of NaIO_4 was added onto the hydrophilic region of the prepared paper-based device, followed by incubation at room temperature for 15 minutes in the absence of light. The aldehyde moieties were generated on the surface of the cellulose substrate by selective oxidation of the hydroxy-functional groups. Thereafter, the aldehyde-modified paper was rinsed two times with ultrapure water to get

rid of the inorganic salts and allowed to dry at ambient temperature. The acpcPNA immobilization was then performed by dropping 2 μL of the acpcPNA working solution onto the aldehyde-modified area. Subsequently, the modified paper was incubated in a humid chamber overnight. Next, the acpcPNA-immobilized sensor was washed with acetonitrile solution (50% v/v in Milli-Q water) for 30 minutes and then left to dry in the open air at ambient condition. Finally, the paper-based biosensor was kept at 4°C until use.

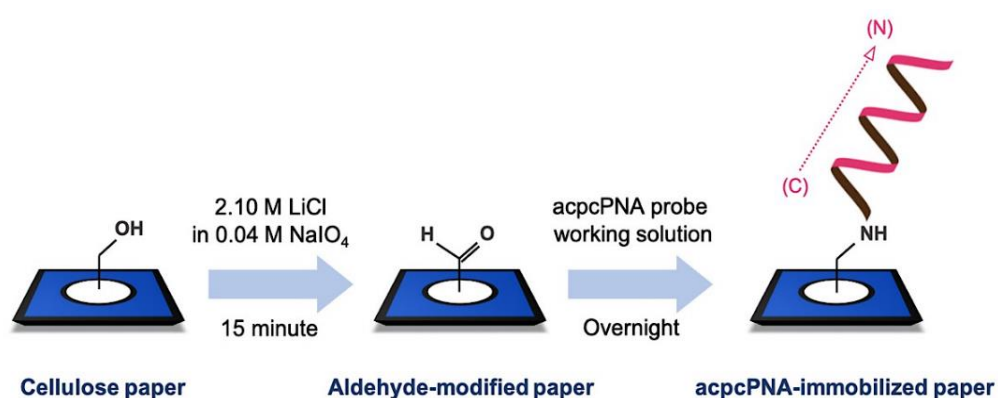


Figure 3.2 The procedure to produce acpcPNA-immobilized paper-based sensor.

3.6 FT-IR characterization

The surface of the Whatman cellulose sheet, aldehyde-modified paper and acpcPNA-immobilized paper-based sensor were characterized using FT-IR optical spectrophotometer (Nicolet iS50) with OMNIC software in the spectral range from 4000 to 500 cm^{-1} at ambient condition. Each infrared spectrum was achieved in transmission mode by an average of the 32 number of scans with a resolution of 4 cm^{-1} . All the solid platforms were allowed to dry in a hot air oven at 50°C for 2 hours before collecting FT-IR data with a diamond ATR crystal. To prevent contamination, the ATR probe was exhaustively cleaned with ethanol before and after the FT-IR measurement.

3.7 XPS characterization

The high-resolution XPS spectra of three elements, including carbon, oxygen and nitrogen that existed onto the acpcPNA-immobilized paper surface were obtained by a Kratos X-ray photospectrometer equipped with a mono aluminium anode and delay-line detector (DLD). In XPS approach, a monochromatic K-alpha X-ray (1486.6 electron volts) was generated by applying a 150 watt of electrical power to the anode material. Charge neutralization (current 1.8 amperes, balance 2.6 volts and bias 1.3 volts) was utilized to stabilize the electrical charge on the surface of an insulating paper. Each XPS spectrum of the defined elements was an average of three sweeps and performed curve-fitting using a Vision 2 processing software. For sample preparation, the paper-based sensor was removed the residual moisture in a hot air oven at 100°C for a minute and then kept in a petri dish which was cleaned with ethanol prior to the XPS analysis.

3.8 Fluorescence-based detection for studying behavior of ssDNA-binding fluorescent dye

The characteristic feature of ssDNA-binding fluorescent dye was studied in the solution phase using a fluorescence spectrophotometer. The assay solutions were firstly mixed by a vortex mixer to ensure the homogeneity. After that, the prepared solution was added into the micro fluorescence cuvette and the fluorescence spectra were measured immediately. All emission spectra in the range of 500–800 nm were obtained by setting the excitation wavelength, excitation slit and emission slit at 492, 5 and 5 nm, respectively. The fluorescence background was recorded using 0.01 M PBS (pH 7.4) solution.

3.9 Hybridization with the target oligonucleotides

For the hybridization experiment, 2 μL aliquot of the target oligonucleotide (synthetic sequence or denature PCR product) was dropped onto the acpcPNA-immobilized paper-based sensor. The hybridization was allowed to proceed at room temperature. After 15 minutes, the non-hybridized or non-specifically adsorbed oligonucleotide was subsequently removed from the detection region by washing with 20 μL of PBST and PBS solution, respectively. Each washing step was performed at ambient condition for 3 minutes.

3.10 Fluorescence-based detection on paper-based biosensor

The detection zone of the oligonucleotide-bounded paper-based sensor was prepared by dropping 20 μL of fluorescent dye working solution (2% v/v), followed by incubation for 5 minutes in a dark box at room temperature. Next, the sensor was photographed under black light (340 nm) to obtain a fluorescent image using iPhone SE coupled with fluorescent camera gadget (Figure 3.3). The green fluorescent response in the form of mean color intensity (green channel) was digitally obtained by the ColorMeter RGB Colorimeter application on the iOS system as illustrated in Figure 3.4. The oligonucleotide-free sensor was performed in the same condition and its color intensity was defined as a background signal.

3.11 Influence of the total length of HCV DNA on the signal response

Effect of the total length of incubated oligonucleotides on the fluorescent signal was evaluated by measuring the mean color intensity of the acpcPNA-immobilized sensors according to the above-mentioned procedure. The paper-based device was incubated with four target sequences having a different total length, including 25, 35, 45 and 55 nucleotides. All experiments were performed using 50 μM of complementary oligonucleotide and 1% v/v of ssDNA-binding fluorescent dye (10 μL) as the assay condition.

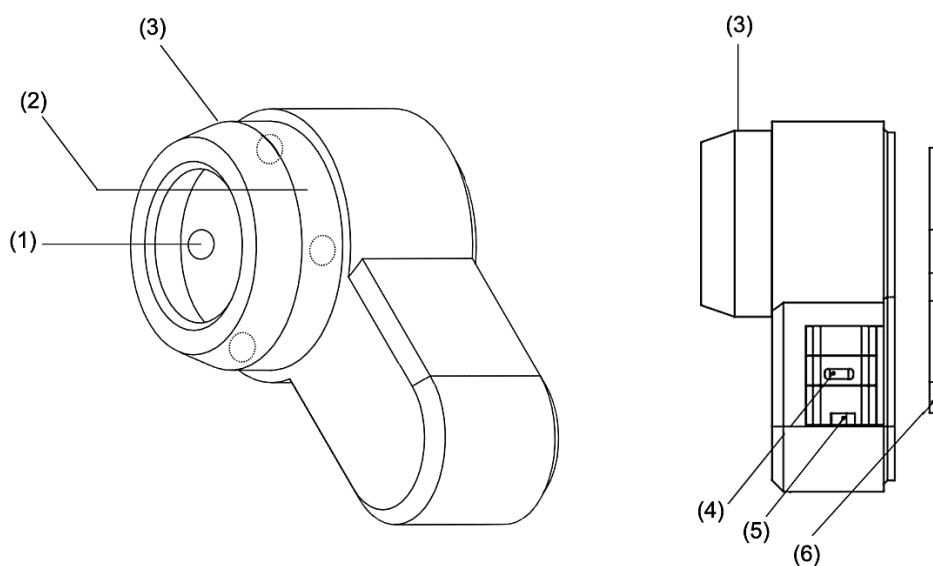


Figure 3.3 Schematic of fluorescent camera for smartphone consisting of (1) 4 pieces of 340 nm light source, (2) 500 nm long-pass filter with anti-reflection filter, (3) body part for covering the paper-based sensor and preventing the interference of external light, (4) USB-C charging port, (5) switch and (6) smartphone case attachment.



Figure 3.4 The mean color intensity obtained from ColorMeter RGB Colorimeter application (version 1.95, developed by White Marten).

3.12 Optimization of the experimental conditions

All optimization experiments, the fluorescence response in the term of mean color intensity (green value, G_{analyte}) was obtained and subtracted with the background intensity (G_{blank}). Each detection was performed for three times repeatedly. After that, the ΔI_G ($G_{\text{analyte}} - G_{\text{blank}}$) and studied parameters were plotted to obtain the best condition.

3.12.1 Concentration of acpcPNA probe

Because the quantity of acpcPNA probe is directly related to the amount of hybridized target on the detection zone of paper-based sensor, it is necessary to optimize the probe concentration in the immobilization process. Therefore, the range of 25 to 75 μM of acpcPNA working solution was investigated. In this study, a synthetic HCV DNA (55 nucleotides) was employed as the target sequence. The 10 μL of ssDNA-binding fluorescent dye (1% v/v) was also used in the fluorescence-based detection step.

3.12.2 Hybridization time

The time required for completion of the binding between the immobilized-acpcPNA probe (50 μM) and target oligonucleotide (50 μM) was studied by varying the hybridization time between 5 and 30 minutes. To measure the mean color intensity, the working solution of 1% v/v fluorescent dye with a volume of 10 μL was used in this assay.

3.12.3 Incubation time

The incubation time of ssDNA-binding fluorescent dye onto the paper-based sensor was optimized next. The incubation time in the dark condition from 0 to 30 minutes was examined using 50 μM of both target oligonucleotide and acpcPNA probe. The same condition of fluorescence-based measurement as the assay of hybridization time was applied in this study.

3.12.4 Concentration of ssDNA-binding fluorescent dye

The mean color intensity in the green channel related to the total amount of ssDNA-binding fluorescent dye. Therefore, the investigation of the dye concentration was optimized by varying in the range of 0.5 to 5% v/v. Each fluorescent dye solution was prepared in a final volume of 20 μL onto the paper-based device. Signal intensities were quantified using 50 μM of incubated HCV DNA onto the probe-immobilized paper (50 μM).

3.12.5 Volume of ssDNA-binding fluorescent dye

The volume of the fluorescent dye is another factor that control the total amount of fluorescent dye and also associated with the fluorescence response. Hence, the color intensity of oligonucleotide-bounded paper was detected using 2% v/v of ssDNA-binding fluorescent dye with different total volumes, including 5, 10, 20 and 30 μL . The incubated amount of target DNA and acpcPNA probe were equal to those used in the optimization of dye concentration.

3.13 Analytical performance

Under optimized conditions, the analytical performance of the developed paper-based DNA sensor relying on label-free assay for detecting HCV DNA (55 nucleotides oligomer) was determined. The various concentrations of target sequences in the range of 2.5 to 50 μM were incubated onto the prepared sensor. Each concentration was examined in triplicate. The average ΔI_G were plotted as a function of the amount of incubated oligonucleotide (pmol) to obtain a calibration curve. The detection limit, defined as the smallest amount of test HCV DNA that can generate the significant difference of the intensity of analyte (G_{analyte}) from the background (G_{blank}), as statically calculated by the Student's t-test in spreadsheet software (Microsoft Excel) after variance testing by F-test. A t-test at the 95% confidence level was selected in this calculation.

3.14 Specificity study

The specificity of the acpcPNA was evaluated by comparing the numerical signal intensities obtained from the fluorescent image between complementary HCV DNA (45 nucleotides oligomer), single-base-mismatch, two-base-mismatch and non-complementary sequence. Each synthetic oligonucleotide used in this evaluation had a working concentration of 50 μM .

3.15 Stability evaluation

To achieve the shelf-life of the developed paper-based DNA sensor, the prepared sensor was kept under a dry condition at 4°C and ambient temperature (25°C) prior to measuring the fluorescent response every other day after hybridization with 50 μM target sequence (45 nucleobases). The signal intensity obtained from the sensing-device after storage was normalized with the freshly prepared sensor on the first day.

3.16 Sample preparation

The extracted HCV oligonucleotides from clinical samples were obtained from the Center of Excellence in Hepatitis and Liver Cancer, Department of Biochemistry, Faculty of Medicine, Chulalongkorn University (Thailand). The complementary HCV DNA was generated by reverse transcription-polymerase chain reaction (RT-PCR). The obtained PCR amplicons were stored at -8°C for further analysis. Prior to the data collection from the PCR-amplified samples, the PCR-amplified dsDNA were denatured to generated ssDNA targets. The denaturation was done by heating the sample in a PCR tube at 100°C for 10 minutes, followed by instant freezing in an ice bath.

CHAPTER IV

RESULTS AND DISCUSSION

This chapter explains the results and discussion of acpcPNA-immobilized paper-based sensor characterization, fluorescence behavior of ssDNA-binding dye, sensing principle, influence of the total length of target oligonucleotide and optimization of experimental conditions. In addition, the analytical performances, specificity study, stability evaluation and real sample analysis using this proposed sensor are also described.

4.1 Characterization of the acpcPNA-immobilized paper-based sensor

Due to the beneficial features of the acpcPNA system including outstanding affinity with DNA target and extraordinary selectivity, the acpcPNA molecule is a promising recognition element that has been extensively applied in various sensing platforms. This study is one of the efforts to utilize acpcPNA as a specific probe to construct a paper-based analytical device for screening of HCV DNA. In this work, the tethering process of the lysine-modified acpcPNA on the cellulose substrate using inexpensive reagents and uncomplicated procedures was adopted from a previous report [31]. In order to confirm the success of acpcPNA immobilization, the fabricated acpcPNA-immobilized paper was characterized by infrared spectroscopy (FT-IR with ATR accessory) and elemental analysis (XPS), respectively.

The obtained FT-IR spectra of three kinds of substrate, namely Whatman cellulose-based paper, aldehyde-modified cellulose and acpcPNA-immobilized sensor are shown in Figure 4.1. The C=O stretching at around 1730 cm^{-1} [98] in the infrared spectrum of the aldehyde-modified paper was clearly different from the unmodified cellulose paper. The presence of carbonyl absorption originates from the periodate oxidation of 1,2-glycol side-chain of the glucose residual on the cellulose. This reaction arises from the Malaprade mechanism [99], contributing to the generation of two aldehyde groups per

glucopyranose unit. After the periodate-oxidized cellulose was incubated with the acpcPNA solution, there was no carbonyl signal (1730 cm^{-1}) left in the FT-IR spectrum. This signal disappearance was consistent with the reaction between the aldehyde groups on the modified-cellulose and the amine groups of lysine-terminated acpcPNA. Additionally, a newly peak near 1640 cm^{-1} related to the stretching vibration of N-C=O [102] was observed. This characteristic band can be assigned to the peptide-like backbone of the acpcPNA probe.

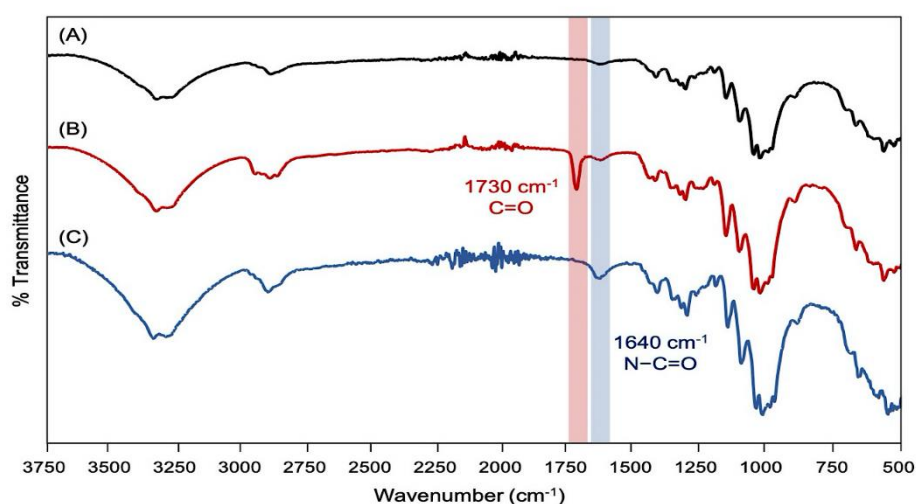


Figure 4.1 ATR-FT-IR spectra of (A) Whatman cellulose sheet, (B) aldehyde-modified paper and (C) acpcPNA-immobilized sensor.

To verify the existence of the acpcPNA probe, an XPS analysis was performed to observe the elemental composition on the surface of the prepared sensor. As illustrated in Figure 4.2, the high-resolution C 1s spectrum of acpcPNA-based PAD was deconvoluted to reveal three peaks at 284.60, 286.14 and 288.37 eV corresponding to C-C (sp^2), C-O and C=O, respectively [103]. Two components of the O 1s peak at 532.06 and 533.05 eV was attributed to C=O and N-O-C [104]. In addition, one peak of N 1s signal was presented at 399.40 eV [105], which denoted the appearance of tertiary nitrogen $\text{N}(\text{C})_3$ moiety in the structure of immobilized-acpcPNA probe. These results clearly confirm that the acpcPNA probe was successfully immobilized on the surface of the periodate-oxidized cellulose.

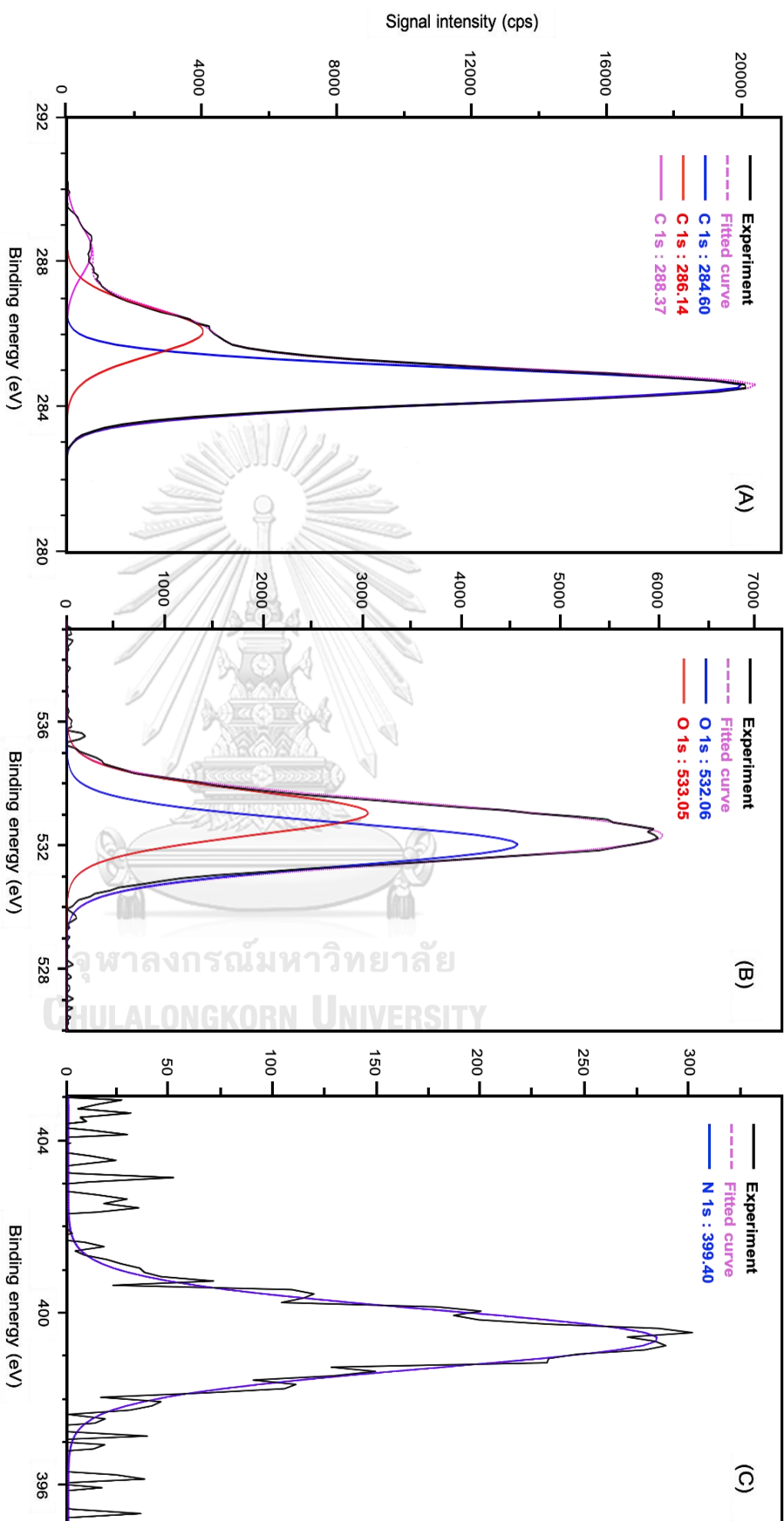


Figure 4.2 High resolution XPS spectra of (A) C 1s, (B) O 1s and (C) N 1s on the surface of acppPNA-immobilized paper-based device.

4.2 Fluorescent behavior of ssDNA-binding fluorescent dye

The fluorescence spectra of the ssDNA-binding dye in 0.01 M PBS (curve A) and the dye mixtures with the acpcPNA probe and the target ssDNA were displayed in Figure . It can be found that the control with the addition of only acpcPNA probe exhibited a negligible fluorescent signal at around 520 nm (curve B) indicating the ineffective binding between the fluorescent dye and the neutral backbone of the acpcPNA probe. In contrast, the target (HCV) ssDNA in the presence of the dye showed an extremely large enhancement (ca. 450-fold) in fluorescent response (curve C) compared with the control solution (curve A). The mixture provided an outstanding emission peak centered at 525 nm when the excitation wavelength was operated at 492 nm. The sensitive fluorescence emission should occur according to the electrostatic binding between the anionic phosphate backbone of ssDNA and the cationic dye. Moreover, the fluorescent intensity at the defined peak of this mixture slightly declined upon hybridization with acpcPNA probe (curve D); about a 7% decrease in the presence of an equivalent acpcPNA. This could be attributed to the formation of the PNA:DNA duplex, resulting in the less accessible sites for fluorescent dye binding. The obtained photographs of these solutions under UV irradiation are shown in the inset of Figure 4.3. As seen, the mixture of ssDNA-binding dye and ssDNA target presents a bright green color that confirmed the strong fluorescent feature of the assay solution. These results indicated that the ssDNA-binding fluorescent dye could be served as a suitable signaling element for the fluorescence-based detection of ssDNA and its binding behavior significantly related to the electrostatic attraction of the dye and target ssDNA as depicted in Figure 4.4.

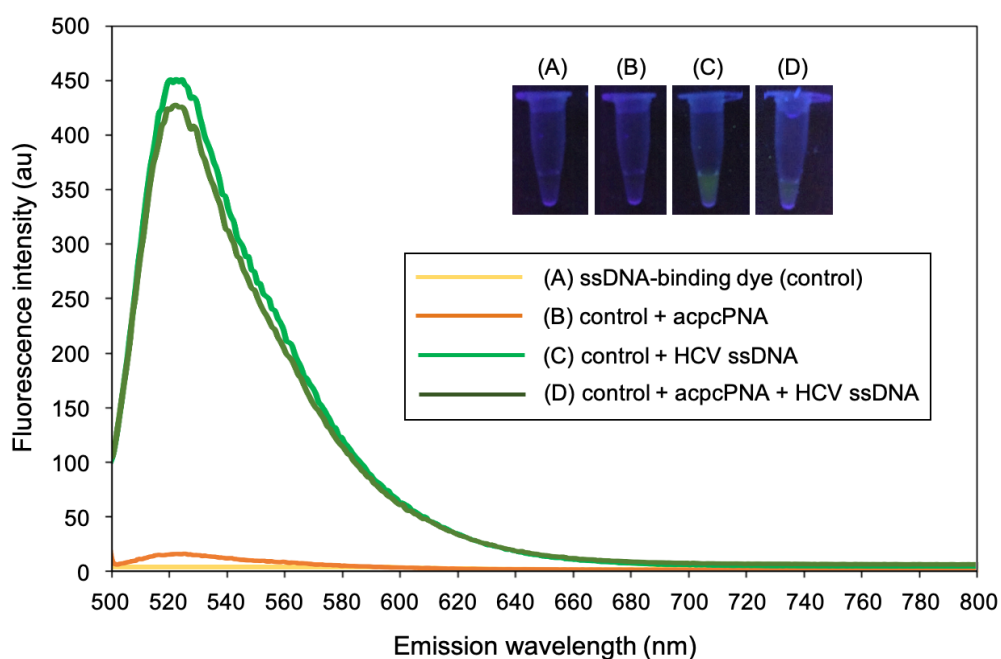


Figure 4.3 Fluorescence spectra of ssDNA-binding dye solution (0.5% v/v) with the addition of acpcPNA probe and target ssDNA (55 oligomers). All concentration of acpcPNA and ssDNA are $0.3 \mu\text{M}$. The inset is the photographs of the assay solutions under UV light (365 nm).

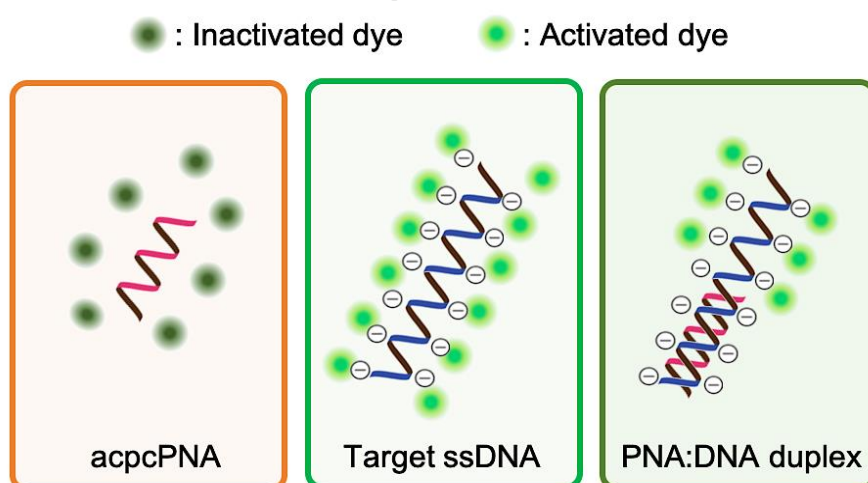


Figure 4.4 The proposed schematic representation of ssDNA-binding dye behavior.

4.3 Sensing principle

The concept for the detection of HCV DNA using the acpcPNA-immobilized PAD was demonstrated in Figure 4.5. In the absence of target sequence (Figure 4.5A), the acpcPNA-immobilized sensor was non-fluorescence due to the lack of binding event between the ssDNA specific dye and the acpcPNA probe. On the contrary, when the complementary HCV DNA was added (Figure 4.5B), the fluorescent dye would bind to the remaining region of the ssDNA target that was not involved in the specific hybridization with the probe. As a result, a bright-green color of fluorescent response was visually observed on the detection zone of the sensor under UV irradiation (340 nm) generated from a handheld camera gadget. The fluorescent color change can be quantified by detecting the mean intensity of green color (G_{analyte}) and subtracted by the intensity of the blank acpcPNA-immobilized paper (G_{blank}). The different color (ΔI_G) value can be utilized as the numerical signal intensity in the further experiment.

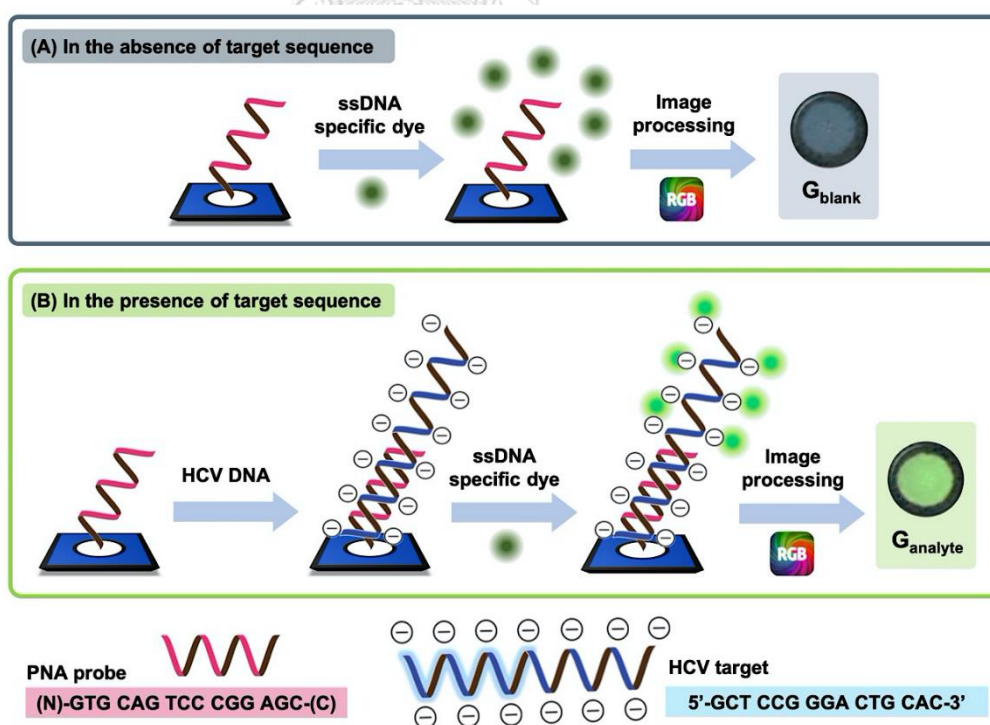


Figure 4.5 The detection concept of acpcPNA-immobilized PAD in the absence (A) and presence (B) of target sequence.

4.4 Influence of the total length of HCV DNA

In this work, fluorescence response of the sensing platform is expected to increase with the increasing of the length of the oligonucleotide target. Thus, the influence of the total length of synthetic HCV DNA on a fluorescent signal was evaluated to prove this hypothesis as shown in Figure 4.6. It can be observed that the ΔI_G value of this system tends to enhance with the increasing length of target oligonucleotide. This phenomenon is due to the expansion in the hanging tail of ssDNA target which leading to higher accessible sites for binding interaction with the fluorescent dye. The fluorescent images of this assay were shown in Figure 4.7. The result pointed out that the total length of target nucleotide was a key factor to achieve the signal amplification in this detection method. In our case, the longest DNA strand (55 nucleotides) was chosen as the target sequence in both experimental optimization and analytical performance study because it provided the highest signal intensity.

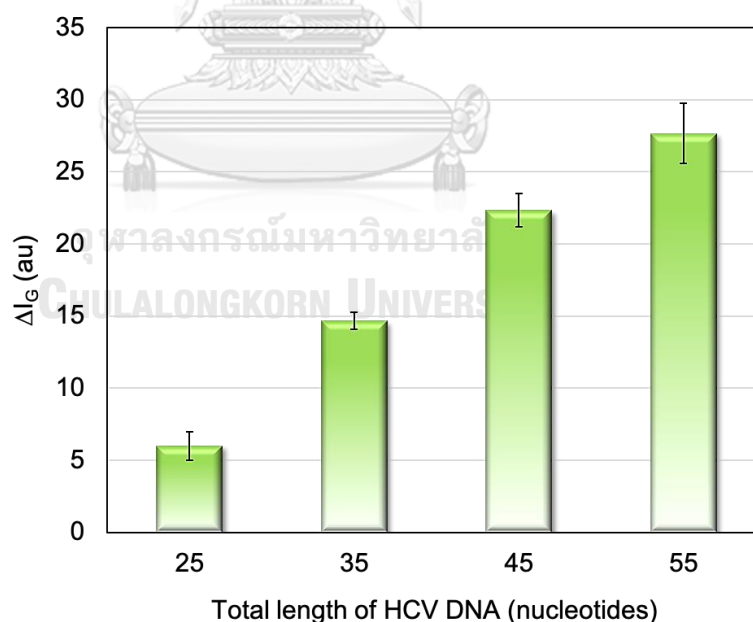


Figure 4.6 Influence of the total length of HCV DNA on the signal intensity.

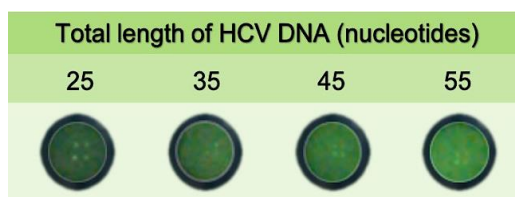


Figure 4.7 Fluorescent images of 50 μM of HCV DNA at different total lengths (25–55 nucleotides).

4.5 Optimization of experimental conditions

To achieve the high sensitivity for HCV DNA measurement using the propose sensor, variation of experimental parameters, including acpcPNA probe concentration, hybridization time and incubation time were investigated. The concentration and volume of fluorescent dye were also examined. All optimization experiments were carried out by observation of the sensor with 50 μM complementary HCV DNA (55 nucleotides) using the fluorescence-based measurement combined with a smartphone application.

4.5.1 Effect of acpcPNA concentration

The optimization of acpcPNA probe concentration in the immobilization process was investigated by varying the concentration of the probe in the range of 25 to 75 μM . As displayed in Figure 4.8, the results revealed that the fluorescent change gradually amplified with an increase of probe concentration from 25 to 50 μM and subsequently remained constant. All photographs of the detection zone were also demonstrated in Figure 4.9. Accordingly, the concentration acpcPNA probe at 50 μM was chosen for further studies because it was the minimum concentration that provided the maximum signal.

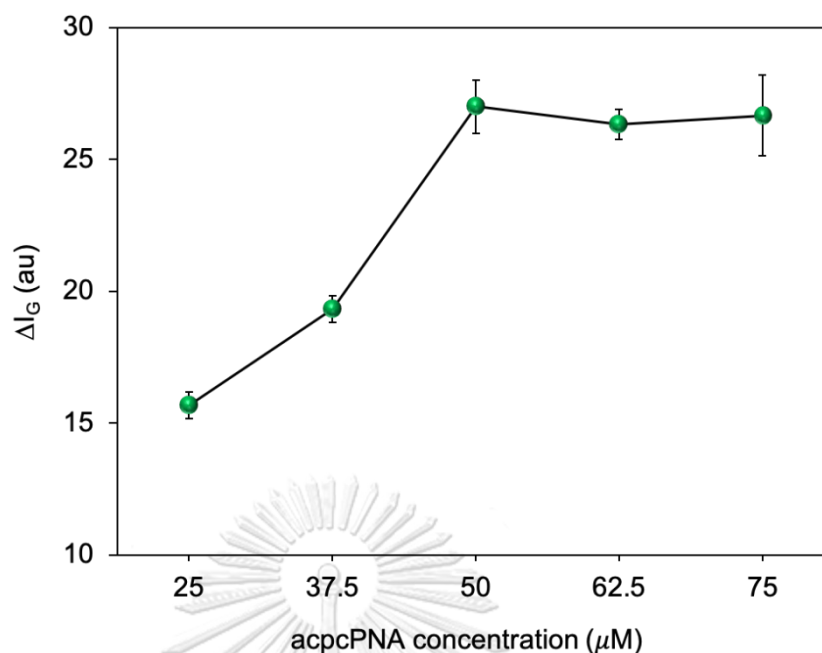


Figure 4.8 Effect of acpcPNA concentration on the fluorescence response of 50 μM of HCV DNA.

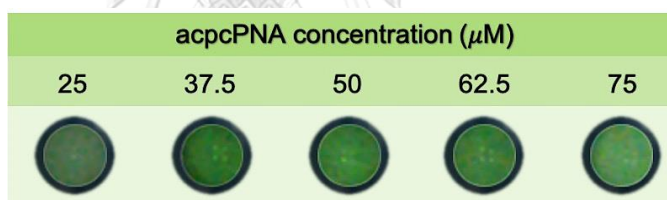


Figure 4.9 Fluorescent images of target HCV DNA (50 μM) at different probe concentrations (25–75 μM).

4.5.2 Effect of hybridization time

Next, the effect of DNA hybridization time on the signal intensity was considered over the time range from 5 to 30 minutes. As shown in Figure 4.10, the numerical intensity slightly increased with the lengthening of time after the addition of the target DNA within 10 minutes, and sharply reached the maximum value at 15 minutes. Then, a signal plateau was observed upon increasing the hybridization time that could be explained by the saturation of the immobilized acpcPNA probe by the DNA target. These results were supported by the obtained photographs (Figure 4.11). Considering the

hybridization efficiency, this method requires only 15 minutes to use as the optimal time for the hybridization process.

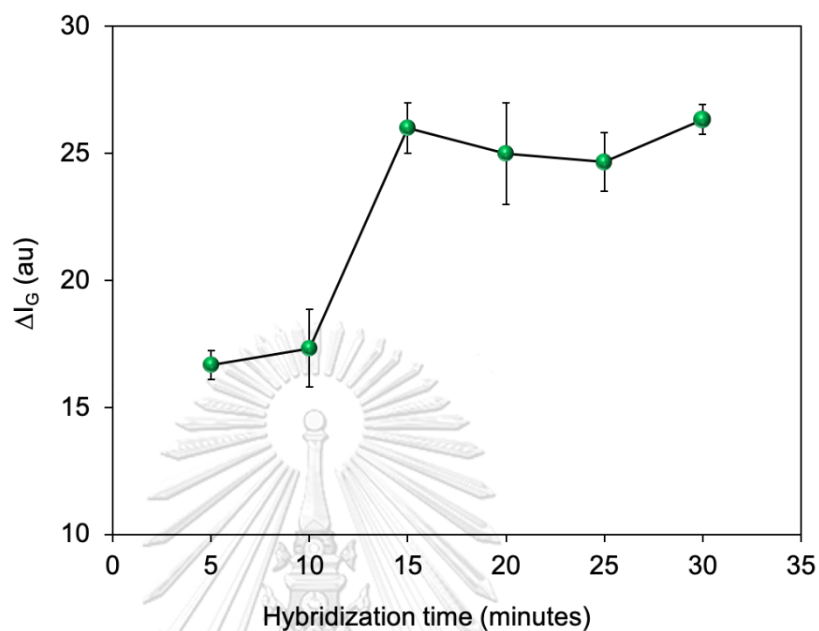


Figure 4.10 Effect of hybridization time on the fluorescence response of 50 μM of HCV DNA.

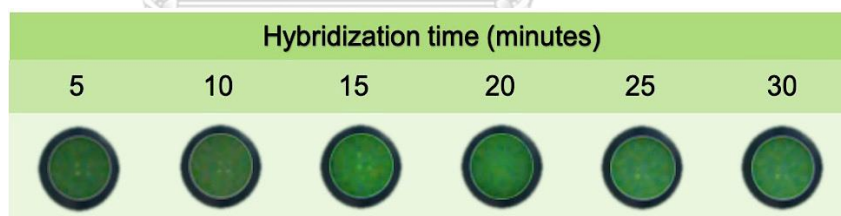


Figure 4.11 Fluorescent images of target HCV DNA (50 μM) at different hybridization times (5–30 minutes).

4.5.3 Effect of incubation time

The influence of incubation time between fluorescent dye and target oligonucleotide that bound onto the acpcPNA-immobilized sensor was examined next. As illustrated in Figure 4.12, the immediate measurement after dropping the dye onto the paper-based sensor resulted in imperfect interaction between the dye and the bound target. The obtained signal reached its highest intensity after the incubation for 5 minutes. Then, the signal intensity declined instantly when the incubation was longer than 10 minutes. This is due to the increase of incubation time would reduce the light performance of the dye. From the product description, the active-time of dye working solution is limited and directly associates with the exposure of light. In addition, the decrease of intensity could be influenced by the photo-bleaching effect caused by undesirable interaction between the dye and surrounding molecules [68]. The change of fluorescent color was obviously observed as presented in Figure 4.13. Therefore, the incubation time of 5 minutes was selected as an optimal condition for subsequent experiments.

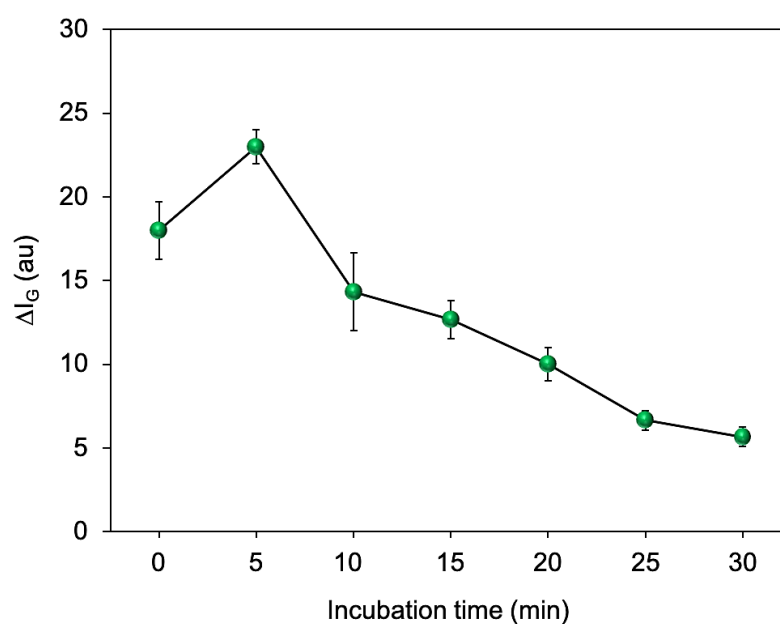


Figure 4.12 Effect of hybridization time on the fluorescence response of 50 μM of HCV DNA.

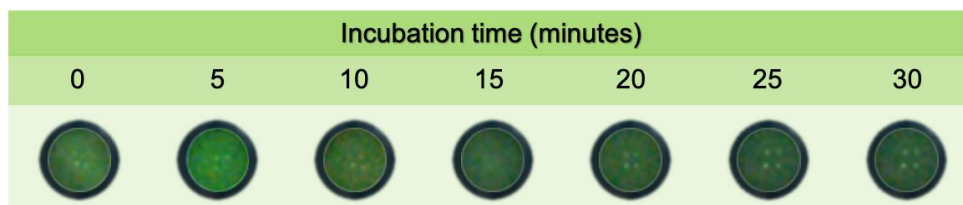


Figure 4.13 Fluorescent images of target HCV DNA ($50 \mu\text{M}$) at different incubation times (0–30 minutes).

4.5.4 Effect of fluorescent dye concentration

Fluorescent dye concentration is another important parameter that influences the sensitivity of this proposed platform since the fluorescent intensity directly depends on the amount of fluorophore molecule used in the solid sensing-device. The range of dye concentration between 0.5 to 5% v/v was studied. As shown in Figure 4.14, the outstanding enhancement of ΔI_G value was observed with the raising of dye concentration and reached a plateau at 2% v/v of fluorescent dye. While the absolute intensity of the obtained photograph was slightly higher at the dye concentration of 5% v/v. At the same time, its blank system also exhibited the highest intensity among other concentrations as illustrated in Figure 4.15. As a result, in the ΔI_G value in this case was close to the case that using the 2% dye (v/v). These results indicated that the probe could interact with the fluorescent dye at high concentration. Hence, 2% v/v of ssDNA-binding dye was utilized as the appropriate concentration for the next optimization.

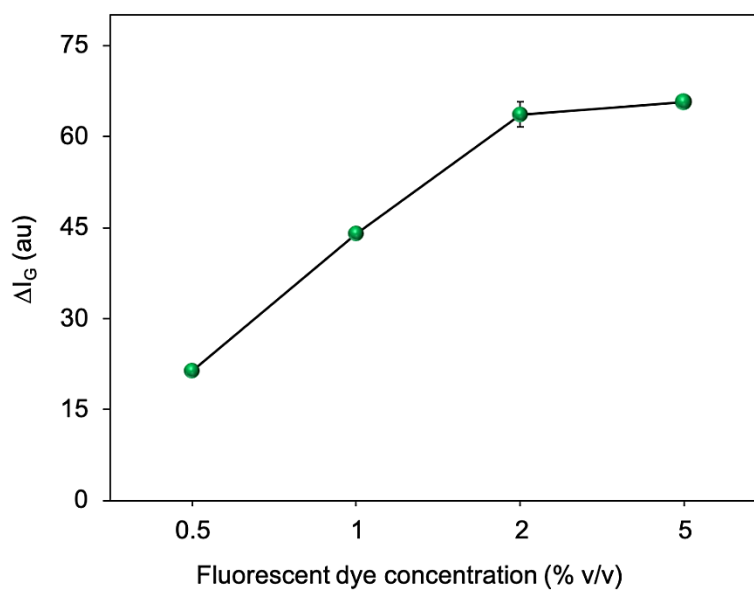


Figure 4.14 Effect of fluorescent dye concentration on the fluorescence response of 50 μM of HCV DNA.

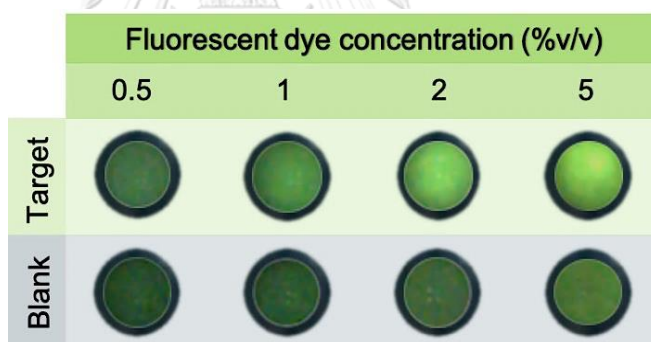


Figure 4.15 Fluorescent images of blank and target HCV DNA (50 μM) at different fluorescent dye concentration (0.5–5% v/v).

4.5.5 Effect of fluorescent dye volume

Finally, the volume of fluorescent dye was optimized over the range of 5 to 30 μL using the previous optimal condition. As presented in Figure 4.16, the trend line showed that the green fluorescent signal continuously increased from the volume of 5 to 20 μL and the intensity was constant after 20 μL . All fluorescent images were also shown in Figure 4.17. This could be described that the increase in dye volume might increase the amount of the fluorophore molecule. Thus, the volume of 20 μL was selected for the fluorescence-based detection.

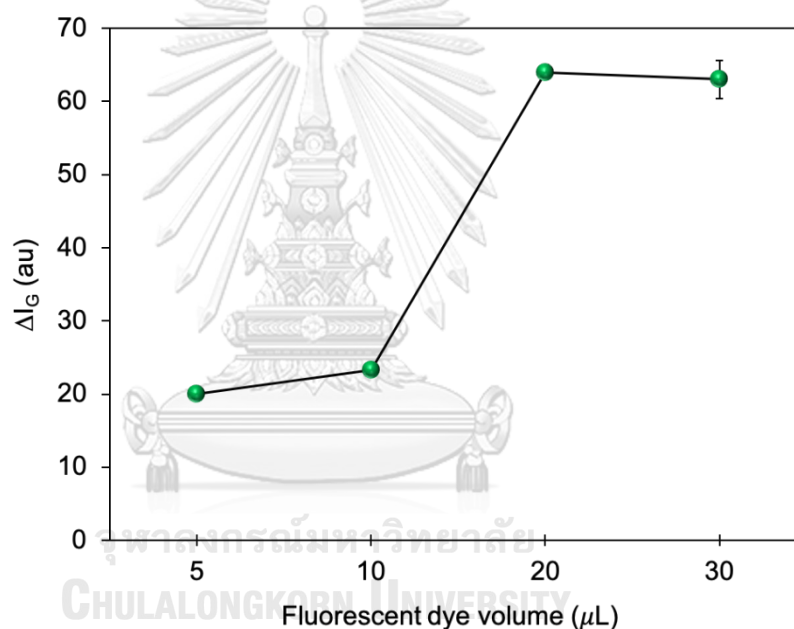


Figure 4.16 Effect of fluorescent dye volume on the fluorescence response of 50 μM of HCV DNA.

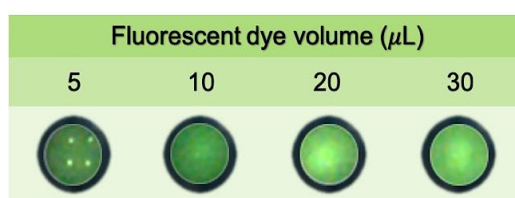


Figure 4.17 Fluorescent images of target HCV DNA (50 μM) at different fluorescent dye volume (5–30 μL).

4.6 Analytical performance

The analytical performance of the acpcPNA-immobilized paper-based DNA sensor for the fluorescence measurement of HCV DNA was assessed under the optimized conditions. To evaluate the dynamic range of this proposed method, the incubated amount of HCV DNA (pmol) as a function of the color change in the green channel (ΔI_G) of the digital images (Figure 4.18) was examined. As clearly seen in Figure 4.19, the ΔI_G values increase with the increasing amount of test DNA. A good linear relationship between the ΔI_G value and the amount of target oligonucleotide in the range of 5–100 pmol was observed. The linear regression of this relationship was $y = 0.6348x + 5.6227$; $R^2 = 0.9956$.

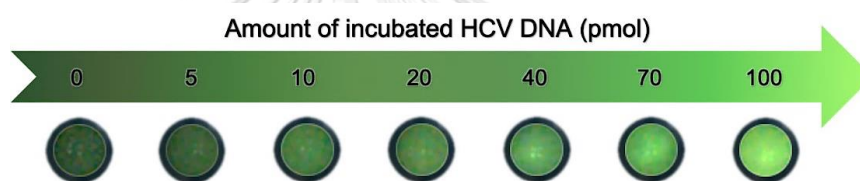


Figure 4.18 The enhancement of green colors onto the proposed DNA sensor for various amounts of incubated HCV DNA (pmol).

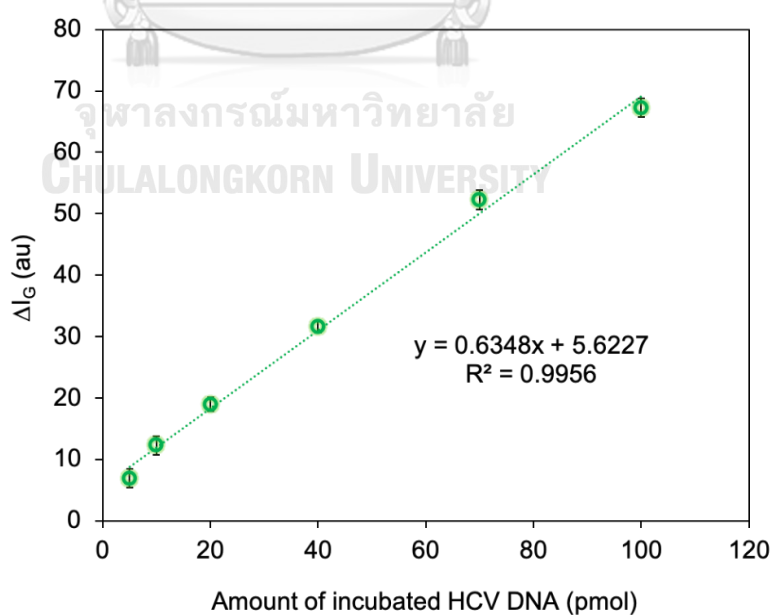


Figure 4.19 The calibration plot of ΔI_G value against the amount of incubated HCV DNA.

Thereafter, the detection limit of the HCV DNA amount was determined by observing the lowest amount of target DNA that exhibited distinguishable green value compared to the background. In this study, ten pieces of both the paper-based DNA sensor having HCV DNA (5 pmol) and the blank were detected and statically evaluated by F-test and Student's t-test, respectively. The result of variance analysis (F-test) is displayed in Table 4.1. The variance between the target-incubated paper and the blank was not significant difference since the calculated F value (1.433) was less than the F critical (3.179) at a significant level (denoted as α) of 0.05. Then, this couple of data groups was analyzed by a t-test that assuming equal variances. As presented in Table 4.2, the resulting value of t stat was equal to 14.146 and higher than the critical value (1.734) given in the t-table ($\alpha = 0.05$). This data indicated that the mean of the green value obtained from the test sensor and the blank was statistic inequality. Consequently, the detection limit for this sensing platform was found to be 5 pmol. These results showed a promising performance of the proposed acpcPNA-based sensor for screening of HCV DNA in clinical samples as a point-of-need approach. In addition, it should be noticed that, in the sensing of real DNAsamples, the detection limit should be further enhanced when the length of the target sequence was extended. That is highly possible to apply in the real sample analysis because the DNA target is regularly hundreds of nucleotide length.

Table 4.1 *F-test for the determination of detection limit.*

Parameters	Test sensor (5 pmol)	Blank
Mean	84.9	77.4
Variance	1.66	1.16
Observations (N)	10	10
Degree of freedom (N-1)	9	9
F value	1.433	
F critical one-tail	3.179	

Table 4.2 *t-test for the determination of detection limit.*

	Test sensor (5 pmol)	Blank
Mean	84.9	77.4
Variance	1.66	1.16
Observations (N)	10	10
Degree of freedom ($N_{\text{total}}-2$)	18	
Pooled variance	1.406	
t value	14.146	
t critical one-tail	1.734	

4.7 Specificity study

In case of detecting HCV DNA in the real sample of PCR-amplified products, the specificity of the proposed DNA sensor is unavoidable for the reason that the fluorescent dye binds to ssDNA target without the selectivity of nucleobase sequence. Thus, the dye can interact with non-complementary oligonucleotide and provide fluorescent emission as in the case of a complementary target. The use of immobilized PNA probe to capture the specific DNA target should solve this problem provided that the specificity of the PNA probe-DNA target is sufficiently high. To determine the specificity of this system, the ΔI_G value obtained from the paper-based sensor after hybridization with the fully complementary HCV DNA (45 nucleotides) was compared to the single-base mismatch (mis-1), two-base mismatch (mis-2) and non-complementary (nc) DNA targets as shown in Figure 4.20. All digital images obtained from this experiment were also displayed in Figure 4.21. In the presence of complementary HCV DNA, the ΔI_G value enhanced remarkably; whereas the ΔI_G values were negligible for the mis-1, mis-2 and ncDNA targets. These results suggested that the mismatched and non-complementary oligonucleotides should not significantly affect the fluorescence measurement in this method. Hence, the proposed strategy exhibited the expected specificity for HCV DNA detection, which confirms the high-performance of acpPNA probes.

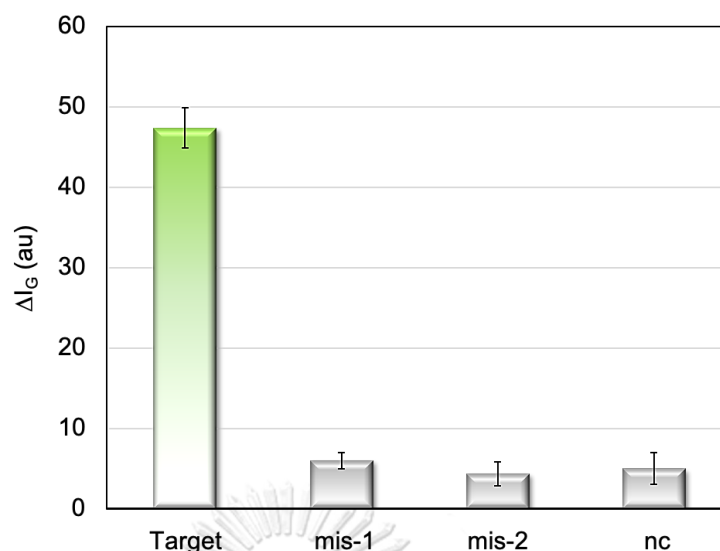


Figure 4.20 ΔI_G values obtained from the paper-based sensor after hybridization of target, mis-1, mis-2 and ncDNA, respectively. All concentration of test DNA are $50 \mu\text{M}$.

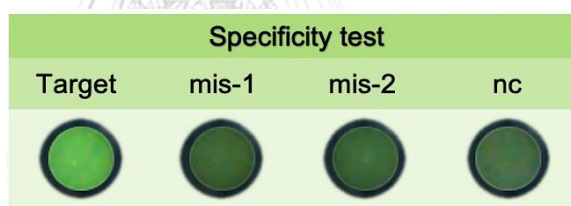


Figure 4.21 The digital images of paper-based sensor in specificity test.

4.8 Stability evaluation

To evaluate the stability of the proposed system, the prepared acpcPNA-immobilized paper-based sensor was kept at room temperature (25°C) and 4°C in a dry chamber for 1, 3, 5, 7, 9 and 11 days, and subsequent measuring the ΔI_G value following hybridization with $50 \mu\text{M}$ of target DNA (45 nucleotides). The obtained signal was normalized with the initial intensity. As illustrated in Figure 4.22, the relative change of green fluorescent color remained over 95% after storage for 5 days (kept at 25°C) and 9 days (kept at 4°C). These steady responses suggest that the proposed DNA sensor affords satisfactory stability for long-term storage.

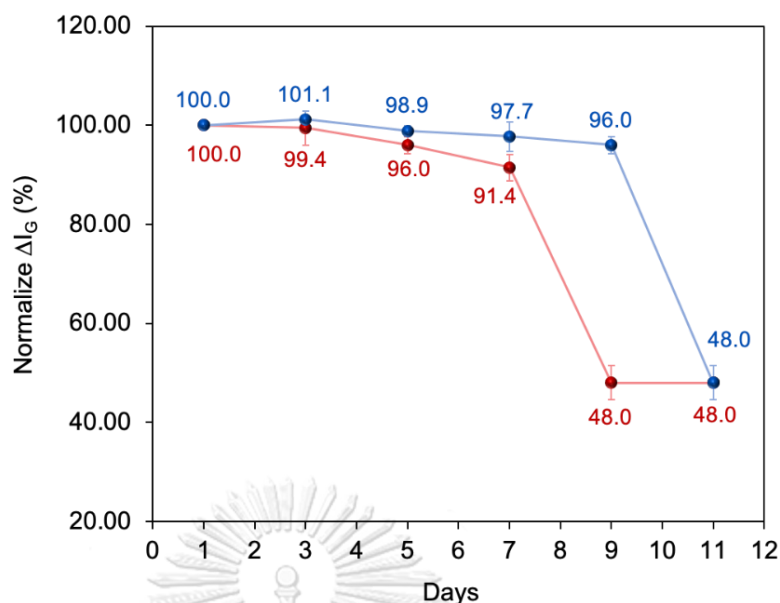


Figure 4.22 Long-term stability of the proposed sensor for detecting 50 μM of HCV DNA (45 nucleotides) in room temperature (red line) and 4°C (blue line).

4.9 Real sample analysis

To test the feasibility of the proposed sensor for the analysis of real samples, the developed DNA sensor was evaluated in the HCV DNA detection of PCR-amplified products from HCV patients with known HCV RNA concentration as listed in Table 4.3. As mentioned in the sensing principle, this sensing-device relied on the detection of ssDNA. In addition, the probe must bind to a single stranded region in the target DNA. Therefore, the duplex DNA in the PCR-amplified real DNA sample should be denatured prior to the hybridization and signal collection. It was found that the average ΔI_G was increased in a concentration-dependent manner in the presence of positive samples at different levels of viral load (Figure 4.23). For the negative control (SiHA), the obtained intensity was insignificantly increased compared to the blank system. The results validated the target hybridization with the acpcPNA probe in the proposed system. In addition, it was observed that the signal intensity enhances with the addition of the amount of PCR sample (C132) as

displayed in Figure 4.24. From these results, it obviously shows that this fluorescent label-free paper-based biosensor could be applicable for the screening of HCV DNA in amplified products from real clinical samples.

Table 4.3 The concentration of HCV-RNA and viral load in test samples.

Code	HCV-RNA (IU/mL)	Viral load Log (logIU/mL)
C118	431,130	5.63
C132	1,215,642	6.08
C264	960,316	5.98
C342	3,431,992	6.54

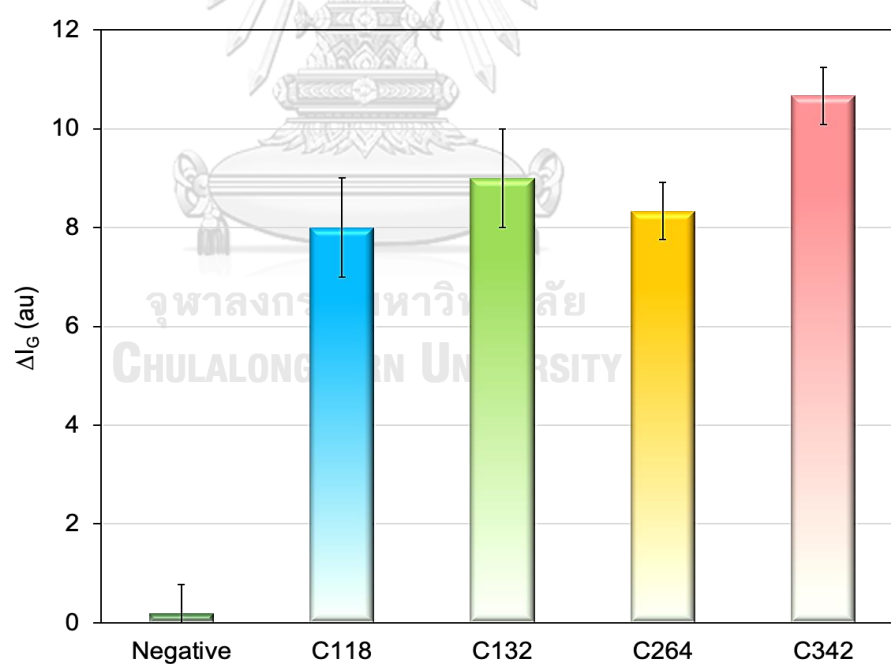


Figure 4.23 The ΔI_G values for the detection of real HCV DNA in PCR-amplified samples ($n=3$).

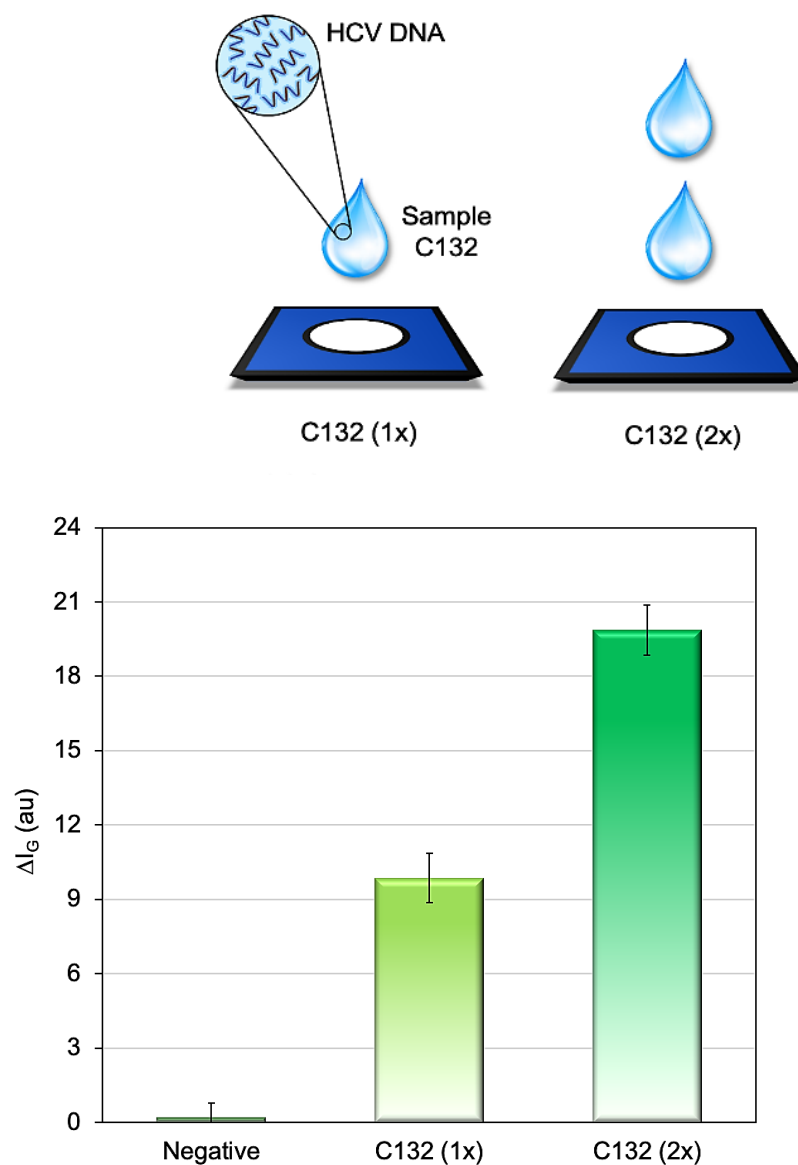


Figure 4.24 The schematic illustration for real sample analysis (upper) and ΔI_G response of the proposed DNA sensing-device in the occurrence of negative control (SiHA) and C132 samples (1x, 2x) (lower).

CHAPTER V

CONCLUSIONS AND FUTURE PERSPECTIVE

5.1 Conclusion

In this research, a novel strategy for the fluorescence-based detection of HCV DNA has successfully established using acpcPNA probes integrated with a paper-based sensing device. The developed platform offers a simple-to-use, rapid measurement, long-term storage, disposability, portability and low sample volume requirement. Moreover, this proposed method exhibits straightforward probe fabrication without the use of costly chemical reagents and complicated steps. The immobilization of the acpcPNA probe onto the surface of PAD was confirmed by surface characterization techniques, namely FT-IR with ATR mode and XPS analysis. The change of green fluorescent color correlates with the amount of the HCV target DNA, which could be observed by naked-eyes and smartphone-based measurements. Under the optimal conditions, the acpcPNA-based device can be utilized to directly observe the HCV oligonucleotide (55 nucleotides) in the dynamic range from 5 to 100 pmol/spot. The detection limit was found to be 5 pmol/spot, as verified by the Student's t-test. The linear relationship equation is $y = 0.6348x + 5.6227$; R^2 is equal to 0.9956. Furthermore, the prepared biosensor provides an acceptable specificity to detect complementary HCV targets over the mismatched and non-complementary oligonucleotides. Additionally, the relative fluorescent response remains constant after storage for 5 days (at ambient temperature) and 9 days (at 4°C) under a dry environment. Finally, this approach was satisfactorily applied for detecting HCV DNA from PCR-amplified products. Accordingly, this proposed DNA sensor combined with the smartphone-based measurement can be employed as a potential alternative and easy-to-handle tool for the point-of-care screening of HCV DNA in the clinical diagnosis.

5.2 Future perspective

Due to genetic variability of HCV which can divide into seven main genotypes and multiple subtypes [34]. Thus, this device can be developed for HCV genotyping in biomedical purposes using the specific acpcPNA probes that are designed to be complementary with the defined HCV targets. The pattern of the paper-based DNA sensor can be also designed for simultaneous detection providing the improvement of high-throughput screening. Nevertheless, the level of HCV DNA in clinical samples is available at a low concentration. Therefore, the superior performance technique that provided higher sensitivity is demanded to continuously evolve. To improve the analytical performance, one should increase the fluorescent response by using the novel dyes or other signaling agents that exhibited better fluorescence change. Additionally, the adjustment of the optical path in the smartphone gadgets to obtain a low background intensity will be beneficial for the signal amplification.

REFERENCES

- [1] Lee, M. H.; M. H.; Yang, H. I.; Yuan, Y.; L'Italien, G.; Chen, C. J. "Epidemiology and natural history of hepatitis C virus infection" *World J. Gastroenterol.* **2014**, *20*, 9270–9280.
- [2] World Health Organization 2014. "Guidelines for the screening, care and treatment of persons with hepatitis C infection" Available online: <https://www.who.int/hepatitis/publications/hepatitis-c-guidelines-2016/en/> (accessed April 4, 2020).
- [3] Manns, M. P.; Buti, M.; Gane, E.; Pawlotsky, J. M.; Razavi, H.; Terrault, N.; Younossi, Z. "Hepatitis C virus infection" *Nat. Rev. Dis. Primers* **2017**, doi: 10.1038/nrdp.2017.6.
- [4] European Association for the Study of the Liver. "EASL recommendations on treatment of hepatitis C 2018" *J. Hepatol.* **2018**, *69*, 461–511.
- [5] Alborino, F.; Burighel, A.; Tiller, F. W.; Helden, J. V.; Gabriel, C.; Raineri, A.; Catapano, R.; Stekel, H. "Multicenter evaluation of a fully automated third-generation anti-HCV antibody screening test with excellent sensitivity and specificity" *Med. Microbiol. Immunol.* **2011**, *200*, 77–83.
- [6] Glynn, S. A.; Wright, D. J.; Kleinman, S. H.; Hirschhorn, D.; Tu, Y.; Heldebrandt, C.; Smith, R.; Giachetti, C.; Gallarda, J.; Busch, M. P. "Dynamics of viremia in early hepatitis C virus infection" *Transfusion* **2005**, *45*, 994–1002.
- [7] Morota, K.; Fujinami, R.; Kinukawa, H.; Machida, T.; Ohno, K.; Saegusa, H.; Takeda, K. "A new sensitive and automated chemiluminescent microparticle immunoassay for quantitative determination of hepatitis C virus Core antigen" *J. Virol. Methods* **2009**, *157*, 8–14.
- [8] Muerhoff, A. S.; Jiang, L.; Shah, D. O.; Gutierrez, R. A.; Patel, J.; Garolis, C.; Kyrk, C. R.; Leckie, G.; Frank, A.; Stewart, J. L.; Dawson, G. J. "Detection of

- HCV Core antigen in human serum and plasma with an automated chemiluminescent immunoassay" *Transfusion* **2002**, *42*, 349–356.
- [9] Chevaliez, S. "Virological tools to diagnose and monitor hepatitis C virus infection" *Clin. Microbiol. Infect.* **2011**, *17*, 116–121.
- [10] European Association for the Study of the Liver. "EASL clinical practice guidelines: management of hepatitis C virus infection" *J. Hepatol.* **2011**, *55*, 245–264.
- [11] Crignis E. D.; Re, M. C.; Cimatti, L.; Zecchi, L.; Gibellini, D. "HIV-1 and HCV detection in dried blood spots by SYBR Green multiplex real-time RT-PCR" *J. Virol. Methods.* **2010**, *165*, 51–56.
- [12] Liu, S.; Hu, Y.; Jin, J.; Zhang, H.; Cai, C. "Electrochemical detection of hepatitis C virus based on site-specific DNA cleavage of BamHI endonuclease" *Chem. Commun.* **2009**, 1635–1637.
- [13] Liu, S.; Wu, P.; Li, W.; Zhang, H.; Cai, C. "Ultrasensitive and selective electrochemical identification of hepatitis C virus genotype 1b based on specific endonuclease combined with gold nanoparticles signal amplification" *Anal. Chem.* **2011**, *83*, 4752–4758.
- [14] Donmez, S.; Arslan, F.; Arslan, H. "A nucleic acid biosensor for detection of hepatitis C virus genotype 1a using poly(L-glutamic acid)-modified electrode" *Appl. Biochem. Biotechnol.* **2015**, *176*, 1431–1444.
- [15] Singhal, C.; Ingle, A.; Chakraborty, D.; Pn, A. K.; Pundir, C. S.; Narang, J. "Impedimetric genosensor for detection of hepatitis C virus (HCV1) DNA using viral probe on methylene blue doped silica nanoparticles" *Int. J. Biol. Macromol.* **2017**, *98*, 84–93.
- [16] Lereau, M.; Wirth, C. F.; Mayen, J.; Farre, C.; Meyer, A.; Dugas, V.; Cantaloube, J. F.; Chaix, C.; Vasseur, J. J.; Morvan, F. "Development of innovative and versatile polythiol probes for use on ELOSA or

- electrochemical biosensors: application in hepatitis C virus genotyping" *Anal. Chem.* **2013**, *85*, 9204–9212.
- [17] Liu, L.; Wang, X.; Ma, Q.; Lin, Z.; Chen, S.; Li, Y.; Lu, L.; Qu, H.; Su, X. "Multiplex electrochemiluminescence DNA sensor for determination of hepatitis B virus and hepatitis C virus based on multicolor quantum dots and Au nanoparticles" *Anal. Chim. Acta* **2016**, *916*, 92–101.
- [18] Ulep, T. H.; Yoon, J. Y. "Challenges in paper-based fluorogenic optical sensing with smartphones" *Nano Converg.* **2018**, doi: 10.1186/s40580-018-0146-1.
- [19] Zeng, P.; Hou, P.; Jing, C. J.; Huang, C. Z. "Highly sensitive detection of hepatitis C virus DNA by using a one-donor-four-acceptors FRET probe" *Talanta* **2018**, *185*, 118–122.
- [20] Wang, Q. X.; Xue, S. F.; Chen, Z. H.; Ma, S. H.; Zhang, S.; Shi, G.; Zhang, M. "Dual lanthanide-doped complexes: the development of a time-resolved ratiometric fluorescent probe for anthrax biomarker and a paper-based visual sensor" *Biosens. Bioelectron.* **2017**, *94*, 388–393.
- [21] Jiao, Y.; Du, C.; Zong, L.; Guo, X.; Han, Y.; Zhang, X.; Li, L.; Zhang, C.; Ju, Q.; Liu, J.; Yu, H.-D.; Huang, W. "3D vertical-flow paper-based device for simultaneous detection of multiple cancer biomarkers by fluorescent immunoassay" *Sens. Actuators B Chem.* **2020**, doi: 10.1016/j.snb.2019.127239.
- [22] Na, M.; Zhang, S.; Liu, J.; Ma, S.; Han, Y.; Wang, Y.; He, Y.; Chen, H.; Chen, X. "Determination of pathogenic bacteria-Bacillus anthrax spores in environmental samples by ratiometric fluorescence and test paper based on dual-emission fluorescent silicon nanoparticles" *J. Hazard. Mater.* **2020**, doi: 10.1016/j.jhazmat.2019.121956.
- [23] Maruthupandi, M.; Thirupathi, D.; Vasimalai, N. "One minute synthesis of green fluorescent copper nanocluster: The preparation of smartphone aided paper-based kit for on-site monitoring of nanomolar level mercury

- and sulfide ions in environmental samples" *J. Hazard. Mater.* **2020**, doi: 10.1016/j.jhazmat.2020.122294.
- [24] Song, X.; Wang, Y.; Ru, J.; Yang, Y.; Feng, Y.; Cao, C.; Wang, K.; Zhang, G.; Liu, W. "A mitochondrial-targeted red fluorescent probe for detecting endogenous H₂S in cells with high selectivity and development of a visual paper-based sensing platform" *Sensors. Actuators B: Chem.* **2020**, doi: 10.1016/j.snb.2020.127982.
- [25] Wittung, P.; Nielsen, P. E.; Buchardt, O.; Egholm, M.; Nordén, B. "DNA-like double helix formed by peptide nucleic acid" *Nature* **1994**, *368*, 561–563.
- [26] M.; Buchardt, O.; Christensen, L.; Behrens, C.; Frelert, S. M.; Drivert, D. A.; Bergt, R. H.; Kim, S. K.; Nordén, B.; Nielsen, P. E. "PNA hybridizes to complementary oligonucleotides obeying the Watson–Crick hydrogen-bonding rules" *Nature* **1993**, *365*, 566–568.
- [27] Tomac, S.; Sarkar, M.; Ratilainen, T.; Wittung, P.; Nielsen, P. E.; Nordén, B.; Gräslund, A. "Ionic effects on the stability and conformation of peptide nucleic acid complexes" *J. Am. Chem. Soc.* **1996**, *118*, 5544–5552.
- [28] Demidov, V. V.; Potaman, V.; Frank-Kamenetskii M. D.; Egholm, M.; Buchard, O.; Sönnichsen, S. H.; Nielsen, P. E. "Stability of peptide nucleic acids in human serum and cellular extracts" *Biochem. Pharmacol.* **1994**, *48*, 1310–1133.
- [29] Vilaivan, T. "Pyrrolidinyl PNA with alpha/beta-dipeptide backbone: from development to applications. *Acc. Chem. Res.* **2015**, *48*, 1645–1656.
- [30] Jirakittiwut, N.; Panyain, N.; Nuanyai, T.; Vilaivan, T.; Praneenararat, T. "Pyrrolidinyl peptide nucleic acids immobilised on cellulose paper as a DNA sensor" *RSC Advanc.* **2015**, *5*, 24110–24114.
- [31] Teengam, P.; Siangproh, W.; Tuantranont, A.; Vilaivan, T.; Chailapakul, O.; Henry, C. S. "Electrochemical impedance-based DNA sensor using

- pyrrolidinyl peptide nucleic acids for tuberculosis detection" *Anal. Chim. Acta* **2018**, *1044*, 102–109.
- [32] Srisomwat, C.; Teengam, P.; Chuaypen, N.; Tangkijvanich, P.; Vilaivan, T.; Chailapakul, O. "Pop-up paper electrochemical device for label-free hepatitis B virus DNA detection" *Sensors. Actuators B: Chem.* **2020**, doi: 10.1016/j.snb.2020.128077.
- [33] Choo, Q.-L.; Richman, K. H.; Han, J. H.; Berger, K.; Lee, C.; Dong, C.; Gallegos, C.; Coit, D.; Medina-Selby, A.; Barr, P. J.; Weiner, A. J.; Bradley, D. W.; Kuo, G.; Houghton, M. "Genetic organization and diversity of the hepatitis C virus" *Proc. Natl. Acad. Sci. USA* **1991**, *88*, 2451–2455.
- [34] Pozzetto, B.; Bourlet, T.; Grattard, F.; Bonneval, L. "Structure, genomic organization, replication and variability of hepatitis C virus" *Nephrol. Dial. Transpl.* **1996**, *11*, 2–5.
- [35] Saeed, U.; Waheed, Y.; Ashraf, M. "Hepatitis B and hepatitis C viruses: a review of viral genomes, viral induced host immune responses, genotypic distributions and worldwide epidemiology" *Asian Pac. J. Trop. Dis.* **2014**, *4*, 88–96.
- [36] Ohno, T.; Mizokami, M.; Wu, R.-R.; Saleh, M. G.; Ohba, K.-I.; Orito, E.; Mukaide, M.; Williams, R.; Lau, J. Y. N. "New hepatitis C virus (HCV) genotyping system that allows for identification of HCV genotypes 1a, 1b, 2a, 2b, 3a, 3b, 4, 5a and 6a" *J. Clin. Microbiol.* **1997**, *35*, 201–207.
- [37] Zeisel, M. B.; Felmler, D. J.; Baumert, T. F. "Hepatitis C virus entry" *Curr. Top. Microbiol. Immunol.* **2013**, *369*, 87–112.
- [38] Lohmann, V. "Hepatitis C virus RNA replication" *Curr. Top. Microbiol. Immunol.* **2013**, *369*, 167–198.
- [39] Lindenbach, B. D. "Virion assembly and release" *Curr. Top. Microbiol. Immunol.* **2013**, *369*, 199–218.

- [40] Choo, Q. L.; Kuo, G.; Weiner, A. J.; Overby, L. R.; Bradley, D.W.; Houghton, M. "Isolation of a cDNA clone derived from a blood-borne non-A, non-B viral hepatitis genome" *Science* **1989**, *244*, 359–362
- [41] Ismail, N.; Fish, G. E.; Smith, M. B. "Laboratory evaluation of a fully automated chemiluminescence immunoassay for rapid detection of HBsAg, antibodies to HBsAg, and antibodies to hepatitis C virus" *J. Clin. Microbiol.* **2004**, *42*, 610–617.
- [42] Covalab R&D in Biotechnology. "Chemiluminescent reagent-covalight" Available online: <https://www.covalab.com/products-covalight> (accessed April 4, 2020).
- [43] Shivkumar, S.; Peeling, R.; Jafari, Y.; Joseph, L.; Pai, N. P. "Accuracy of rapid and point-of-care screening tests for hepatitis C" *Ann. Intern. Med.* **2012**, *157*, 558–566.
- [44] United States Food and Drug Administration (US FDA). "OraQuick HCV rapid antibody test-P080027/s001" Available online: <http://www.fda.gov/MedicalDevices/ProductsandMedicalProcedures/DeviceApprovalsandClearances/Recently-ApprovedDevices/ucm246401.html> (accessed April 4, 2020).
- [45] Saludes, V.; González, V.; Planas, R.; Matas, L.; Ausina, V.; Martró, E. "Tools for the diagnosis of hepatitis C virus infection and hepatic fibrosis staging" *World J. Gastroenterol.* **2014**, *20*, 3431–3442.
- [46] Park, Y.; Lee, J. H.; Kim, B. S.; Kim, D. Y.; Han, K. H.; Kim, H. S. "New automated hepatitis C virus (HCV) Core antigen assay as an alternative to real-time PCR for HCV RNA quantification" *J. Clin. Microbiol.* **2010**, *48*, 2253–2256.
- [47] Descamps, V.; Op de Beeck, A.; Plassart, C.; Brochet, E.; Francois, C.; Helle, F.; Adler, M.; Bourgeois, N.; Degre, D.; Duverlie, G.; Castelain, S. "Strong correlation between liver and serum levels of hepatitis C virus Core

- antigen and RNA in chronically infected patients" *J. Clin. Microbiol.* **2012**, *50*, 465–468.
- [48] Alberti, A.; Benvegnù, L. "Management of hepatitis C" *J. Hepatol.* **2003**, *38*, 104–118.
- [49] Aoyagi K.; Ohue, C.; Iida, K.; Kimura, T.; Tanaka, E.; Kiyosawa, K.; Yagi, S. "Development of a simple and highly sensitive enzyme immunoassay for hepatitis C virus Core antigen" *J. Clin. Microbiol.* **1999**, *37*, 1802–1808.
- [50] Miedouge, M.; Saune, K.; Kamar, N.; Rieu, M.; Rostaing, L.; Izopet, J. "Analytical evaluation of HCV Core antigen and interest for HCV screening in haemodialysis patients" *J. Clin. Virol.* **2010**, *48*, 18–21.
- [51] Gonzalez, V.; Padilla, E.; Diago, M.; Gimenez, M. D.; Sola, R.; Matas, L.; Montoliu, S.; Morillas, R. M.; Perez, C.; Planas, R. "Clinical usefulness of total hepatitis C virus Core antigen quantification to monitor the response to treatment with peginterferon alpha-2a plus ribavirin" *J. Viral. Hepat.* **2005**, *12*, 481–487.
- [52] Coppola, N.; Pisapia, R.; Marrocco, C.; Martini, S.; Vatiro, L. M.; Messina, V.; Tonziello, G.; Sagnelli, C.; Filippini, P.; Piccinino, F.; Sagnelli, E. "Anti-HCV IgG avidity index in acute hepatitis C" *J. Clin. Virol.* **2007**, *40*, 110–115.
- [53] Firdaus, R.; Saha, K.; Biswas, A.; Sadhukhan, P. C. "Current molecular methods for the detection of hepatitis C virus in high risk group population: a systematic review" *World J. Virol.* **2015**, *4*, 25–32.
- [54] Zitzer, H.; Heilek, G.; Truchon, K.; Susser, S.; Vermehren, J.; Sizmman, D.; Cobb, B.; Sarrazin, C. "Second-generation Cobas AmpliPrep/Cobas TaqMan HCV quantitative test for viral load monitoring: a novel dual-probe assay design" *J. Clin. Microbiol.* **2013**, *51*, 571–577.
- [55] Martinez, A. W.; Phillips, S. T.; Butte, M. J.; Whitesides, G. M. "Patterned paper as a platform for inexpensive, low-volume, portable bioassays" *Angew. Chem. Int. Ed. Engl.* **2007**, *46*, 1318–1320.

- [56] Xia, Y.; Si, J.; Li, Z. "Fabrication techniques for microfluidic paper-based analytical devices and their applications for biological testing: a review" *Biosens. Bioelectron.* **2016**, *77*, 774–789.
- [57] Chaiyo, S.; Mehmeti, E.; Siangproh, W.; Hoang, T. L.; Nguyen, H. P.; Chailapakul, O.; Kalcher, K. "Non-enzymatic electrochemical detection of glucose with a disposable paper-based sensor using a cobalt phthalocyanine-ionic liquid-graphene composite" *Biosens. Bioelectron.* **2018**, *102*, 113–120.
- [58] Yao, Y.; Ping, J. "Recent advances in graphene-based freestanding paper-like materials for sensing applications" *Trac-Trend. Anal. Chem.* **2018**, *105*, 75–88.
- [59] Deng, D.; Lin, Q.; Li, H.; Huang, Z.; Kuang, Y.; Chen, H.; Kong, J. "Rapid detection of malachite green residues in fish using a surface-enhanced Raman scattering-active glass fiber paper prepared by in situ reduction method" *Talanta* **2019**, *200*, 272–278.
- [60] Mettakoonpitak, J.; Boehle, K.; Nantaphol, S.; Teengam, P.; Adkins, J. A.; Srisa-Art, M.; Henry, C. S. "Electrochemistry on Paper-based Analytical Devices: a Review" *Electroanalysis* **2016**, *28*, 1420–1436.
- [61] Fu, L.-M.; Wang, Y.-N. "Detection methods and applications of microfluidic paper-based analytical devices" *Trac-Trend. Anal. Chem.* **2018**, *107*, 196–211.
- [62] Chen, C.-A.; Wang, P.-W.; Yen, Y.-C.; Lin, H.-L.; Fan, Y.-C.; Wu, S.-M.; Chen, C.-F. "Fast analysis of ketamine using a colorimetric immunosorbent assay on a paper-based analytical device" *Sensors. Actuators B: Chem.* **2019**, *282*, 251–258.
- [63] Pungjunun, K.; Chaiyo, S.; Praphairaksit, N.; Siangproh, W.; Ortner, A.; Kalcher, K.; Chailapakul, O.; Mehmeti, E. "Electrochemical detection of NO_x gas based on disposable paper-based analytical device using a

- copper nanoparticles-modified screen-printed graphene electrode" *Biosens. Bioelectron.* **2019**, doi: 10.1016/j.bios.2019.111606.
- [64] Lim, W. Y.; Goh, B. T.; Khor, S. M. "Microfluidic paper-based analytical devices for potential use in quantitative and direct detection of disease biomarkers in clinical analysis" *J. Chromatogr. B Analyt. Technol. Biomed. Life Sci.* **2017**, *1060*, 424–442.
- [65] Guzman, J. M. C. C.; Tayo, L. L.; Liu, C.-C.; Wang, Y.-N.; Fu, L.-M. "Rapid microfluidic paper-based platform for low concentration formaldehyde detection" *Sensors. Actuators B: Chem.* **2018**, *255*, 3623–3629.
- [66] Peters, J. J.; Almeida, M.; O'Connor Sraja, L.; McKelvie, I. D.; Kolev, S. D. "Development of a micro-distillation microfluidic paper-based analytical device as a screening tool for total ammonia monitoring in freshwaters" *Anal. Chim. Acta* **2019**, *1079*, 120–128.
- [67] Noomnam, U.; Clegg, R. M. "Fluorescence lifetimes: fundamentals and interpretations" *Photosynth. Res.* **2009**, *101*, 181–194.
- [68] Wu, M.; Lai, Q.; Ju, Q.; Li, L.; Yu, H. D.; Huang, W. "Paper-based fluorogenic devices for in vitro diagnostics" *Biosens. Bioelectron.* **2018**, *102*, 256–266.
- [69] Kanchi, S.; Sabela, M. I.; Mdluli, P. S.; Inamuddin; Bisetty, K. "Smartphone based bioanalytical and diagnosis applications: a review" *Biosens. Bioelectron.* **2018**, *102*, 136–149.
- [70] Noor, M. O.; Shahmuradyan, A.; Krull, U. J. "Paper-based solid-phase nucleic acid hybridization assay using immobilized quantum dots as donors in fluorescence resonance energy transfer" *Anal. Chem.* **2013**, *85*, 1860–1867.
- [71] Yang, Z.; Xu, G.; Reboud, J.; Ali, S. A.; Kaur, G.; McGiven, J.; Bobby, N.; Gupta, P. K.; Chaudhuri, P.; Cooper, J. M. "Rapid veterinary diagnosis of bovine reproductive infectious diseases from semen using paper-origami DNA microfluidics" *ACS Sens.* **2018**, *3*, 403–409.

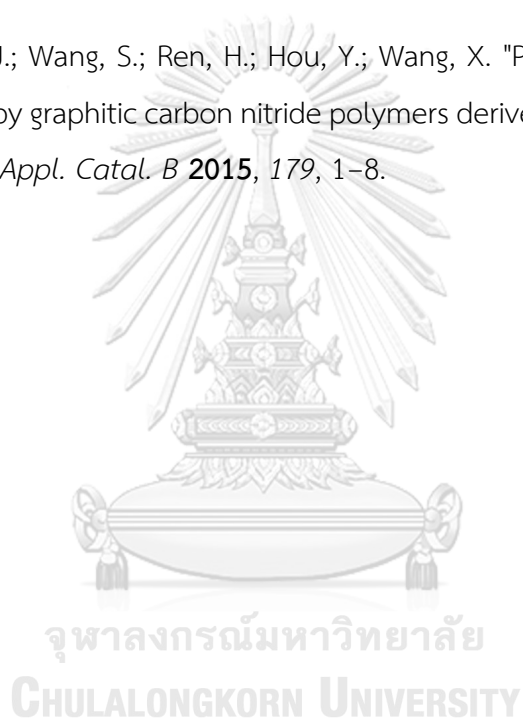
- [72] Calabretta, M. M.; Alvarez-Diduk, R.; Michelini, E.; Roda, A.; Merkoci, A. "Nano-lantern on paper for smartphone-based ATP detection" *Biosens. Bioelectron.* **2020**, doi: 10.1016/j.bios.2019.111902.
- [73] Rong, Z.; Wang, Q.; Sun, N.; Jia, X.; Wang, K.; Xiao, R.; Wang, S. "Smartphone-based fluorescent lateral flow immunoassay platform for highly sensitive point-of-care detection of Zika virus nonstructural protein 1" *Anal. Chim. Acta* **2019**, *1055*, 140–147.
- [74] Nielsen, P. E.; Egholm, M.; Berg, R. H.; Buchardt, O. "Sequence-selective recognition of DNA by strand displacement with a thymine-substituted polyamide" *Science* **1991**, *254*, 1497–1500.
- [75] Tackett, A. J.; Corey, D. R.; Raney, K. D. "Non-Watson–Crick interactions between PNA and DNA inhibit the ATPase activity of bacteriophage T4 Dda helicase" *Nucleic Acids Res.* **2002**, *30*, 950–957.
- [76] Braasch, D. A.; Corey, D. R. "Synthesis, analysis, purification, and intracellular delivery of peptide nucleic acids" *Methods* **2001**, *23*, 97–107.
- [77] Pokorski, J. K.; Witschi, M. A.; Purnell, B. L.; Appella, D. H. "(S,S)-trans-cyclopentane-constrained peptide nucleic acids. a general backbone modification that improves binding affinity and sequence specificity" *J. Am. Chem. Soc.* **2004**, *126*, 15067–15073.
- [78] Govindaraju, T.; Kumar, V. A.; Ganesh, K. N. "Synthesis and evaluation of (1S,2R/1R,2S)-aminocyclohexylglycyl PNAs as conformationally preorganized PNA analogues for DNA/RNA recognition" *J. Org. Chem.* **2004**, *69*, 1858–1865.
- [79] Dragulescu-Andrasi, A.; Rapireddy, S.; Frezza, B. M.; Gayathri, C.; Gil, R. R.; Ly, D. H. "A simple gamma-backbone modification preorganizes peptide nucleic acid into a helical structure" *J. Am. Chem. Soc.* **2006**, *128*, 10258–10267.

- [80] Sahu, B.; Sacui, I.; Rapireddy, S.; Zanotti, K. J.; Bahal, R.; Armitage, B. A.; Ly, D. H. "Synthesis and characterization of conformationally preorganized, (*R*)-diethylene glycol-containing gamma-peptide nucleic acids with superior hybridization properties and water solubility" *J. Org. Chem.* **2011**, *76*, 5614–5627.
- [81] Sahu, B.; Chenna, V.; Lathrop, K. L.; Thomas, S. M.; Zon, G.; Livak, K. J.; Ly, D. H. "Synthesis of conformationally preorganized and cell-permeable guanidine-based gamma-peptide nucleic acids (gammaGPNAs)" *J. Org. Chem.* **2009**, *74*, 1509–1516.
- [82] Jain, D. R.; Anandi, V. L.; Lahiri, M.; Ganesh, K. N. "Influence of pendant chiral C(γ)-(alkylideneamino/guanidino) cationic side-chains of PNA backbone on hybridization with complementary DNA/RNA and cell permeability" *J. Org. Chem.* **2014**, *79*, 9567–9577.
- [83] Jain, D. R.; Ganesh, K. N., "Clickable $C\gamma$ -azido(methylene/butylene) peptide nucleic acids and their clicked fluorescent derivatives: synthesis, DNA hybridization properties, and cell penetration studie" *J. Org. Chem.* **2014**, *79*, 6708–6714.
- [84] Lowe, G.; Vilaivan, T. "Solid phase synthesis of novel peptide nucleic acids" *J. Chem. Soc., Perkin Trans. 1* **1997**, 555–560.
- [85] Ananthanawat, C.; Vilaivan, T.; Hoven, V. P. "Synthesis and immobilization of thiolated pyrrolidiny l peptide nucleic acids on gold-coated piezoelectric quartz crystals for the detection of DNA hybridization" *Sensors. Actuators B: Chem.* **2009**, *137*, 215–221.
- [86] Ananthanawat, C.; Hoven, V. P.; Vilaivan, T.; Su, X. "Surface plasmon resonance study of PNA interactions with double-stranded DNA" *Biosens. Bioelectron.* **2011**, *26*, 1918–1923.
- [87] Thipmanee, O.; Samanman, S.; Sankoh, S.; Numnuam, A.; Limbut, W.; Kanatharana, P.; Vilaivan, T.; Thavarungkul, P. "Label-free capacitive DNA sensor using immobilized pyrrolidiny l PNA probe: effect of the length and

- terminating head group of the blocking thiols" *Biosens. Bioelectron.* **2012**, *38*, 430–435.
- [88] Jampasa, S.; Wonsawat, W.; Rodthongkum, N.; Siangproh, W.; Yanatatsaneejit, P.; Vilaivan, T.; Chailapakul, O. "Electrochemical detection of human papillomavirus DNA type 16 using a pyrrolidinyl peptide nucleic acid probe immobilized on screen-printed carbon electrodes" *Biosens. Bioelectron.* **2014**, *54*, 428–434.
- [89] Teengam, P.; Siangproh, W.; Tuantranont, A.; Vilaivan, T.; Chailapakul, O.; Henry, C. S. "Multiplex paper-based colorimetric DNA sensor using pyrrolidinyl peptide nucleic acid-induced AgNPs aggregation for detecting MERS-CoV, MTB, and HPV oligonucleotides" *Anal. Chem.* **2017**, *89*, 5428–5435.
- [90] Jampasa, S.; Siangproh, W.; Laocharoensuk, R.; Yanatatsaneejit, P.; Vilaivan, T.; Chailapakul, O. "A new DNA sensor design for the simultaneous detection of HPV type 16 and 18 DNA" *Sensors. Actuators B: Chem.* **2018**, *265*, 514–521.
- [91] Long, Y.; Zhou, J.; Yang, M.-P.; Yang, B.-Q. "A selective and sensitive off-on probe for palladium and its application for living cell imaging" *Chinese Chem. Lett.* **2016**, *27*, 205–210.
- [92] Feng, W.; Qiao, Q.-L.; Leng, S.; Miao, L.; Yin, W.-T.; Wang, L.-Q.; Xu, Z.-C. "A 1,8-naphthalimide-derived turn-on fluorescent probe for imaging lysosomal nitric oxide in living cells" *Chinese Chem. Lett.* **2016**, *27*, 1554–1558.
- [93] Promega Corporation. "QuantiFluor ssDNA System" Available online: <https://worldwide.promega.com/products/RNA-analysis/DNA-and-RNA-quantitation/quantifluor-ssDNA-system/?catNum=E3190> (accessed April 4, 2020).
- [94] Rye, H. S.; Glazer, A. N. "Interaction of dimeric intercalating dyes with single-stranded DNA" *Nucleic Acids Res.* **1995**, *23*, 1215–1222.

- [95] Thermo Fisher Scientific. "Quant-iT Oligreen reagent and kit" Available online:
http://tools.thermofisher.com/content/sfs/manuals/Quant_iT_OliGreen_ssDNA_Reagent_UG.pdf (accessed April 4, 2020).
- [96] Barrios, V. A. E.; Méndez, J. R. R.; Aguilar, N. V. P.; Espinosa, G. A.; Rodríguez, J. L. D. "FTIR - An Essential Characterization Technique for Polymeric Materials" In: Theophile, T. (Ed.), *Infrared Spectroscopy-Materials Science, Engineering and Technology*, InTech, Croatia, 2012, 195–212.
- [97] Aton Paar. "Attenuated total reflectance" Available online:
<https://wiki.anton-paar.com/en/attenuated-total-reflectance-atr/> (accessed April 4, 2020).
- [98] Fan, Q. G.; Lewis, D. M.; Tapley, K. N. "Characterization of cellulose aldehyde using Fourier transform infrared spectroscopy" *J. Appl. Polym. Sci.* **2001**, *82*, 1195–1202.
- [99] Verma, V.; Verma, P.; Ray, P.; Ray, A. R. "2, 3-Dihydrazone cellulose: prospective material for tissue engineering scaffolds" *Mater. Sci. Eng. C* **2008**, *28*, 1441–1447.
- [100] Konno, H. "X-ray Photoelectron Spectroscopy" In: Inagami, M.; Kang, F. (Eds.), *Materials Science and Engineering of Carbon*, Elsevier, US, 2016, 153–171.
- [101] Vilaivan, T.; Srisuwannaket, C. "Hybridization of Pyrrolidinyl Peptide Nucleic Acids and DNA: Selectivity, Base-Pairing Specificity, and Direction of Binding" *Org. Lett.* **2006**, *8*, 1897–1900.
- [102] Seol, Y. G.; Trung, T. Q.; Yoon, O-J; Sohn, I. Y.; Lee, N. E. "Nanocomposites of reduced graphene oxide nanosheets and conducting polymer for stretchable transparent conducting electrode" *J. Mater. Chem.* **2012**, *22*, 23759–23766.

- [103] Ren, H.; Shao, H.; Zhang, L.; Guo, D.; Jin, Q.; Yu, R.; Wang, L.; Li, Y.; Wang, Y.; Zhao, H.; Wang, D. "A New Graphdiyne Nanosheet/Pt Nanoparticle-Based Counter Electrode Material with Enhanced Catalytic Activity for Dye-Sensitized Solar Cells" *Adv. Energy Mater.* **2015**, doi: 10.1002/aenm.201500296.
- [104] Zhan, G.; Zeng, H. C. "Synthesis and Functionalization of Oriented Metal-Organic-Framework Nanosheets: Toward a Series of 2D Catalysts" *Adv. Funct. Mater.* **2016**, doi: 10.1002/adfm.201505380.
- [105] Qin, J.; Wang, S.; Ren, H.; Hou, Y.; Wang, X. "Photocatalytic reduction of CO₂ by graphitic carbon nitride polymers derived from urea and barbituric acid" *Appl. Catal. B* **2015**, 179, 1–8.





APPENDIX

จุฬาลงกรณ์มหาวิทยาลัย
CHULALONGKORN UNIVERSITY

BLAST Results					
Job title: Nucleotide Sequence (15 letters) 5'-GCTCCGGGACTGCAC-3'					
RID	4S3KSOA001R (Expires on 01-27 14:38 pm)				
Query ID	Id Query_210159	Database Name	nr		
Description	None	Description	Nucleotide collection (nt)		
Molecule type	nucleic acid	Program	BLASTN 2.8.1+		
Query Length	15				
Hepacivirus C isolate IBTO.IR.DONOR188 non-structural protein 5b (NS5b) gene, partial cds					
Sequence ID: MG704793.1 Length: 280 Number of Matches: 1					
Range 1: 231 to 245					
Score	Expect	Identities	Gaps	Strand	Frame
30.2 bits(15)	304()	15/15(100%)	0/15(0%)	Plus/Plus	
Features:					
Query	1	GCTCCGGGACTGCAC	15		
Sbjct	231	GCTCCGGGACTGCAC	245		
Hepacivirus C isolate IBTO.IR.DONOR231 non-structural protein 5b (NS5b) gene, partial cds					
Sequence ID: MG704785.1 Length: 318 Number of Matches: 1					
Range 1: 231 to 245					
Score	Expect	Identities	Gaps	Strand	Frame
30.2 bits(15)	304()	15/15(100%)	0/15(0%)	Plus/Plus	
Features:					
Query	1	GCTCCGGGACTGCAC	15		
Sbjct	231	GCTCCGGGACTGCAC	245		
Hepacivirus C isolate IBTO.IR.DONOR61 non-structural protein 5b (NS5b) gene, partial cds					
Sequence ID: MG704790.1 Length: 390 Number of Matches: 1					
Range 1: 267 to 281					
Score	Expect	Identities	Gaps	Strand	Frame
30.2 bits(15)	304()	15/15(100%)	0/15(0%)	Plus/Plus	
Features:					
Query	1	GCTCCGGGACTGCAC	15		
Sbjct	267	GCTCCGGGACTGCAC	281		
Hepacivirus C isolate IBTO.IR.DONOR15 non-structural protein 5b (NS5b) gene, partial cds					
Sequence ID: MG704787.1 Length: 384 Number of Matches: 1					
Range 1: 270 to 284					
Score	Expect	Identities	Gaps	Strand	Frame
30.2 bits(15)	304()	15/15(100%)	0/15(0%)	Plus/Plus	
Features:					
Query	1	GCTCCGGGACTGCAC	15		
Sbjct	270	GCTCCGGGACTGCAC	284		
Hepacivirus C isolate IBTO.IR.DONOR226 non-structural protein 5b (NS5b) gene, partial cds					
Sequence ID: MG704784.1 Length: 318 Number of Matches: 1					
Range 1: 231 to 245					
Score	Expect	Identities	Gaps	Strand	Frame
30.2 bits(15)	304()	15/15(100%)	0/15(0%)	Plus/Plus	
Features:					
Query	1	GCTCCGGGACTGCAC	15		
Sbjct	231	GCTCCGGGACTGCAC	245		

Figure A1 Nucleotide sequences report from NCBI BLAST database.

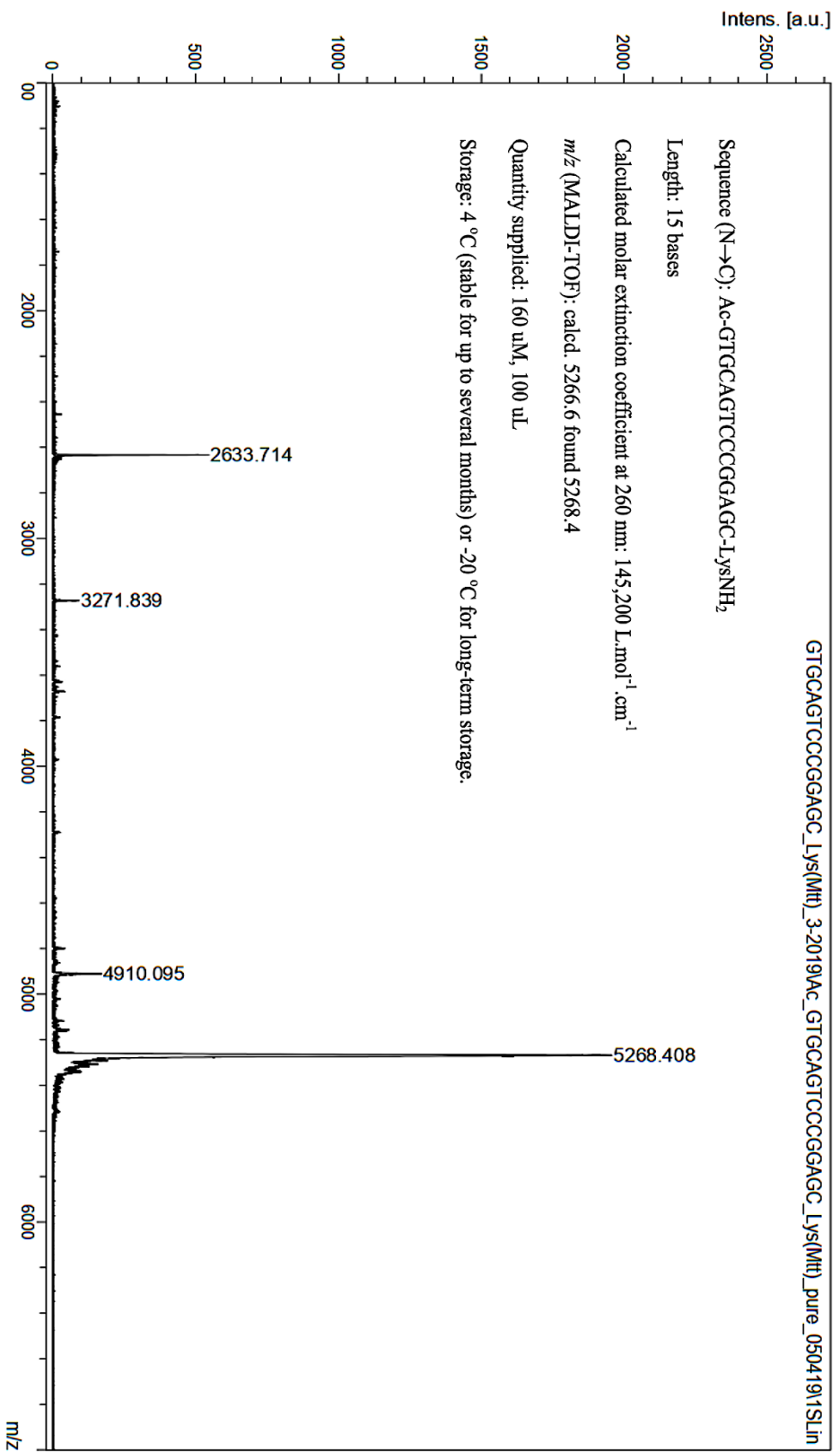


Figure A2 MALDI-TOF mass spectrum and the specific information of HCV acpPNA probe

Table A1 Chemical compounds that interfere with the ssDNA-binding fluorescent dye (QuantiFluor[®] ssDNA System) [93].

Compounds	Concentration shown to affect the dye ¹	Change in fluorescence signal
Agarose	0.08%	44% decrease
Ammonium acetate	20 mM	8% decrease
Bovine serum albumin (BSA)	1%	17% decrease
Chloroform	0.4%	22% increase
Ethanol	10%	24% decrease
IgG	0.5%	15% decrease
Sodium chloride	20 mM	14% decrease
Magnesium chloride	2 mM	25% decrease
Zinc chloride	1 mM	1% increase
dsDNA	10 ng	9% increase
RNA	60 ng	11% increase
dNTPs	0.5 mM	8% decrease
rNTPs	0.5 mM	7% decrease
Urea	3 M	13% decrease
Phenol	0.2%	9% decrease
Polyethylene glycol	10%	3% increase
Sodium acetate	15 mM	6% decrease
Sodium dodecyl sulfate (SDS)	0.02%	17% decrease
Triton [®] X-100	0.2%	17% decrease

¹ Compounds were tested at the indicated concentration with an initial dye dilution of 1:200 and a final concentration of 990 ng/mL ssDNA standard in a 200 μ L assay.

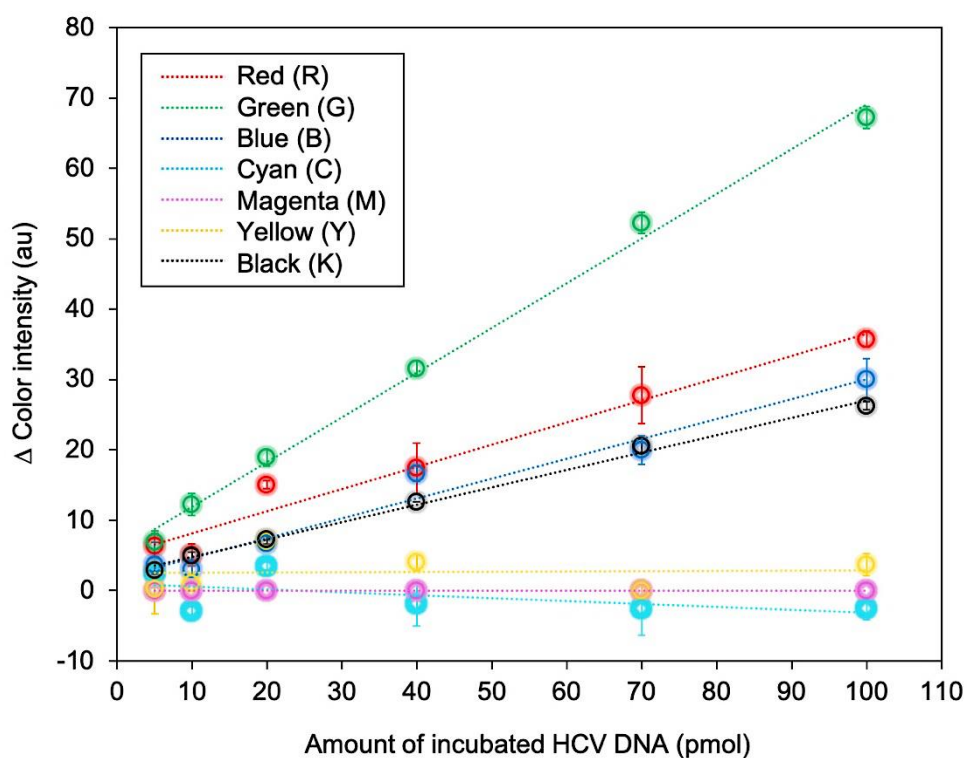


Figure A3 The calibration plots of the proposed DNA sensor in multiple color channels.

Table A2 The regression analysis of the calibration plots in Figure A3.

Color channel	Linear regression equation	Correlation coefficient
Red (R)	$y = 0.3259x + 4.8148$	0.9697
Green (G)	$y = 0.6348x + 5.6227$	0.9956
Blue (B)	$y = 0.2682x + 2.1037$	0.9624
Cyan (C)	$y = -0.0419x + 1.0681$	0.3076
Magenta (M)	-	-
Yellow (Y)	$y = 0.0037x + 2.5140$	0.0026
Black (K)	$y = 0.2472x + 2.3377$	0.9951

Table A3 *T-distribution table (one tail).*

Degree of freedom (df)	Significant level, α		
	0.1	0.05	0.01
1	3.078	6.314	31.821
2	1.886	2.920	6.965
3	1.638	2.353	4.541
4	1.533	2.132	3.747
5	1.476	2.015	3.365
6	1.440	1.943	3.143
7	1.415	1.895	2.998
8	1.397	1.860	2.896
9	1.383	1.833	2.821
10	1.372	1.812	2.764
11	1.363	1.796	2.718
12	1.356	1.782	2.681
13	1.350	1.771	2.650
14	1.345	1.761	2.624
15	1.341	1.753	2.602
16	1.337	1.746	2.583
17	1.333	1.740	2.567
18	1.330	1.734	2.552
19	1.328	1.729	2.539
20	1.325	1.725	2.528
∞	1.282	1.645	2.326

Table A4 F distribution table (one tail) at significant level of 0.05.

	df ₁ =1										
	2	3	4	5	6	7	8	9	10	∞	
df ₂ =1	161.448	199.500	215.707	224.583	230.162	233.986	236.768	238.883	240.543	241.882	254.314
2	18.513	19.000	19.164	19.247	19.296	19.330	19.353	19.371	19.385	19.396	19.496
3	10.128	9.552	9.277	9.117	9.014	8.941	8.887	8.845	8.812	8.786	8.526
4	7.709	6.944	6.591	6.388	6.256	6.163	6.094	6.041	5.999	5.964	5.628
5	6.608	5.786	5.410	5.192	5.050	4.950	4.876	4.818	4.772	4.735	4.365
6	5.987	5.143	4.757	4.534	4.387	4.284	4.207	4.147	4.099	4.060	3.669
7	5.591	4.737	4.347	4.120	3.972	3.866	3.787	3.726	3.677	3.636	3.230
8	5.318	4.459	4.066	3.838	3.688	3.581	3.500	3.438	3.388	3.347	2.928
9	5.117	4.256	3.862	3.633	3.482	3.374	3.293	3.230	3.179	3.137	2.707
10	4.965	4.103	3.708	3.478	3.326	3.217	3.136	3.072	3.020	2.978	2.538
∞	3.842	2.996	2.605	2.372	2.214	2.099	2.010	1.938	1.880	1.831	1.000

VITA

NAME Narathorn Nisab

DATE OF BIRTH 4 October 1996

PLACE OF BIRTH Bangkok, Thailand

INSTITUTIONS ATTENDED High school at Bhadungsit Pittaya School, Bangkok, Thailand
Bachelor's degree of Science, majoring in Chemistry from Chulalongkorn University, Bangkok, Thailand

HOME ADDRESS 363/59 Techawanit Road, Bangsue Sub-district, Bang Sue District, Bangkok 10800

AWARD RECEIVED Gold Medal (according to academic criteria), a Higher education level (Group 2: Health and medicine) from Thailand New Gen Inventors Award 2020, National research council of Thailand (NRCT)